TWO- AND THREE-DIMENSIONAL FINITE ELEMENT ANALYSES OF THE INTACT AND RECONSTRUCTED HEMIPELVIS

By

Greg Austin

Submitted to the University of Cape Town in partial fulfilment of the requirements for the degree of Master of Science in Biomedical Engineering.

August 1993

I, Greg Austin, hereby declare that the work on which this thesis is based is my original work (except where acknowledgements indicate otherwise) and that neither the whole work nor any part of it has been, is being or is to be submitted for another degree in this or any other University.

I empower the university to reproduce for the purpose of research either the whole or any portion of the contents in any manner whatsoever.

.......Signed..............

SIGNATURE

..............05/08/93..............

DATE

ABSTRACT

Cemented Total Hip Arthroplasty has up to now failed to ensure adequate long-term fixation of the acetabular component. This is due primarily to the aseptic loosening that occurs at the implant/bone interface. The cementless procedure was recently introduced in an attempt to address and overcome such problems, the emphasis of current research being aimed at improving component design to provide the necessary fixation. A porous coating on the metal backing of the cup is one cementless concept whereby the long-term fixation is achieved by means of bony ingrowth into the porous surface.

This study makes use of a powerful computational stress-analysis tool, Finite Element Analysis (FEA), to investigate a number of features of both the intact and reconstructed hip joint. The effect of cup orientation, cup metal backing material and assumed implant/bone interface conditions on the stresses in the pelvis was investigated, by means of two-dimensional plane strain FEA models. These two simulated interface conditions were those of a fully bonded and an unbonded cup, representing the "full-ingrowth" situation and the press-fit cup immediately post-operatively. A fully three-dimensional FEA model of the right hemipelvis was then developed in order to analyse the stresses in the intact bone. The strain-related bone remodelling in the hemipelvis was examined by means of a numerical algorithm. Finally, a method is presented for simulating the insertion of a three-dimensional cementless cup - complete with anti-rotational pegs - into bone.

We are able to conclude that the angle of cup insertion has a marked effect on the bone stresses compared to those predicted for the intact bone. Of the orientations investigated, a "neutral" angle of 45° is shown to be the best angle for cup insertion. Cup/bone interface modelling assumptions are shown to affect the bone stresses to a large degree, since the maximum principal stresses for the unbonded condition are twice those found for the fully bonded condition. The biomaterials used for metal backing of these cups have a negligible effect on both the stress magnitudes and distribution in the bone.

It was found that the three-dimensional hemipelvis is fully constrained at the pubis symphysis, while being able to displace in an antero-posterior direction at the sacro-iliac joint. The muscles are best modelled as fully constrained when these bony constraints are imposed on the hemipelvis, and a resultant hip reaction force is acting at the acetabulum. The maximum principal tensile stresses in the cortical and cancellous bone for these boundary and loading conditions were 9.29 and 1.29 MPa respectively, while the corresponding compressive stresses were 1.43 and 0.105 MPa respectively.

A strain-related adaptive bone remodelling simulation predicts a similar distribution of bone densities to that seen in a cadaveric bone. This "adapted" density distribution is conclusive in indicating that a single assumed bone density in each of the cancellous and cortical bone regions is an inadequate representation of the actual distribution in the hemipelvis.

The proposed pegged cup simulation using beam elements was shown to be an accurate indicator of bone stress magnitudes over the whole bone, but provide a relatively poor predictor of the bone stresses adjacent to the pegs themselves.

It is felt that this study can be useful in understanding the biomechanical behaviour of the hemipelvis. The three-dimensional model developed can also be easily adapted to examine differences in surgical technique (e.g. orientation of the cup and extents of reaming), the use of cemented cups and different pathological conditions (e.g. dysplasia and protrusio acetabulae).

ACKNOWLEDGEMENTS

I would like to thank the following people and departments for their contributions to this study:

Thanos Spirakis for his commitment to and supervision of this thesis. In particular, my understanding of the broader biomechanical issues has been vastly improved through my association with him.

Colin Mercer for his supervision of the implementation of the finite element code, and his insight into some of the difficult numerical problems which were encountered.

The FRD/UCT Centre for Research in Computational and Applied Mechanics (CERECAM) at the University of Cape Town for the use of their computing facilities. Also the staff and students of the unit for their input and ideas, and to the general interest shown in this work.

Greg Starke for his help that was always readily available.

Professor ID Learmonth for his useful suggestions on aspects of the surgical implantation of acetabular cups.

Mrs J Michie and Mr A. Sadie of the Radiology Department at Groote Schuur Hospital for performing the CT scanning of the hemipelvis.

TABLE OF CONTENTS

ABSTRACT	i
ACKNOWLEDGEMENTS	iii
TABLE OF CONTENTS	iv
LIST OF ILLUSTRATIONS	vi
LIST OF TABLES	ix
GLOSSARY	x
CHAPTER 1: INTRODUCTION	1
CHAPTER 2: LITERATURE REVIEW & RELEVANT BACKGROUND	4
2.1 Anatomy	4
2.1.1 Anatomy of the hip joint	4
2.1.2 The structure and function of bone	7
2.2 Biomechanics of the hip joint	9
2.3 Total hip arthroplasty	12
2.3.1 Background	12
2.3.2 Principles of total hip arthroplasty	12
2.3.3 Fixation methods of acetabular cups	14
2.4 Clinical results of cup arthroplasty	16
2.4.1 Cemented cups	16
2.4.2 Cementless cups	17
2.5 Finite element analysis in acetabular replacement	24
CHAPTER 3: TWO-DIMENSIONAL FEA MODELS	31
3.1 Model development	31
3.2 Boundary and loading conditions	36
3.3 Material properties	37
3.4 Numerical modelling and implementation	38

3.5 Results 43
3.5.1 Intact hemipelvis 43
3.5.2 Cup orientation and metal backing 46
3.5.3 Cup/bone interface conditions 51
3.5.4 Stresses at the unbonded cup/bone interface 56
3.5.5 Cup stresses 59

3.6 Discussion 62

CHAPTER 4: THREE-DIMENSIONAL FEA MODELS 68

4.1 Model development 68

4.2 Boundary and loading conditions 72

4.3 Material models 75

4.4 Numerical modelling and implementation 78
4.4.1 Hemipelvis and muscles 78
4.4.2 Cup implantation 83

4.5 Results 86
4.5.1 Model constraints 86
4.5.2 Adaptive bone remodelling 96
4.5.3 Cup implantation 103

4.6 Discussion 105

CHAPTER 5: CONCLUSIONS and RECOMMENDATIONS 114

APPENDIX A: REVIEW OF STRESS ANALYSIS METHODS 117

APPENDIX B: BONE REMODELLING 122

APPENDIX C: SAMPLE 2D ABAQUS INPUT DECK 126

APPENDIX D: SAMPLE 3DABAQUS INPUT DECK 129

REFERENCES 133

LIST OF ILLUSTRATIONS

Figure 2.1:	Cross-sectional view of the hip joint.	4
Figure 2.2:	Anterior view of the right hemipelvis and femur showing the important bony landmarks and the attachment sites of six muscles.	6
Figure 2.3:	Posterior view of the right hemipelvis and femur showing the attachment sites of six important muscles.	6
Figure 2.4:	Major forces acting on the hip joint.	9
Figure 2.5:	Components of THA and their relationship with the surrounding bone.	13
Figure 2.6:	a) Schematic diagram showing the acetabular origin of screws b) Schematic diagram showing the location of the screws on the quadrilateral intrapelvic superior surface relative to the iliac venous system.	23
Figure 2.7:	Diagram of three different model sections used in 2D FEA analyses of the hemipelvis.	27
Figure 3.1:	Digitised cross-section of the right hemipelvis.	33
Figure 3.2:	Mesh plots of a) the intact model, b) acetabulum with 30^{o} cup, c) acetabulum with 45^{o} cup and d) acetabulum with 60^{o} cup	35
Figure 3.3:	Boundary and loading conditions applied to the sectioned hemipelvis	36
Figure 3.4:	Implementation of INTER2 element for use with 2D plane strain elements	39
Figure 3.5:	2D rigid surface representing the artificial femoral head	39
Figure 3.6:	Default pressure-clearance relationship for interface elements	40
Figure 3.7:	"Softened" pressure-clearance relationship for interface elements	41

Figure 3.8:	Maximum principal cortical and cancellous stresses in the intact hemipelvis section	44
Figure 3.9:	Von Mises cortical and cancellous stresses in the intact hemipelvis section	45
Figure 3.10:	Maximum principal stresses in the cortical bone with a fully bonded cup/bone interface	47
Figure 3.11:	Maximum principal stresses in the cortical bone with a fully bonded cup/bone interface	48
Figure 3.12:	Maximum principal stresses in the cancellous bone with a fully bonded cup/bone interface	49
Figure 3.13:	Maximum principal stresses in the cancellous bone with a fully bonded cup/bone interface	50
Figure 3.14:	Maximum principal stresses in the cortical bone with a fully bonded cup/bone interface	52
Figure 3.15:	Maximum principal stresses in the cortical bone with an unbonded cup/bone interface	53
Figure 3.16:	Maximum principal stresses in the cancellous bone with a fully bonded cup/bone interface	54
Figure 3.17:	Maximum principal stresses in the cancellous bone with an unbonded cup/bone interface	55
Figure 3.18:	Cup/bone interface normal stresses with an unbonded cup/bone interface	57
Figure 3.19:	Cup/bone interface normal stresses with an unbonded cup/bone interface	58
Figure 3.20:	Maximum principal stresses in the cup with a fully bonded cup/bone interface	60
Figure 3.21:	Maximum principal stresses in the cup with a fully bonded cup/bone interface	61
Figure 4.1:	Mesh plot of the three-dimensional hemipelvis model	70

Figure 4.2:	Diagram illustrating the development of a Bezier surface	79
Figure 4.3:	Diagram illustrating the ABAQUS INTER4 element.	79
Figure 4.4:	Muscle attachment sites on the hemipelvis	81
Figure 4.5:	(a) Mesh plot of the pegged cup developed in PATRAN (hidden lines removed) (b) The same view of the cup as in Figure 4.5 (a), seen as a shaded image here.	84
Figure 4.6:	Graph of reaction force at the six muscle insertion nodes for different muscle spring k-values used, with the sacro-iliac joint allowed to displace vertically.	87
Figure 4.7:	Graph of reaction force at the six muscle insertion nodes for different muscle spring k-values used, with the sacro-iliac joint allowed to displace in the antero-posterior direction.	90
Figure 4.8:	Maximum principal stresses in the cortical bone	93
Figure 4.9:	Maximum principal stresses in the cancellous bone	94
Figure 4.10:	Displaced shape of the hemipelvis	95
Figure 4.11:	Convergence plot for cortical bone density	97
Figure 4.12:	Cortical bone density distribution	98
Figure 4.13:	Convergence plot for cancellous bone density	100
Figure 4.14:	Cancellous bone density distribution	101
Figure 4.15:	X-ray of dry right hemipelvis showing bone density distribution	102
Figure 4.16:	Maximum principal stresses in the 3D peg and beam test models	104

LIST OF TABLES

Table 2.1:	Summary of porous-coated cup literature review	20
Table 2.2:	Summary of screw-threaded cup literature review	22
Table 2.3:	Description of 2D, axisymmetric and 'alternate' 2D models	28
Table 2.4:	Description of 3D FEA models of the human hemipelvis	29
Table 2.5:	Summary of bone mechanical properties used in FEA models reported in the literature.	30
Table 3.1:	Material properties used in all analyses	37
Table 4.1:	Muscle forces from Goel *et al,* 1978	73
Table 4.2:	Co-ordinates of muscle insertion points extrapolated from Dostal & Andrews, 1981	74
Table 4.3:	Muscle stiffness values for the series of analyses where the sacro-iliac joint is allowed to displace vertically	88
Table 4.4:	Muscle stiffness values for the series of analyses that have the sacro-iliac joint able to displace in the antero-posterior direction	91

GLOSSARY

Abduction: Movement away from the median axis of the body

Acetabulum: The socket portion of the hip joint

Adduction: Movement towards the median axis of the body

Anterior: The front of the body

Anteversion: The angle that the acetabular rim or femoral neck makes with the coronal plane

Arthroplasty: Surgical operation to make a moveable joint

Bone ingrowth: Ingrowth of bone into the porous metal backing of acetabular cups

Coronal plane: A vertical plane through the body in a latero-medial direction

Cranial: Superior; literally, towards the head

Caudal: Inferior; literally, towards the tail

Deformation: The movement of points of the hemipelvis relative to each other

Displacement: A vector quantity which indicates the movement of a point on a body that is subject to a system of forces

Distal: Farther from the trunk; synonymous with inferior

Elastic modulus: A constant representing the stiffness of a material

Extension: The act of straightening a joint

Femur: The thigh bone, the bone of the upper leg

Flexion: The act of bending a joint

Hemipelvis: One half of the whole pelvis, without the sacrum

Joint force: The forces that exist between the articular surfaces of a joint. Joint forces arise as a result of muscle, gravity and inertial forces.

Inferior: The lower end of the body

Intact models: Models of the hemipelvis in the "physiologic" state

In vivo: In the living body

Lateral: Away from the midline of the body

Lateral rotation: Movement of a body part away from the median axis of the body

Medial: Towards the midline of the body

Medial rotation: Movement of a body part towards the median axis of the body

Necrosis: The death of cells or tissue

Normal: Perpendicular to

Orthopaedics: The medical field concerned with the skeletal system

Posterior: The rear side of the body

Prosthesis: A device that replaces a portion of the body

Proximal: Nearer the trunk; synonymous with superior

Reaming: The surgical procedure whereby the acetabulum and surrounding bone is cleared away to accommodate the prosthesis

Rigid body motion: The translation or rotation of the body as a whole.

Sagittal plane: A vertical plane through the body in an antero-posterior direction

Strain: Deformation produced in a solid as a result of stress

Stress: A measurement of the force acting on a unit area of a body

Superior: The top of the body

THA models: Models of the hemipelvis after implantation of an artificial cup

Transverse plane: A horizontal plane through the body

CHAPTER 1
INTRODUCTION

Total Hip Arthroplasty (THA) is regarded as being the most successful procedure in the management of the severe osteo- or rheumatoid- arthritic hip that exists today. These degenerative bone diseases result in extreme discomfort for the sufferer, and THA offers a good solution in terms of pain relief and increased mobility for the patient. As a result, improved quality of life is the ultimate attraction of this procedure.

Sir John Charnley revolutionised the field of hip replacement when he introduced his principle of low-friction arthroplasty in 1961. The principles of this technique are: (1) the use of a smaller diameter prosthetic femoral head for the reduction of torsional forces at the artificial joint surface; and (2) reconstruction of the hip in order to change the moments of forces about the joint, thereby reducing the total load on the joint (Charnley, 1970). Charnley also introduced the use of the selfcuring acrylic cement polymethylmethacrylate to achieve both initial and long-term fixation of the prosthesis to bone (Charnley, 1960, 1970; Morscher, 1989).

However, long-term clinical results have indicated that problems do exist with the procedure as implemented today, which results in failure of THA's in a percentage of patients. Failure may be due to several causes including (i) biological e.g. infection, (ii) technical e.g. poor cementing technique, poor placement of the prosthesis and (iii) mechanical failure, which usually presents as loosening or migration of the components (Hungerford and Jones, 1988; Petty *et al*, 1980). Of these factors, the most common cause of late failure in THA is aseptic loosening of the prosthetic component(s) (Amstutz *et al*, 1982; Apel *et al*, 1989; Dorr *et al*, 1983; Engh *et al*, 1988; Harris and Penenberg, 1987; Hungerford and Jones, 1988; Mehlhoff and Sledge, 1990; Moreland *et al*, 1980;

Morscher *et al*, 1989; Morscher, 1989; Petty *et al*, 1980). It should be noted, however, that poor surgical technique is probably largely accountable for the short- and medium-term occurrences of loosening. This is reflected in the fact that the best and the worst results ten years after the primary operation differ by a factor of twenty (Ling, 1986).

The primary site at which aseptic loosening of the cemented THA's occurs has been identified as the cement/bone interface (Hungerford and Jones, 1988; Morscher, 1989; Mehlhoff and Sledge, 1990). Loosening of the femoral component occurs relatively early and has therefore been studied extensively (Svensson *et al*, 1977; Jacob *et al*, 1978; Amstutz *et al*, 1976). Aseptic loosening of the acetabular component (cup) is relatively rare during the first six to eight years but tends to increase exponentially after the eighth to tenth post-operative year (Carlsson, 1981; Maistrelli *et al*, 1986; Morscher *et al*, 1989; Rapperport *et al*, 1987). The identification of this aseptic loosening led to research into alternative methods of ensuring improved cup fixation. This process has resulted in a return to the first attempts at hip arthroplasty: the use of cementless cups.

Cementless fixation of acetabular cups can be achieved by press-fit, bony ingrowth and screw-threaded methods. Each of these cementless concepts incorporates different types of initial fixation techniques. The aim of cementless arthroplasty is to provide similarly successful initial fixation to that found in cemented cups while at the same time improving the longevity of the implant.

Unfortunately, the literature reports controversial clinical and biomechanical results for the different cementless cups in use today. As a result, these provide the surgeon with an informed choice for or against usually only one specific type of fixation method, with different reports emphasising the favourability of different cups. This in turn may lead to a situation where market-related factors may have more influence on the surgeon's choice of cup than the available (conflicting) information. It is therefore important that comparative biomechanical studies are undertaken in an attempt to address some of these issues.

The aims of this study are four-fold. The first objective is to investigate, by means of two-dimensional plane strain finite element models, the effect of cup orientation on the pelvic bone stresses. Other analysis variables are the assumed cup/bone interface conditions, representing different post-operative states, and the materials used for the metal backing of the cup.

Since it is acknowledged that a two-dimensional biomechanical analysis of the hemipelvis is crude when considering its complex geometry, and that a full three-dimensional model of the bone is required, the second aim of the thesis is to develop such a model. The boundary and loading conditions on the bone are modelled by an extremely complicated set of constraints, and are analysed in this study in order to provide a good working model of the hemipelvis' behaviour in the single-legged stance phase of gait.

The third objective is the analysis of the strain-related adaptive bone remodelling process that takes place in the three-dimensional hemipelvis. This consists of an investigation of the bone density distribution in the hemipelvis, by means of an existing algorithm which simulates this remodelling process.

The final aim of this thesis is to develop a method of numerically simulating the implantation of acetabular cups in three-dimensional models. By combining all of the three-dimensional modelling features into one comprehensive model of the hemipelvis will ultimately provide a powerful tool for analysing the bone stresses following THA. The capability to model design characteristics of the implanted acetabular component suggests that the abnormal stress distribution in the acetabular region after THA - when compared to an intact hip - could be improved by altering these design features. Such improvements may diminish the incidence of long-term acetabular component loosening, migration and failure.

CHAPTER 2
LITERATURE REVIEW AND RELEVANT BACKGROUND

2.1. ANATOMY

Basic knowledge of the gross musculoskeletal anatomy, the structure of bone and the biomechanics of the hip joint is required to understand the "philosophy" and principles of Total Hip Arthroplasty (THA). This and the following section describe these aspects of the human hemipelvis.

2.1.1. Anatomy of the hip joint

Figure 2.1 shows a cross-sectional view of the hip joint in the coronal plane. The hip joint is a ball-and-socket, multiaxial self-centering joint connecting the trunk to the lower extremities. It is formed by the articulation of the femoral head with the cup-shaped fossa

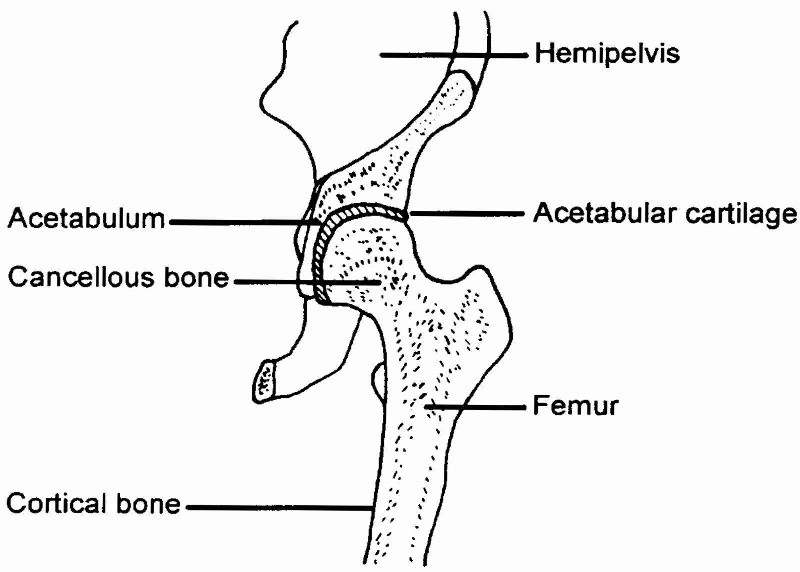

Figure 2.1: Cross-sectional view of the hip joint. (Adapted from Spirakis, 1988)

of the acetabulum. The articular surfaces are more spheroid than spherical, approximately congruent and covered with hyaline cartilage.

The mechanical demands on the hip joint are severe. The joint should therefore possess maximum stability, whilst achieving maximum mobility. The joint's stability derives largely from the shapes of the femoral head and the deep acetabular fossa, the strong ligaments and the capsule holding the femur and pelvis together. At the same time, the joint "enjoys" a large range of movement, limited only by the above stabilising structures.

Figures 2.2 and 2.3 show the main bony landmarks on the pelvis and femur, and the areas of attachment of the six muscles included in this study. The landmarks are useful when describing the position of the bones and the points of attachment of the muscles to them. The understanding of the hip muscles' functions, as described below, can be facilitated by referring to these diagrams for the origin and insertion points of the muscles.

The most important muscles which act around the hip joint, moving the thigh, are most conveniently grouped according to their function: flexion, extension, abduction and adduction. Some of the muscles that fall within these four groups also provide a further function, that of lateral or medial rotation. It would have been beyond the purpose of this review to describe in detail all these different muscles and functions. Only aspects essential to this study are therefore described.

Flexion of the thigh is brought about by iliopsoas (iliacus and psoas major muscles) and rectus femoris. The opposite action, extension, is performed by the massive gluteus maximus muscle. The most important group of muscles for support when standing on one leg (hereafter single-legged stance) are the abductor muscles. These include gluteus medius and minimus, tensor fasciae latae and the anterior fibres of gluteus maximus. The tensor fasciae latae is a muscle which exerts a "pull" on the deep fascia (fascia lata) of the thigh via a thickening on its lateral aspect termed the iliotibial tract. Finally, adduction of the thigh is performed by the adductor group: adductor brevis, longus and magnus.

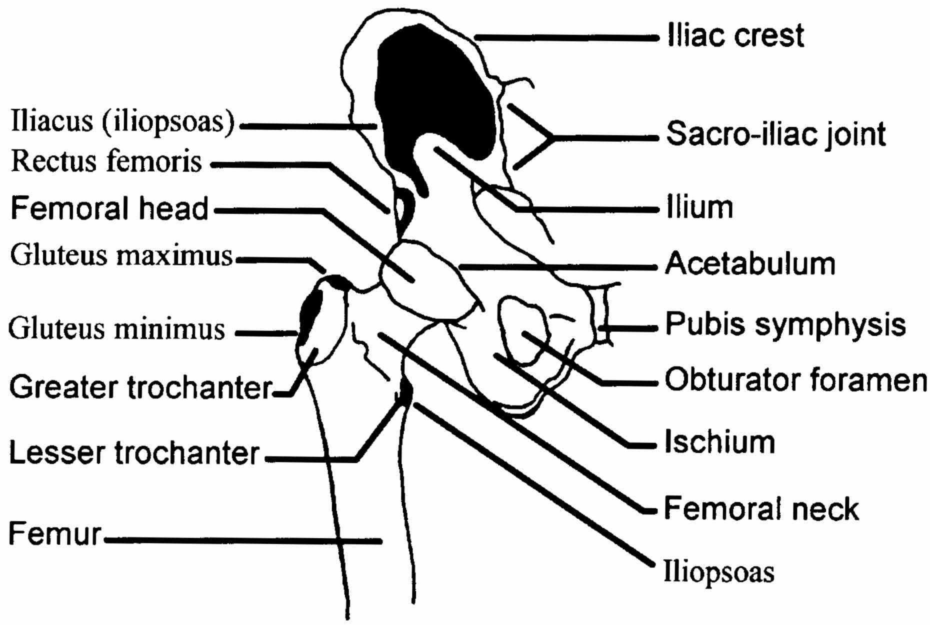

Figure 2.2: Anterior view of the right hemipelvis and femur showing the important bony landmarks and the attachment sites of six muscles. (Adapted from Basmajian, 1981)

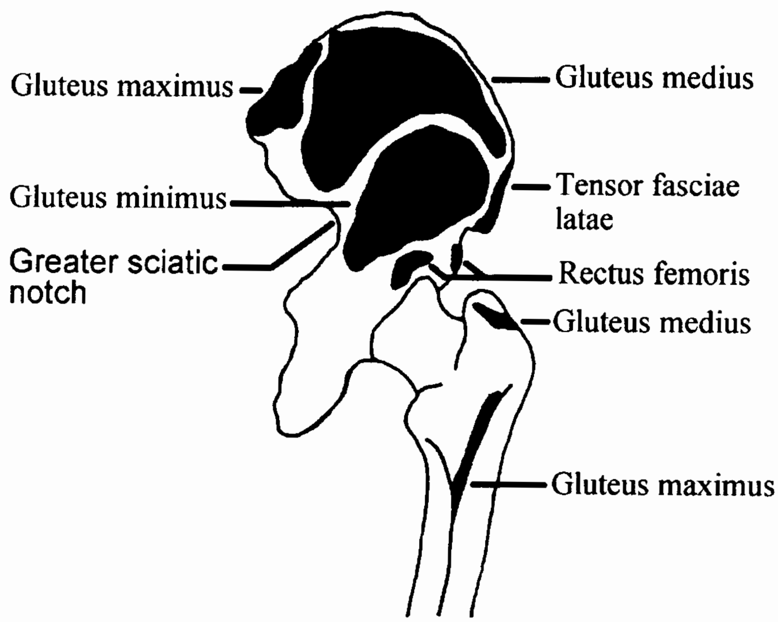

Figure 2.3: Posterior view of the right hemipelvis and femur showing the attachment sites of six important muscles. (Adapted from Basmajian, 1981)

Muscles are essentially a collection of soft-tissue fibres which, by contraction, produce movements of limbs by pulling on the skeleton. They vary considerably in size, shape and arrangement of fibres. The direction of the fibres composing a muscle is significant because of its direct link to function, while the size and shape of the whole muscle determines the amount of force that it can exert. It is necessary to investigate the actions of these muscles around the hip joint more accurately in order to understand the forces that act upon it. This field of investigation is known as functional anatomy/biomechanics, and is discussed in Section 2.2.

2.1.2. The structure and function of bone

Bone is the primary structural element of the human body. It is unique among structural materials in that it is self-repairing and can alter its properties and configuration in response to changes in mechanical demand (Woo *et al*, 1981). Morphologically, bone tissue is organised in two ways. It is composed of an outer shell of hard, compact substance called cortical bone. This encloses the spongy substance which consists of delicate bone trabeculae, and is hence called trabecular (or cancellous) bone. The major physical difference between cancellous and cortical bone is the increased porosity of the cancellous bone.

The jointed levers that ensure mobility of the body consist essentially of muscles and ligaments (the tension members) acting on a bony framework (the compression members). The articular surfaces of joints, such as the hip, are smooth and normally covered by a thin adherent layer of smooth, well-lubricated articular cartilage. The articular cartilage is bonded to its subjacent bone at a region called the subchondral plate. This subchondral bone is less spongy than the cancellous bone, yet not as compact and stiff as the cortical bone. It is supported by bony trabeculae which meet it at approximately right angles. On loading the subchondral bone transmits the stresses first to the cancellous bone and then to the cortical bone.

The material properties of cortical bone are dependant on the rate at which the bone is loaded. Bone is a visco-elastic, or time-dependant, material. This means that the stress-strain characteristics and strength properties are dependant upon the applied strain rate. The stress-strain behaviour of cortical bone is also very dependant upon the orientation of its microstructure with respect to the direction of loading. Such materials are said to be anisotropic materials.

Bone has a remarkable characteristic of constantly regenerating and resorbing itself throughout life. This process is called bone remodelling, and is involved in bone development, growth and repair. The process of bone remodelling includes both the external geometry changes and the internal property changes that result from local cellular activity (Hart *et al*, 1984). New bone is laid down by special cells called osteoblasts, while bone is resorbed by multi-nucleate cells called osteoclasts. Remodelling of articular cartilage and bone tissue can be provoked in two ways: a change of the cartilage and bony matrix may occur because of alterations in the loading conditions of the joint, and changes in structural and mechanical properties may be caused by alterations in the biochemical composition. Thus the remodelling characteristics of bone can determine the success or failure of total joint replacements.

The remodelling process is sustained in response to the mechanical demands made upon it throughout the first forty or fifty years of life. The mechanical loading provides a continuous stimulus and the remodelling process continues. However, as an individual ages, the process proceeds at a slower rate. Further aspects of strain-related bone remodelling will be discussed in more detail in Chapter 4 and Appendix B.

2.2. BIOMECHANICS OF THE HIP JOINT

Biomechanical analyses of the hip joint have been performed using methods such as strain gauge measurement, force plate measurement, electromyographic (EMG) studies and mathematical models. Often the force plate and EMG data is used as input to a mathematical model of the hip joint. The mathematical studies are often limited to analysing the forces acting around the hip joint in two dimensions, usually in the coronal plane (Koch, 1917; Inman, 1947; Johnston and Larson, 1969; Maistrelli *et al*, 1986; Noble *et al*, 1987).

Figure 2.4(a) shows a simplified anatomical model of the two-dimensional forces around the hip joint for normal stance. The weight W can be conveniently represented by a vertical vector through the body's centre of gravity. A system of forces is established across the hip joint that balances this downward gravitational force.

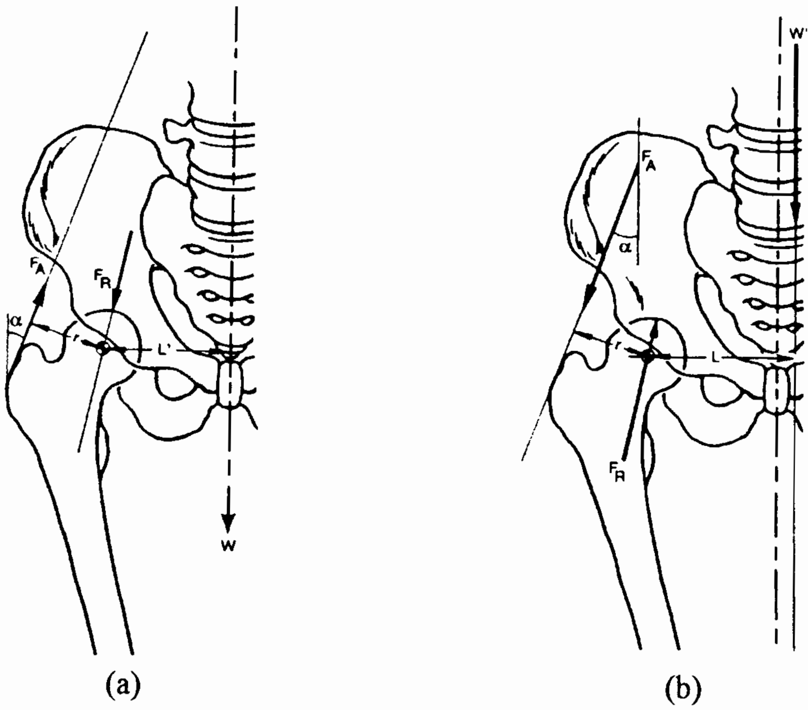

Figure 2.4: Major forces acting on the hip joint. a) Normal (two-legged) stance; b) Single-legged stance. W = weight, F_A = total abductor muscle force, F_R = hip joint resultant reaction force, α = angle at which abductor muscles act, W' = body weight in single-legged stance ≅ 5/6 W, L & r = body weight and abductor muscles lever arms respectively. (Adapted from Noble *et al*, 1987)

For the case of the single-legged stance (Figure 2.4(b)) the body's centre of gravity is shifted away from the supporting leg. This shift is due to the weight of the suspended leg, which has the effect of moving the centre of gravity towards itself. W' represents the weight of the body proximal to the hip joint and is approximately five sixths of the total body weight.

In both cases, equilibrium is reached when the leverage of the abductor force equals that of the body weight acting around the hip joint fulcrum. The hip joint fulcrum is the centre of the femoral head. For the single-legged stance, this balance is expressed mathematically by the following equation:

$$F_A * r = W' * L = \frac{5}{6} W * L$$

where r is the minimum distance from the abductor force to the centre of the femoral head and L is the distance from body weight line of action to the centre of the femoral head. Rearranging the above equation to solve for F_A, we obtain

$$F = \frac{5}{6} W * \left(\frac{L}{r} \right)$$

Thus the magnitude of the abductor force necessary to maintain hip stability is proportional to the ratio between L and r.

The joint reaction force (F_R) acting through the hip joint fulcrum can be calculated from its vertical and horizontal components, namely F_{RV} and F_{RH} :

$$F_{RV} = W' + F_A \cos\alpha = \frac{5}{6} W + F_A \cos\alpha$$

$$F_{RH} = F_A \sin\alpha$$

The resultant reaction force F_R can therefore be calculated as follows:

$$F_A = \sqrt{(F_{RV}{}^2 + F_{RH}{}^2)} = \sqrt{\left[F_A{}^2 \sin^2\alpha + \left(\frac{5}{6}W + F_A\cos\alpha\right)^2\right]}.$$

For typical values of the angle α (20°- 22°), the total hip joint force in single-legged stance is approximately twice the body weight (Maistrelli *et al*, 1986; Noble *et al*, 1987).

Rydell (1966), in a strain gauge study of the femoral head prosthesis, found the resultant hip reaction force to be 3.3 times the body weight. This value was confirmed by Williams and Svensson (1968), who found the hip reaction force to be 3.43 times body weight. McLeish and Charnley (1970), in their 2D force analysis, found that this reaction force ranged from 1.8 to 2.7 times body weight, as the pelvis moved from an elevated to a "sagging" position relative to the supporting leg. Crowninshield *et al* (1978), in their landmark investigation of the biomechanics of the hip joint, reported the hip resultant force components over the entire gait cycle. This results in a resultant hip reaction force, acting in the coronal plane, with a magnitude of approximately 3.6 times body weight, at an angle of 15° to the vertical. An almost identical result can be determined from the gait cycle analysis reported by Johnston *et al* (1979).

The muscles of interest in this study are primarily the abductor group. Crowninshield *et al* (1978) depicted the muscular activity of 16 muscles over the gait cycle, thus providing us with a very good understanding of the phasic behaviour of these different muscles. Jacob *et al* (1976) reported the forces in gluteus medius, gluteus minimus and tensor fasciae latae as being 500N, 330N and 155 N respectively. Goel *et al* (1978), in their 3D stress analysis of the pelvis, used muscle forces based on the work done by Williams and Svensson (1968). They reported that the muscle forces for the abovementioned muscles are 640N, 320N and 290N respectively. The iliopsoas muscle and rectus femoris muscles were assigned forces of 135N and 580 N respectively. All the above muscle force analyses have assumed that the line of action of a muscle is a straight line from the origin to the insertion point. This admittedly simplified approach is taken in preference to the more complex centroid method, which proposes that the line of action of a muscle passes through the centroid of the muscle cross-section at each point (Dostal & Andrews, 1981).

2.3. TOTAL HIP ARTHROPLASTY (THA)

2.3.1. Background

Osteoarthritis, or pathological degeneration of the bone matrix, has affected man since earliest times. In the 19th century this form of arthritis was differentiated from others, prior to which it was thought of as being a variant of rheumatism. Osteoarthritis is generally the most common reason for performing THA today. The primary indication for a THA is the situation where both the acetabulum and the femoral head are involved in this degenerative process. Other indications include rheumatoid arthritis, ankylosing spondylitis, protrusio acetabulae, aseptic necrosis and general hip dysplasiae (McKee, 1970). THA offers pain relief, improved hip function and good overall patient satisfaction.

2.3.2. Principles of THA

Figure 2.5 illustrates the main components of the THA, and their relationship with the surrounding bones. Total hip replacements are similar to the ball-and-socket arrangement of the natural hip joint. The acetabular cup functions as a medium through which the hip reaction force is transmitted to the pelvic bone. The articulating surface of the cup is usually manufactured from Ultra-High-Molecular-Weight Polyethylene (UHMWPE), due to its excellent friction and wear properties in contact with the common orthopaedic metal-alloys. Because of this polymer's flexibility, the cup sometimes has a relatively thin metal layer on the surface that comes into contact with bone in an attempt to distribute the stresses across the cup/bone interface more evenly. The femoral component of the total

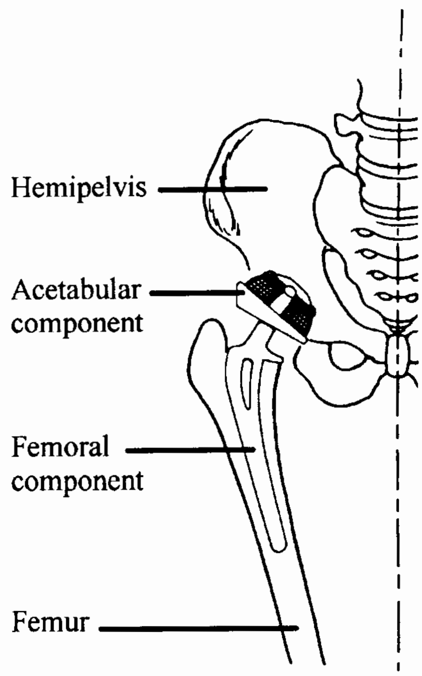

Figure 2.5: Components of THA and their relationship with the surrounding bone. (Adapted from Noble *et al*, 1987)

hip replacement is an intramedullary device since its stem is inserted into the medullary canal of the femur. The artificial femoral head is highly polished and congruent with the shape of the acetabular cup. The materials used are usually stainless steel (316L medical grade) and Cobalt-Chrome-Molybdenum alloy. The articulation of these metallic femoral heads give the best frictional behaviour at their interface with the polyethylene cup.

Two main principles lie behind the rationale to hip arthroplasty: the use of a relatively small prosthetic head and reconstruction of the hip. The use of a small femoral head has the effect of reducing the frictional torque on the acetabular cup, and ensures that the frictional moment transferred from the femoral head, tending to turn the socket, is much less than the frictional moment tending to hold the socket motionless in the acetabulum. Since the outer diameter of the acetabular cup is limited to the hemispherical shape of the acetabulum, another advantage of the small diameter femoral head is the ability to use an acetabular cup with a thicker wall. The Charnley prosthetic head has a diameter of 22 mm (the smallest that can be used to avoid dislocation) which means that it is possible to have an acetabular cup wall thickness of approximately 10 mm. This arrangement is known to substantially reduce the polyethylene wear that takes place, and for the increased energy absorption capability of the thicker cup relative to a thinner one.

During the total hip arthroplasty operation, it is possible to arrange the moments of forces acting on the hip joint in order to reduce the resultant force on the artificial joint by as much as 30%. This emphasises the fact that this operation is ideally a total hip reconstruction rather than a replacement of a hip, since the moment levers might be seriously affected by the preoperative condition (Charnley, 1970).

2.3.3. Fixation methods of acetabular cups

Fixation of acetabular cups is dominated by difficulties associated with attaining durable fixation within the acetabular floor while preserving bone stock (Eftekhar and Pawluk, 1980). In general, the types of fixation methods used are either cemented or cementless.

Cemented cup arthroplasty makes use of an acrylic bone cement (polymethylmethacrylate) to achieve fixation of the acetabular cup to the bone. This is a self-curing cement which releases heat (up to 90^{O} Celsius) during the polymerisation process. After reaming the surface of the acetabulum until good bone stock is reached, and drilling strategic holes into the bone, the cement is packed into the acetabulum. Placement of the cement into the acetabulum under pressure is advocated as being advantageous regarding the longevity of the THA (Ling, 1986). The thickness of this cement mantle is a crucial factor towards ensuring good post-operative results. Carter *et al* (1982) have shown that for acetabular components without a metal backing, a thicker cement mantle leads to lower stresses within the mantle and surrounding bone.

The cup is then pressed into the cement and correctly orientated. Sutherland *et al* (1982) reported a greater incidence of aseptic loosening of those cups which protruded beyond the cover of the superior margin of the acetabulum. Since the difference between the angle that the acetabulum and the artificial cup make to the horizontal in the coronal plane is between 5 and 30 degrees, some cup design features do reflect this disparity by having an additional flange on the superior lip. Alternatively, the cup profile is reduced so that less subchondral bone needs to be reamed and the cup can be orientated at the correct angle without superior protrusion occurring.

The decision as to whether total hip arthroplasty is indicated is complicated by the fact that there are problems associated with the use of cemented cups. Cement ages, is prone to fatigue failure and does lead to tissue necrosis in the immediate vicinity, as a result of the abnormally high temperatures generated during the polymerisation process. "Cement disease", where microfragments of the cement break off leading to granulomata formation, is another problem found with the use of cement. The weakest point of the cup/cement/bone continuum is the cement/bone interface, with the cement itself being prone to premature failure. These factors initiated intensive research into cementless cups, with a view to improving the long-term fixation achieved by the cemented cups.

The cementless approach to cup arthroplasty has encompassed many different designs aimed at providing good initial and long-term fixation of the cup. Since cementless cups were recently introduced it is too early to come to a conclusion about the achievement of these proposed goals. As a result, the use of cementless or cemented cups is still a contentious issue today. The clinical results of cementless cups cannot be generalised because the designs fall into one of three groups: press-fit, bony in- or on-growth and screw-threaded types. Clinical results for both the cemented and the three types of cementless cups are discussed in the following section.

2.4. CLINICAL RESULTS OF CUP ARTHROPLASTY

2.4.1. Cemented cups

In a 4 to 7 year follow-up of 333 cemented THA's, Beckenbaugh and Ilstrup (1978) reported a 91.7% success rate. Charnley and Cupic (1973) and Stauffer (1982) reported 90.4% and 88.7% success rate respectively in their 10 year follow-up of cemented THA's. Garvin *et al* (1991), in a 14 year follow-up of cemented total hip arthroplasties, reported that the total failure rate for the acetabular component was 17 %. They also reported isolated non-progressive radiolucencies of under 1 mm in a few cases. These good figures may be misleading since the reported radiographic evidence of loosening viz. progressive/continuous radiolucent lines at the cement/bone interface, could suggest an impending failure of the implant despite clinical success of the THA. DeLee & Charnley (1976) indicate a 69.5% radiographic lucency in their ten-year follow-up study, while Salvati *et al* (1976), Beckenbaugh & Ilstrup (1978) and Cotterill *et al* (1982) reported 93%, 99% and 95% radiographic lucencies respectively. This evidently conflicting information is almost certainly the result of a lack of a standardised definition of success/failure of an implant, and the lack of definition as to what actually comprises loosening/migration (Brand *et al*, 1986; Harris and White, 1982; Knahr *et al*, 1987; Mjö-berg, 1986; Rothman and Cohn, 1990; Callaghan, 1990).

Patient age is an important factor regarding the incidence of cemented component loosening/migration. In a study by Harris *et al* (1983) all (100%) ten patients who were 30 years or younger at the primary operation showed migration or required revision 10 years later, whereas 7 out of 38 patients (17.5%) older than 30 years showed migration or required revision arthroplasty. Even the latter figure is unacceptably high. Chandler *et al* (1981) reported a 57% incidence of actual or potential loosening of at least one component of the prosthesis after 5 years, with the acetabular component loosening twice as frequently as the femoral (45% compared to 21%). Dorr *et al* (1983), in their study of patients less than

45 years old, reported a similar trend in those patients under the age of 30. These poor results of cemented THA in younger patients is also evidenced in research performed by Halley & Wroblewski (1986) reported a slightly better failure rate with the Charnley prosthesis in their follow-up of 49 patients under the age of 30. The follow-up time averaged 10 years, with a failure rate of 7 %.

Dobbs (1980) went one step further by reporting that mechanical loosening is the predominant reason for failure and that the annual rate of revisions for loosening in his study increased as the follow-up time increased. Similar exponential loosening rates have been reported by Sutherland *et al* (1982), Morscher & Schmassmann (1983) and Morscher (1989).

A major consequence of failure of a cemented prosthesis is minor to massive bone loss surrounding the implant (Engh *et al*, 1988; Hungerford and Jones, 1988). Also, the risk of sepsis and the further bone loss that occur at revision of a failed cemented acetabular component often results in less than optimal fixation of the secondary THA.

It is clear that the use of bone cement entails a number of drawbacks regarding the long-term fixation of the implant. As a result, many researchers have taken to investigating the use of noncemented acetabular components for use in THA. Since primary stability is the most important prerequisite for permanent implant fixation, the absence of bone cement as a stabilising factor therefore demands that the cementless technique will ensure that this initial stability is achieved (Morscher, 1989). The different types of cementless fixation techniques are described below.

2.4.2. Cementless cups

The types of cementless cups that are being / have been investigated and researched are varied, but the rationale behind their design can be classified essentially into three distinct groups: press-fit, bony ingrowth and screw-threaded. Most cementless cups today incorporate two of these fixation principles.

Press-fit cup

The press-fit cup is hemispherical with a number of pegs or fins which provide it with anti-rotational stability. Generally, shallow grooves in its surface are included in the hope of achieving bony ongrowth. Initial fixation is usually achieved by the use of screws through the implant into the surrounding bone, which have the effect of providing the compression necessary for stability and bony ongrowth.

Short term follow-ups of the press-fit cups reported good results. Morscher & Masar (1988), in an initial study of 81 operations performed over 21 months, reported good bone ingrowth and no visible migration of the acetabular component after an average of 16 months follow-up time. A longer, extended follow-up (330 patients), by Morscher *et al* (1989) for the same implantation period indicated that 85.2 % of the components exhibited complete bone ingrowth, while 2.4 % of the implants had migrated.

Bertin *et al* (1985), in a study of 1878 operations, reported no loosening and no migration in all (100 %) of the cases. They reported on an average follow-up time of 24 months, which ranged from 6 to 72 months. This group suggested that migration of the component greater than 5 mm constituted loosening.

The excellent results above are contradicted by a study by Knahr *et al* (1987) of uncemented ceramic acetabular cups. They report a loosening/migration occurrence of 13 % in a study of 67 operations after an average period of 89 months (a range of 72 to 118 months). Using migration of more than 2 mm, followed by a surrounding lucency, as an indication of loosening, a study of 445 cementless THA's by Wilson-MacDonald *et al* (1990) indicated that 9 % of the implants were loose after 7 years. The loosening rate increased to 17 % after 8 years and 28 % after 9 years. They concluded their report by stating that their group has abandoned the use of this prosthesis.

Consensus has not been achieved on the loosening of acetabular components. Migration greater than 2 mm followed by a surrounding lucency might be a good definition, as proposed by Wilson-MacDonald *et al* in 1990. Bertin *et al*'s (1985) suggestion that migration greater than 5 mm constituted loosening gives an indication of why reports on the this problem do vary to such an extent. Another general problem experienced by most researchers undertaking to radiographically determine the extent of loosening of the acetabular components using radiographs is the lack of a radiodense line around the cup (Bobyn *et al*, 1988; Engh *et al*, 1990; Shaw *et al*, 1990). These problems both affect the accuracy of reporting of post-operative results.

Bony ingrowth cup

Like the press-fit cup, the primary fixation of this implant is achieved by means of screws through the surface of the cup into the surrounding bone. The secondary, or long-term, stability is achieved by the porous coating of the cup, which permits bony ingrowth.

Bony ingrowth can be defined as the growth of bone into pores and spaces in the implanted material. Osseointegration is a more exact term for this phenomenon, and describes the bone apposition (i.e. no intervening fibrous layer) to orthopaedic implants fabricated from different materials (Spector, 1988).

The first attempt at texturing the outer surface of the cup to achieve bone ongrowth was the Austin-Moore implant, which was followed by the Mittelmeier, the PM and the Lord prostheses (Morscher, 1989). Galante *et al* (1971) developed the principle of microporosity when he demonstrated the possibility of bony ingrowth into "fibre metal". Satisfactory bony ingrowth into microporous chrome-cobalt alloy and fibre-mesh titanium was performed by Homsy *et al* (1972) and Cameron *et al* (1976). Table 2.1 summarises some of the clinical reports on the incidence of loosening of porous-coated cups.

AUTHOR	NO OF CASES	FOLLOW-UP TIME	EVALUATION of DESIGN (based on loosening/ migration)
Silber, Engh (1990)	13	36 months average (24 - 76). Mean patient age: 45 years	No loosening
Pupparo, Engh (1991)	62 porous-threaded cups	29.5 months average (25 - 50).	No loosening/migration
Engh, *et al* (1990)	285	Mean follow-up 4.8 years, minimum of 2 years.	No loosening, one migration.
Mallory, *et al* (1988)	58 porous-threaded cups (22 primary, 36 revision)	9 months average (6 - 24).	Migration (less than 2 mm) occurred once in the primary group (4.5%); 2 migrations in revision group (5.5%).
Engh, *et al* (1988)	34 revisions	53 months average (24 - 72)	2.9 % unstable
McGann, *et al* (1988)	75 revisions	14 months average (2 - 36).	lucencies (23%), 14 < 1 mm, 3 = 1 mm. No migrations.
Davey, Harris (1989)	32	31 months average (24 - 40).	No loosening, no migration. 4 (8%) showed lucencies
Hwang, *et al* (1991)	81 PCA	Average 47 months (24 - 69)	4 (4.9 %) migrated in the first year; not progressive
Tanzer, *et al* (1992)	140 revisions	Average 41 months (24 - 76)	Migration in 2 hips (1.4 %); 92 (66 %) radiolucencies < 1 mm
Kim YK, Kim VEM (1992)	82 Harris-Galante	Average 62.1 months (60 - 66)	3 (3.7 %) radiolucencies < 1 mm; 1 superior migration
Cracchiolo, Severt, Moreland (1992)	39 (16 PCA, 14 AML, 6 Harris-Galante, 3 other)	Average 44.4 months (24 - 72)	12.8 % radiolucencies; 1 migration
Schmalzried, Harris (1992)	83 Harris-Galante	Average 68 months (60 - 84)	No migration; progressive radiolucent line in 22 hips (27 %)
Maric, Karpman (1992)	52 PCA	Average 29 months (12 - 48)	27 % radiolucencies < 1 mm; no migration

Table 2.1: Summary of porous-coated cup literature review

For bony ingrowth to occur, the design of this porous coating is all-important. Research into the optimal pore size of the porous coating has yielded a number of similar results.

According to Spector (1988), pore sizes between 140 and 350 μm are recommended for the maximum interfacial shear strength to be achieved. This range is generally confirmed by a number of reports (Bobyn *et al*, 1980; Cameron, 1982; Galante *et al*, 1971; Homsy, 1973; Homsy *et al*, 1972; Morscher, 1983; Pilliar and Bratina, 1980; Pilliar *et al*, 1986; Jasty & Harris, 1988).

The types of porous coatings found today are usually beads sintered onto the cup surface, fibre metal, plasma spray or mesh (Crowninshield, 1987). The bead material that is used has to be carefully chosen in respect of its biocompatibility, since the surface area is increased up to ten times with porous surfaces (Morscher, 1989) (release of toxic metallic ions is proportional to the surface area).

Screw-threaded cup

The main technical problem of initial stability is overcome most effectively by the use of a screw-threaded cup, since the fixation takes place over a large surface area (Bobyn *et al*, 1988; Engh *et al*, 1990; Kody *et al*, 1990; Snorrason and Kärrholm, 1990; Tooke *et al*, 1988). The threaded cup utilises torque and compression to gain purchase into the bony margin of the acetabulum. By employing a larger surface area for fixation, the joint load is dispersed over a larger portion of the pelvis (Apel *et al*, 1989).

The initial threaded designs included truncated cones, such as the Mittelmeier, and the ellipsoid used by Lord and Bancel. More recently, the screw-threaded cups feature a hemispheric shape with spheric threads. This arrangement allows for a minimal compromise of bone stock with maximal thread purchase (Mallory *et al*, 1988).

Kody *et al* (1990) found that the quality of the initial fixation in foam of screw-threaded components was dependant on their design features: those with widely spaced, deep threads, and minimal thread interruptions offered the strongest initial fixation (in foam). Cups with a wide variety of screw features are nevertheless commercially available today.

Table 2.2 presents a summary of follow-up results with the use of screw-threaded cups, as reported in the literature.

AUTHOR	NO OF CASES	FOLLOW-UP TIME	EVALUATION of DESIGN (based on loosening/ migration)
Mallory, *et al* (1988)	42 smooth-threaded cups (12 primary, 30 revision)	Follow-up time 9 months average (6 - 24).	No loosening or migration
Engh, *et al* (1988)	73 revisions for cemented failures	Follow-up time 53 months average (24 - 72)	stable, 31.5% loose
Apel, *et al* (1989)	121	Follow-up time 30 months average (22 - 49)	(3.3%) loose, 29 (24%) radiolucencies of 1-2 mm
Silber, Engh (1990)	6	Follow-up time 36 months average (24 - 76). Mean patient age: 45 years	One optimum fixation, 5 unstable: migration measured as being 4-5 mm superiorly
Engh, *et al* (1990)	130	Mean follow-up 3.9 years, minimum of 2.	(21%) unstable; 9: progressive lucencies, 18: migration
Pupparo, Engh (1991)	82 smooth-threaded cups	Follow-up time 33.3 months average (24 - 49).	(29%) unstable; 7: progressive lucencies, 9: migration 3-11 mm (mean 5.5 mm)
Shaw, *et al* (1990)	48 (25 primary, 23 revision)	Follow-up time 31.6 months average (24 - 44)	Progressive lucencies: 2 (8%) primary, 1 (4.3%) revision; loose: 1 (4%) primary, 8 (34.7%) revision
Snorrason & Kärrholm (1990)	20	Follow-up time 24 months	cups migrated a mean of 1.1 mm (0.3 - 2.5)
Wykman, *et al* (1991)	75	Follow-up time 5 years	(18.7%) revisions for mechanical loosening

Table 2.2: Summary of screw-threaded cup literature review

It is evident that these results are not at all promising. The first six studies shown in Table 2.2 report in a comparative manner results obtained with both the porous-coated and the screw-threaded cups. The results with the screw-threaded cups are relatively poor, and this explains the unpopularity of these types of cup, especially in North America. Engh *et al* (1990) concluded their comparison of screw-threaded and porous-coated cups by saying that the latter have been abandoned in favour of the former type of implant.

Attention has been drawn above to the fact that the porous-coated and the press-fit types of cups require some additional measure to ensure that primary stability occurs. While pegs and fins have also been used to provide anti-rotational stability, this initial fixation is invariably performed by the use of screws which anchor the prosthesis to the surrounding bone. However, the use of screws for primary stability has some inherent drawbacks to it.

Firstly, the intrapelvic vasculature is at risk from medially placed screws which may penetrate the acetabulum itself (Keating *et al*, 1990). More specifically, the anterior superior and anterior inferior quadrants should be avoided when possible because screws may endanger the external iliac artery and vein, as well as the obturator nerve, artery, and vein. These danger areas are shown in Figures 2.6 (a) and (b).

In addition to these risks, screw-fixed acetabular components may increase the incidence of vascular injury because of the increased use of drills into the acetabulum, in close proximity to major vessels (Kirkpatrick *et al*, 1990; Wasielewski *et al*, 1990).

Secondly, most researchers indicate that a number of screws are found to be broken after

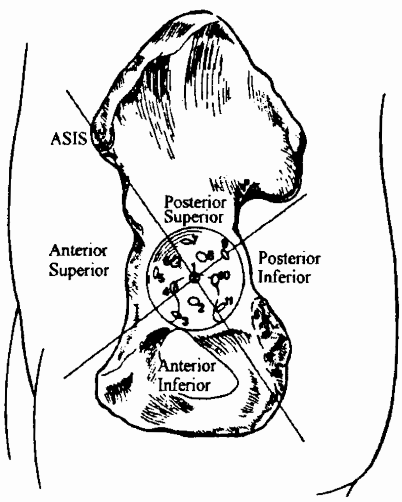

(a)

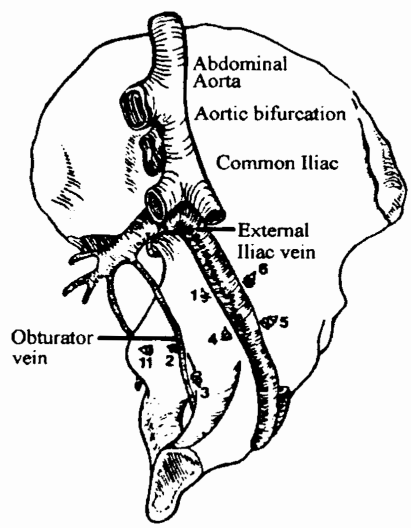

(b)

Figure 2.6: a) Schematic diagram showing the acetabular origin of screws (numbered 1 through 11); ASIS = anterior superior iliac spine. b) Schematic diagram showing the location of the screws on the quadrilateral intrapelvic superior surface relative to the iliac venous system. (Adapted from Wasielewski *et al*, 1990)

time (Andrew *et al*, 1986; Davey and Harris, 1989; Engh *et al*, 1990; Morscher *et al*, 1982; Pupparo and Engh, 1991; Wilson-MacDonald *et al* 1990) which has two note-worthy implications: the screws are not performing very well as primary fixators, and further damage and/or foreign body action might occur.

There is one further case that has not been mentioned thus far: the group of patients who do not fall into the stable or unstable categories. These patients show progressive radiolucencies at the bone/cement interface despite the absence of clinical symptoms, which raises doubts about their long-term outcome. Pellicci *et al* (1985) reported that 42% of the patients in this questionable group went on to definite failure in five years. Thus to be able to determine the effectiveness of a particular cup design a follow-up time of at least ten years is required. On this basis alone, most of the reported results described above are not an accurate indicator of the longevity of the implants. Long-term information is certainly necessary and desirable before conclusion can be reached regarding noncemented cup design.

2.5. FINITE ELEMENT ANALYSIS IN ACETABULAR REPLACEMENT

Finite Element Analysis (FEA) is one method by which stress-analysis problems can be approached. It involves the construction of a mathematical model which resembles the real object with regard to geometry, the properties of the material involved, the nature of the connections between the material and the boundaries of the model, and the loading conditions. The model is discretised into small blocks, or finite elements, connected at nodal points. After defining the boundary conditions, these separate elements are assigned material properties, and boundary nodes are provided with the appropriate loads. The finite element program then calculates the strains and stresses at integration points by solving a set of equations in matrix format. These integration point results are then extrapolated to the nodes of the elements.

Measurements on the physical structure and measurements on a model of the structure are alternative approaches. The former option is not relevant here since it would be very difficult, if not impossible, to conduct such an analysis of the human hip. There are, however, a number of methods of performing a stress analysis of the physically modelled hip. Such methods include the use of strain gauges, photoelasticity and holographic interferometry. These experimental stress analysis methods are reviewed together with FEA in Appendix A.

FEA is very well suited to an investigation of the biomechanics of the intact and replaced hip joint because of the relative ease with which variables such as material properties, interface conditions and cup geometries can be altered to analyse the effects these changes have on the resultant stress distributions.

The different types of FEA models of the acetabular region that have been developed and analysed thus far include plane strain two-dimensional (2D), axisymmetric - which is mathematically a 2D type - and pure three-dimensional (3D) types. Most models reported have been 2D, for a number of reasons. These include the ease of model development and the reduced computer time (and therefore costs) associated with such an analysis. Vasu *et al* (1982) state that they developed a 2D model because it was felt that 3D analyses are extremely time consuming and expensive while the 2D model has the advantage that a finer mesh can be economically used in the analysis. These motivations for the use of their 2D model are perhaps no longer applicable since the recent advancement of both computer hardware and software has been such to virtually eliminate these considerations.

For their 2D model, Vasu *et al* (1982) selected the section of high loading through the pelvis. This section extended in a superior-inferior direction through the centre of the acetabulum. Unfortunately, the FEA models presented in their paper appear to have been rotated out of the physiologic position, for reasons unstated and unknown. Since the loading conditions were not altered accordingly it is difficult to judge whether their results are realistic. Although the size of the cup they inserted into their model is not reported, it appears to have been inserted incorrectly: it only covers the superior portion of the acetabulum. The same section and these apparent inconsistencies are repeated in the papers by Carter *et al* (1982) and Carter *et al* (1983).

Axisymmetric FEA's of the acetabular region have been undertaken in studies by Pedersen *et al* (1982), Crowninshield *et al* (1983), Stiehl *et al* (1990) and Huiskes (1987). This type of analysis is possible since a part of the acetabular region can be regarded as being approximately symmetrical about a central axis. The axisymmetric model is a much simplified one, where the largest assumption is approximating the geometry of the surrounding hip bone as being symmetric about this central axis. Hence it is limited as to the extent of the pelvis that can be modelled, since the symmetry is only localised around the acetabulum.

Rapperport *et al* (1985) developed a 2D model of the hip, but with a different section plane to that discussed above. This section passes through the pubic bone, the acetabulum and the sacro-iliac joint on the ilium. Their model is geometrically similar to the axisymmetric model developed by Pedersen *et al* (1982). This section will be referred to in future as the *alternate 2D* model. Brown and DiGioia (1984) developed a similar model, but only of the immediate acetabular region.

Figures 2.7 (a), (b) and (c) illustrate the three different model types as used in the studies mentioned above. The loading and boundary conditions used in these models are described in Table 2.3.

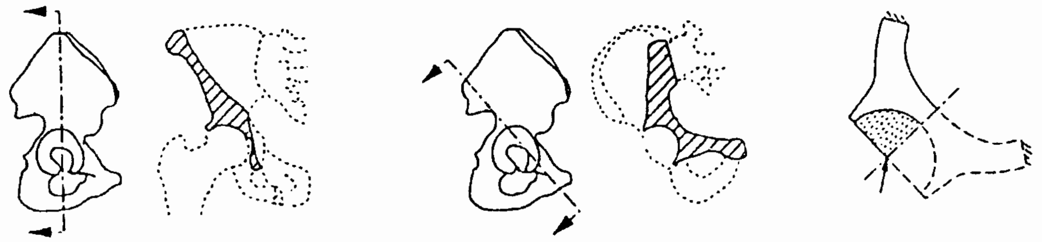

(a) (b) (c)

Figure 2.7: Diagram of three different model sections used in 2D FEA analyses of the hemipelvis. a) Section chosen by Vasu *et al* (1982), Carter *et al* (1982) and Carter *et al* (1983); b) Alternate section used by Rapperport *et al* (1985); and c) Axisymmetric model used by Pedersen *et al* (1982), Crowninshield *et al* (1983), Stiehl *et al* (1990) and Huiskes (1987). (Adapted from Hansen & Koeneman, 1991)

3D FEA models of the pelvis have been developed by Oonishi *et al* (1983), Goel *et al* (1978), Hansen & Koeneman (1991) and Dalstra & Huiskes (1990, 1992). These models, except for the last two, vary greatly in most respects; certainly the greatest differences between them lies in the degree of complexity of the final three-dimensional model and the boundary conditions imposed. Each model's specific attributes/ assumptions are presented in Table 2.4.

The use of material properties reported in the literature covers a very wide range of values, and remains a contentious issue still today. This controversy is reflected in the reviewed research papers, since most studies report the FEA models to be sensitive to material values used. This issue is underscored by research by Pedersen *et al* (1982), who state that a relative insensitivity to particular material properties exists regarding the trends of stress distribution about the acetabulum, while Vasu *et al* (1982), in their comparison of a realistic material model and a model with homogeneous properties, reported a marked change in stresses depending on the values used.

	AUTHOR	MODEL PARTICULARS	LOADING	BOUNDARY CONDITIONS
TWO DIMENSIONAL	Vasu *et al* (1982)	Four-noded isoparametric elements used throughout. Intact/THA models consisted of 393/278 elements with 437/424 nodes respectively.	Based on contact pres-sure distributions by Rushfeldt *et al* (1979), resultant load = 89.9N at 21.1^{o} to the vertical.	Fully constrained the iliac crest and the inferior rim of the acetabulum.
	Carter *et al* (1982)	Used 4-noded quadrila teral elements throughout. The most extensive model incorporated 589 elements with 825 nodes.	As above.	As above.
	Carter *et al* (1983	Used 4-node and 3-noded elements exclusively. The most extensive model incorporated 601 elements with 1012 nodes.	As above.	As above.
AXISYMMETRIC	Pedersen *et al* (1982); Crowninshield *et al* (1983)	Used 330 3-noded elements.	Resultant hip load was not quantified. Authors describe it as being conically distributed around the resultant load at 20^{o} to the vertical. Applied by means of an assumed pressure distribution to the acetabular cup.	Peripheral surface of the model is constrained.
	Huiskes (1987)	Included the femoral head in the analysis. Used 8-noded quadrilateral elements throughout.	Investigated different loading assumptions.	Constrained the medial surface of the hip model.
ALTERNATE 2D	Rapperport *et al* (1987)	Used 1313 quadrilateral and triangular elements (1198 nodes) with about 30 contact elements at the cup/ bone interface to model component loosening. Included the femoral head in the analysis.	1000N/cm applied at angles of 20^{o} and 40^{o} to the vertical. Loading applied to the node at the centre of the sphere representing the artificial femoral head, which was rigidly attached to the cup.	Pubic symphysis: free to rotate, and to displace in the sagittal plane. Sacro-iliac joint: free to displace only in the plane of the joint. Extreme margin of the iliac crest was rigidly fixed.
	Brown & DiGioia (1984)	Included the femoral head in the analysis. Used 4 and 8 noded 2D elements for the bone regions, as well as Coulomb frictional elements at the contact surface	Loading simulated by 14 incremental displacements of the acetabulum inferiorly and of the femur along the line of action of the abductor muscles.	Femur: constrained vertically at its distal (intertrochanteric) section. Pelvis: medial edge constrained horizontally.

Table 2.3: Description of 2D, axisymmetric and 'alternate' 2D models

AUTHOR	MODEL PARTICULARS	LOADING	BOUNDARY CONDITIONS
Oonishi *et al* (1983)	Membrane elements used to model the cortical bone. Cancellous region very crudely meshed (only one element deep everywhere). Total number of elements was 2251, with 930 nodes.	Loaded (assumed a proportional amount of the body weight) 25 points in the acetabulum. 28 muscle elements were applied, with loading taken from Crowninshield *et al* (1978).	Constrained the symmetrical plane of the pelvis viz. the medial edge. The femoral head and the acetabulum were constrained only in the normal direction at 25 nodal points in the acetabulum.
Goel *et al* (1978)	A very crude model, consisting of 209 solid 3D elements for the cancellous bone and 378 joint elements (similar to membrane elements) for the cortical bone, with a total of 809 nodes.	Loading included both hip reaction force and muscles, uniformly distributed over respective areas of application of the bone. Values taken from Williams & Svensson (1968)	Completely fixed the pelvis at the pubis symphysis in order to stop its rigid body motion, even though their table of forces indicates that a reaction force exists only in the medial-lateral direction. No mention made of any constraint at sacroiliac joint.
Hansen & Koeneman (1991)	Used solid elements for the cancellous bone, membrane elements for the cortical bone, interface elements for the bone-implant interface and spar elements for the muscle loading.	Loading conditions based on McLeish and Charnley's (1970) investigation of the abduction forces in single-legged stance. Application of muscle loading is not described.	Completely fixed the sacroiliac joint and the pubis symphysis.
Dalstra & Huiskes (1990, 1992)	Used 365 brick elements to model the cancellous bone and 632 membrane elements to represent the cortical bone.	Used hip reaction force of 600N; compared results with experimental. Used QCT to determine bone densities.	Completely fixed the sacroiliac joint and the pubis symphysis.
Shüller *et al* (1993)	Mesh consisted of 1260 elements of both 8-noded solid brick elements (cancellous bone) and 4-noded membrane elements (cortical bone)	Used a hip reaction force of 3 times body weight = 2158 N modelled as distributed load on prosthetic head. Included 15 muscle forces in their analysis.	Completely fixed the sacro-iliac joint and pubis symphysis.

Table 2.4: Description of 3D FEA models of the human hemipelvis

Table 2.5 describes available information from the literature on material properties used by various authors, without attempting to explain the basis of each researcher's assumptions.

It can be noted just how diverse the reported material properties are for different bony regions of the pelvis. All researchers have assumed that all of the bone in each particular region of the pelvis is linearly elastic, isotropic and homogeneous. This alone is a large assumption, since it is well known that in fact bone is both an anisotropic and non-homogeneous material.

AUTHOR	MECH. PROP.	TRABECULAR BONE	CORTICAL BONE	SUBCHONDRAL BONE	UHMWPE
Vasu *et al* (1982)	E (GPa)	0.04/0.352/1.025	6.188	-	0.5
	ν	0.18/0.22/0.247	0.326	-	0.4
Carter *et al* (1982)	E (GPa)	0.04/0.352/1.025	6.188	-	0.5
	ν	0.18/0.22/0.247	0.326	-	0.4
Carter *et al* (1983)	E (GPa)	0.04/0.352/1.025	6.188	-	0.5
	ν	0.18/0.22/0.247	0.326	-	0.4
Pedersen *et al* (1982)	E (GPa)	1/1.5/3	17	17	0.69
	ν	-	-	-	0.35
Crowninshield *et al* (1983)	E (GPa)	1/1.5/3	17	17	0.69
	ν	0.3	-	-	0.35
Huiskes (1987)	E (GPa)	1/1.5/3	17	-	0.7
	ν	-	-	-	-
Rapperport *et al* (1987)	E (GPa)	0.08/0.3/0.6	1.1	0.7	-
	ν	0.2	0.3	0.3	-
Brown & DiGioia (1984)	E (GPa)	1	6.9	6.9	-
	ν	0.3	0.25	0.25	-
Oonishi *et al* (1983)	E (GPa)	1	15	3	-
	ν	0.2	0.2	0.2	-
Goel *et al* (1978)	E (GPa)	0.3246	17.26	-	-
	ν	0.29	0.29	-	-
Hansen & Koeneman (1991)	E (GPa)	0.04/0.352/1.025	1.5	1.17	0.6
	ν	0.18/0.22/0.28	0.3	0.3	0.375

Table 2.5: Summary of bone mechanical properties used in FEA models reported in the literature. E: elastic (Young's) modulus; ν: Poisson's ratio. It should be noted that the properties for cancellous bone were assigned up to three different values in some of the studies, according to the different bone regions.

CHAPTER 3
TWO-DIMENSIONAL FEA MODELS

This chapter describes in detail the development of the model, boundary and loading conditions applied to the model and specific information regarding the FEA program features that were used. The presentation of the above information is complicated by the fact that both 2D and 3D model types have been analysed. It was therefore decided to present and discuss each model type separately.

3.1. MODEL DEVELOPMENT

A number of dry hemipelves were examined for any gross abnormalities or signs of osteoporosis at the Department of Anatomy at the University of Cape Town's Medical School. The best one of those inspected was used for the FEA model development.

After consultation with technicians in the Department of Radiology at Groote Schuur Hospital, it was decided that the most accurate mapping of the hemipelvis would result if it was first cast into a resin block and then scanned. Computer Tomographic (CT) scanning would be the scanning method used. This method was chosen for the mapping of the hemipelvis because of its greater accuracy over other reported methods. Alternatives would have been to simply place the dry hemipelvis on the CT scanning table, or to immerse it in a container of water. The former option would have resulted in artifacts around the surface of the bone, which would have made the final mapping of the surface extremely difficult and possibly inaccurate. The latter option was avoided because it was not known what effect the water would have on the image obtained; recent CT scanning of the tibia under these conditions appeared to be perfectly adequate, and at least as accurate as the cast resin approach.

A rectangular box was constructed, with dimensions which ensured that a two centimetre border was left around the extreme points on the bone, when placed in the optimal scanning position. Polyester resin was used for the casting process, as was recommended by specialists in the field.

The casting process is a difficult and sensitive one, especially with a geometry as complex as the hemipelvis. For example, air can become trapped in the acetabulum if it is face down when being cast. Also, the curing process is a relatively strong exothermic one. It is controlled essentially by the amount of catalyst used for hardening the resin. Too much catalyst accelerates the curing to such an extent that the resin warps, and cracks develop down specific propagation planes. However, the use of a large amount of catalyst can be advantageous, since this results in an extremely clear cast. Too little catalyst results in an opaque cast, and seems to remain rather sticky days after the cast is made. Fortunately, because the opaqueness of the cast does not affect the outcome of the CT scanning, the amount of catalyst was decreased so that warping and cracking did not occur.

The resin block was cast by layers, each about 15 mm high. The heat generated while curing limited the height of these layers: too great a heat would warp the block and crack the resin. Mixing of the resin and the catalyst resulted in a large amount of air bubbles being trapped within the mixture. This was exacerbated by the pouring of the resin mixture into the moulding block. To remove the air bubbles, the wooden block, complete with hemipelvis and resin, were placed in a vacuum chamber for about 5 minutes, or until all the bubbles had been removed. Curing time was about 12 hours, after which the next layer could be cast.

The CT scanning of the hemipelvis was a relatively simple procedure for the 2D models that were developed, since only one section through it was required. A single CT scan was made of the hemipelvis, in a vertical coronal plane through the centre of the acetabulum. This is similar to the approach taken by Vasu *et al* (1982), Carter *et al* (1982) and Carter *et al* (1983). The two-dimensional section that results from this CT scan corresponds to the superior-inferior plane of high loading in the hemipelvis.

The outline of this 2D cross-section was digitised, in the physiologic position (Figure 3.1). This was performed using a Summagraphics SummaSketch II digitiser (Summagraphics, 1989) linked to an IBM-compatible PC running AutoCAD Release 11 (Autodesk, 1990). The *drawing* file that resulted consisted of approximately 400 digitised points connected by two polylines. A polyline is an AutoCAD drawing entity which joins many points by means of a continuous line. One polyline described the outer surface of the cortical bone, while the other represented the division between the two types of bone.

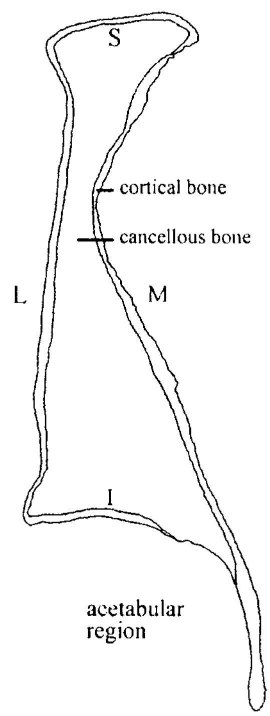

Figure 3.1: Digitised cross-section of the right hemipelvis. Anatomical orientation of the section is as follows: S - superior; I - inferior; L - lateral; and M - medial.

The AutoCAD *drawing* file was then converted into DXF format, using an option within the AutoCAD program itself. DXF is a neutral, ASCII format that links otherwise incompatible CAD and graphics systems. A TruBASIC program was written that read the DXF-translated AutoCAD file and converted it to an *input* format for the graphics package, PATRAN (PDA Engineering, 1992). PATRAN Release 3.2, a general-purpose 3-D interactive graphics pre- and post-processor, reads the *input* file containing the grid points, as if they had been generated within PATRAN itself. This circuitous method was used to overcome problems experienced in interfacing AutoCAD and PATRAN directly.

From these grid points the finite element model was generated, for the finite element analysis code ABAQUS Version 5.2 (Hibbitt, Karlsson & Sorensen, 1992). PATRAN provides the user with a variety of options with which to create FEA meshes. Grid points are joined to form lines, which can themselves be meshed (for the creation of truss or beam elements). Lines can be combined to form virtually any 2D shape, which are called patches. The simplest of these are triangular or quadrilateral patches. In general, the 2D models used quadrilateral patches, often with curved edges.

The patches for the complete 2D model were then meshed. PATRAN offers three options by which to do this: by forcing all the elements in a patch to have approximately the same user-defined size; by fitting a user-defined number of elements to each edge of the patch (this is useful for transition meshes); and by making the lengths of the sides of the elements approximately equal to a user-defined amount. The first two methods were used exclusively in the development of the models. Triangular elements were avoided as much as possible because of their known greater stiffness relative to quadrilateral elements. ABAQUS plane strain 4-noded quadrilateral elements (type CPE4) were used extensively throughout the models.

A PATRAN *neutral* file was generated for each model, from which the ABAQUS input deck was created, using the PATRAN-ABAQUS interfacer, PATABA (PDA Engineering, 1992). PATABA Release 3.1 translates the information regarding the FEA models from the *neutral* format into the standard ABAQUS input deck format. The number of elements varied according to the interface conditions imposed on each model, and on the angle at which the cup was implanted. The minimum number of elements was 685, and the maximum was 803. The number of nodes used ranged between 738 and 867. The cortical bone was two elements "thick" in all the models in order to obtain more accurate "through-thickness" stress variations. All analyses were performed using the ABAQUS Release 5.2 FEA code running on an IBM RISC/6000 Model 560 main-frame computer at the CERECAM unit at the University of Cape Town.

The aims of the 2D analyses were to investigate a number of features of THA. Four different FEA meshes were developed in order to determine the effects of the following:

- Surgical technique: cementless placement of cups at 30, 45 and 60 degrees vertical orientation
- Different biomaterials (Titanium alloy and Cobalt-Chrome alloy) used
- Two cup/bone interface conditions (bonded and unbonded) simulating different post-operative states.

All of the THA models simulated the use of the same uncemented porous ingrowth cup, the dimensions of which were based on a commercially available implant (PCA), without the pegs. The cup had an inner (artificial femoral head) diameter of 32 mm, and an external diameter of 55 mm. The two eccentric pegs on the standard PCA cup were not included since they are out of the plane of these models. The four FEA meshes are shown in Figure 3.2.

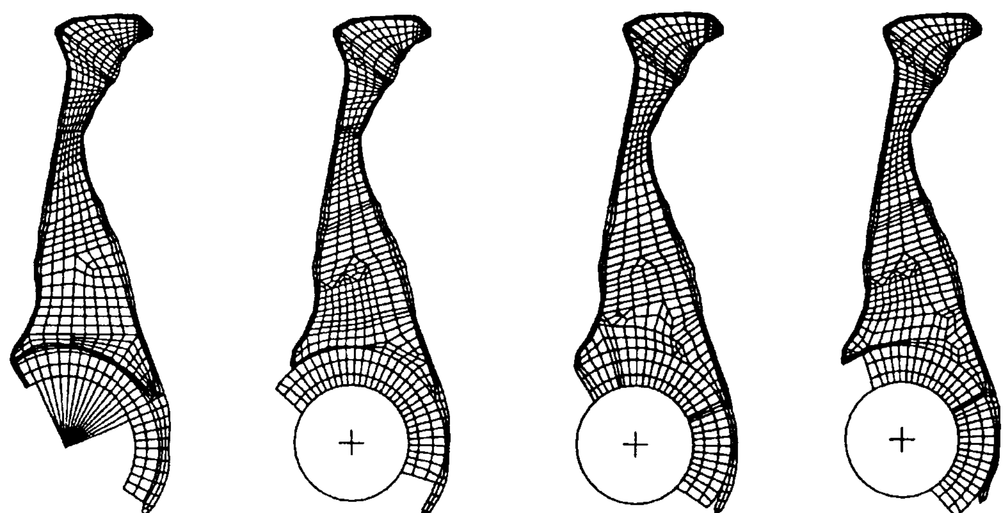

Figure 3.2: Mesh plots of a) the intact model, b) acetabulum with 30° cup, c) acetabulum with 45° cup and d) acetabulum with 60° cup

3.2. BOUNDARY AND LOADING CONDITIONS

The superior tip of the ilium and the inferior margin of the acetabulum were constrained in both horizontal and vertical directions (Figure 3.3), according to Vasu *et al* (1982), Carter *et al* (1982) and Carter *et al* (1983). These constraints on the bone are felt to reflect the reaction force at the pubic symphysis and the contraction of the abductor muscles superiorly, both of which oppose the resultant hip joint force. Analyses were performed to verify these boundary conditions, by constraining the inferior rim of the acetabulum only in the horizontal direction. This had the effect of inducing large bending loads in the middle of the iliac trabecular bone, and thus confirmed the validity of the initial boundary conditions.

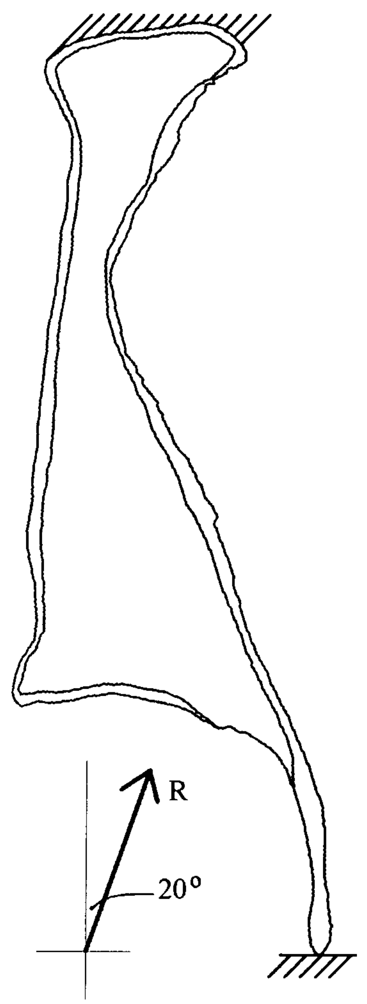

Figure 3.3: Boundary and loading conditions applied to the sectioned hemipelvis

A load of 2550 N, at an angle of 20° to the vertical (Rapperport *et al*, 1987; Pedersen *et al*, 1982; Crowninshield *et al*, 1983; Ducheyne *et al*, 1978; Carter *et al*, 1983; Huiskes, 1987) was applied to the acetabulum, in the coronal plane. This corresponds to a load of 3.4 times body weight in a 750N person. The horizontal and vertical components of the hip reaction force were applied to the models. A detailed account of these loads is given in the Numerical Modelling section.

3.3. MATERIAL PROPERTIES

The choice of bone material properties remains a contentious issue. The values used in these analyses fall well within the central band of those listed in Table 6 of Section 2.5. Table 3.1 below lists the material properties used in both the 2D and 3D studies, where applicable. Values for these material properties have been taken from various sources. The reasons for this include the fact that some of the reported values are not properly representative of the bone properties, and that not all the reviewed research work incorporated all of the values required for this study.

MATERIAL	E (MPa)	ν
cortical bone (Oonishi *et al*, 1983)	15000	0.3
cancellous bone (pelvis) (Huiskes, 1987; Pedersen *et al*, 1982; Crowninshield *et al*, 1983)	1500	0.3
subchondral bone (Oonishi *et al*, 1983; Rapperport *et al*, 1987)	3000	0.3
cartilage (Brown & DiGioia, 1984)	10.35	0.4
cancellous bone (femoral head) (Brown & DiGioia, 1984)	690	0.3
truss elements (femoral head) (Brown & DiGioia, 1984)	690	0.4
UHMWPE (Pedersen *et al*, 1982; Crowninshield *et al*, 1983)	690	0.4
cobalt-chrome (Ashby & Jones, 1980)	208000	0.3
titanium (Huiskes, 1987)	110000	0.3

Table 3.1: Material properties used in all analyses. Note that all the materials are assumed to be isotropic, homogeneous and linearly elastic. E is the Young's modulus of the material and ν is the Poisson's ratio

3.4. NUMERICAL MODELLING AND IMPLEMENTATION

The femoral head was included in the model in order to model the physiologic loading pattern of the hemipelvis. By using this approach it is unnecessary to prescibe an assumed intra-articular loading distribution at the hip joint. The femoral head was assumed to be spherical. The cartilage was also included, with its thickness varied so that a perfect match could be made between it and the (assumed) spherical head of the femur. This approach prevented a mismatch between the irregular contour of the subchondral bone in the acetabulum and the surface of the femoral head. A double layer of 4-noded plane strain elements (ABAQUS type CPE4) represented the outer region of the femoral head (55 mm in diameter). According to Brown & DiGioia (1984) the contact area for loading in the intact hip covers a quadrant. It was therefore decided to connect nodes on this meshed outer region of the femoral head to the centre of the femoral head. These nodes were at 45^{o} medial and lateral to the resultant loading direction, and were connected by 2-noded truss elements, ABAQUS type C1D2. The prescribed loading was then applied to the common node of these truss elements.

The interface between the femoral head and the acetabular cartilage was modelled using ABAQUS type INTER2 elements. These elements allow small relative sliding to occur between the surfaces coming into contact, and are specific for use in a plane strain model. They are positioned on the surface of the body with which the rigid surface comes into contact. In this case, the interface elements were placed on the exterior of the acetabular cartilage. Figure 3.4 indicates how these elements are used, with the numerical integration being performed midway between the element faces.

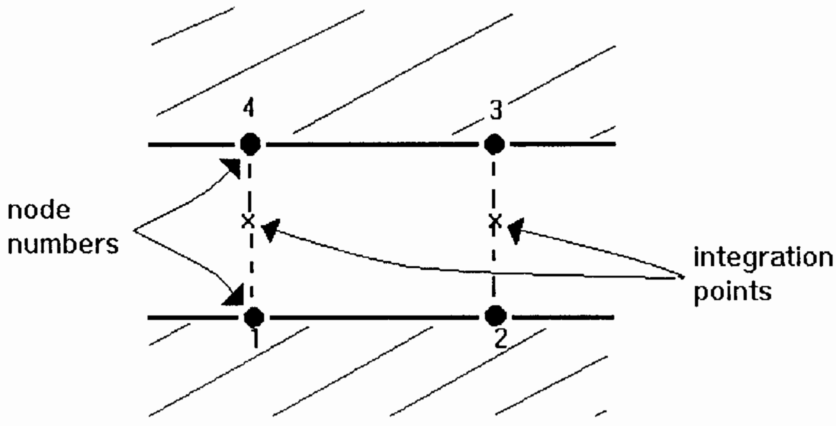

Figure 3.4: Implementation of INTER2 element for use with 2D plane strain elements

The artificial femoral head was simulated by using the RIGID SURFACE option. This option is used to specify the surface of a rigid body that interacts with other parts of the model (Figure 3.5). It has a reference node assigned to it by the user; displacement of this node defines the motion of the entire rigid surface during the analysis.

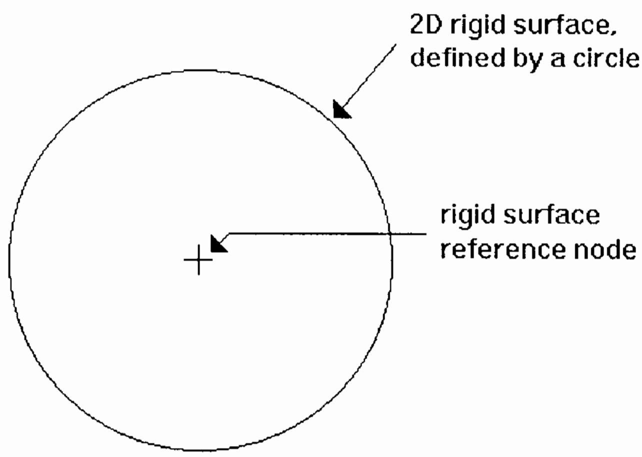

Figure 3.5: 2D rigid surface representing the artificial femoral head

However, the femur can not be realistically considered to be a rigid surface. The ABAQUS SURFACE CONTACT option was therefore utilised, with the SOFTENED parameter enabled. In the future, this ABAQUS option will be referred to as the SOFTENED CONTACT option. It allows the interface conditions between the two interacting surfaces to be altered to suit the specific model requirements. Figure 3.6 illustrates the default pressure-clearance relationship for ABAQUS interface elements. The SOFTENED CONTACT is achieved by modifying this default contact pressure-clearance relationship on the interface elements of the deforming body, in this case the cartilage and acetabulum.

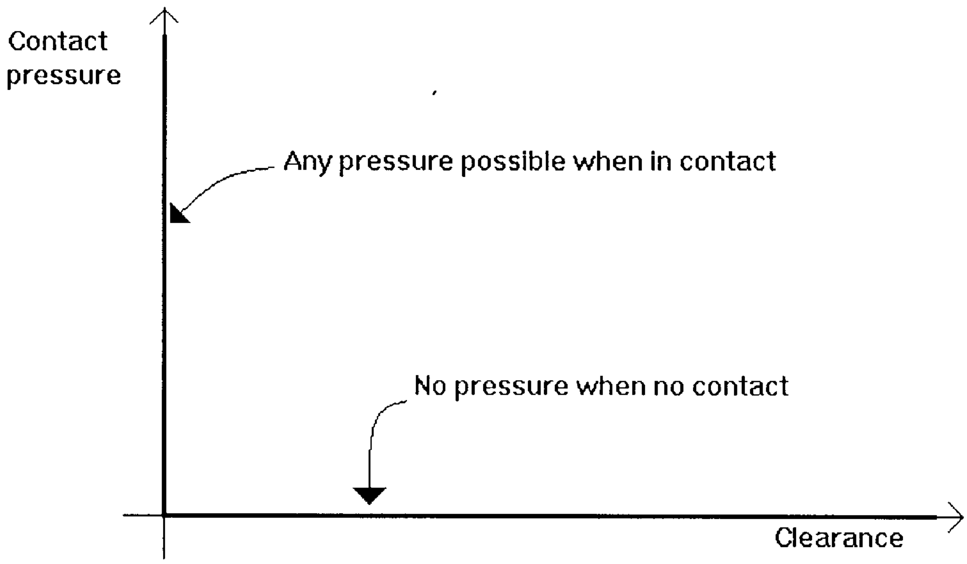

Figure 3.6: Default pressure-clearance relationship for interface elements

In effect, SOFTENED CONTACT allows some pressure to be transmitted across the interface even while there is no contact between the two surfaces. The user defines the clearance (c) at which the interface will begin experiencing pressure, and the value of the pressure when the clearance is zero (p^o). The degree to which the two surfaces overlap is defined as the overclosure h. The pressure is defined, in terms of p^o, c and this overclosure h, by the general equation

$$p = \frac{p^o}{(\exp(1)-1)}\left[\left(\frac{h}{c}+1\right)\left(\exp\left(\frac{h}{c}+1\right)-1\right)\right].$$

ABAQUS iterates the analysis until the calculated softened contact incompatibility error is within 0.5% of the value specified for c, at all the interface element nodes.

This exponential behaviour of the stress transmission across the softened contacting surfaces is illustrated in Figure 3.7.

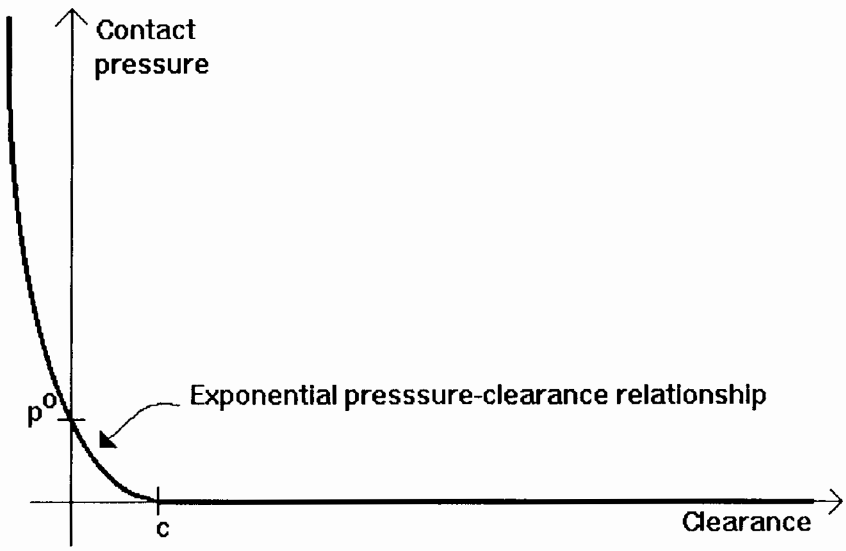

Figure 3.7: "Softened" pressure-clearance relationship for interface elements

The interface between the RIGID SURFACE (i.e. artificial femoral head in the THA models) and the acetabular cup was assumed to be frictionless. Additional runs were performed with a friction coefficient of 0.025 included at this interface, in an attempt to simulate the joint behaviour.

Until recently, many finite element investigations of the acetabular component in THA have assumed the existence of a fully fixed bone/component interface only. In this 2D study, the cup/bone interface was modelled in two ways: fully bonded and unbonded. In the first case, the cup and the bone form a continuum and thus the interface is 'fixed'. In the second, ABAQUS interface elements type INTER2 were used at the cup/bone interface (Figure 3.4). This represents the ideal post-operative situation where full bony ingrowth has occurred into the porous coating of the cup.

The interface elements allow an infinitesimal amount of movement before sliding occurs, dependant on the friction that exists there. The modelled interface assumed by using a co-efficient of friction of 0.3, with the SOFTENED CONTACT parameter enabled. This approach simulates a press-fit situation. It should be noted that all the THA models had the cartilage and subchondral bone of the acetabulum "perfectly reamed" to accommodate the cup. In all analyses the interface between the cup's metal backing and polyethylene liner was assumed to be perfectly bonded.

An example of an ABAQUS input deck for the 2D models can be found in Appendix C.

3.5. RESULTS

The results for the 2D study are subdivided into various sections. Firstly, the predicted stress levels in the intact hemipelvis are presented. Secondly, the effects of cup orientation (30, 45 and 60 degrees vertical orientation) and metal backing (Co-Cr and Titanium alloys) for a fully bonded cup/bone interface are shown. A comparison of the assumed cup/bone interface conditions (fully bonded and unbonded) is then made, for the three cup orientations incorporating only a Co-Cr cup backing.

After a description of the femoral head/cup normal stresses, results are presented for the normal and shear stresses at the unbonded cup/bone interface for both material types and the three orientations. Finally, a comparison is made between the stresses in the acetabular cups with the two different material types used as a metal backing.

The calculated stresses were transformed to a contour spectrum where the lightest shade of grey indicates areas of compressive (negative) stresses, and the darkest shade areas of high tensile stresses. The values of these stresses are seen in the grey-coded scales as Pascals (Pa).

3.5.1. Intact hemipelvis

The maximum principal stress contours obtained for both cortical and cancellous bone of the intact hemipelvis are shown in Figure 3.8. The stresses in the cortex are predominantly tensile in the medial wall, while compressive stresses were predicted in the lateral side of the chosen hemipelvic section. The maximum cortical tensile and compressive stresses are 2.09 and 0.17 MPa respectively. The corresponding stresses in the cancellous bone are 0.16 and 0.045 MPa.

The ratio of the stress magnitudes in the cortical bone to that in the cancellous bone is approximately 13:1, which is similar to the ratio of their Young's moduli.

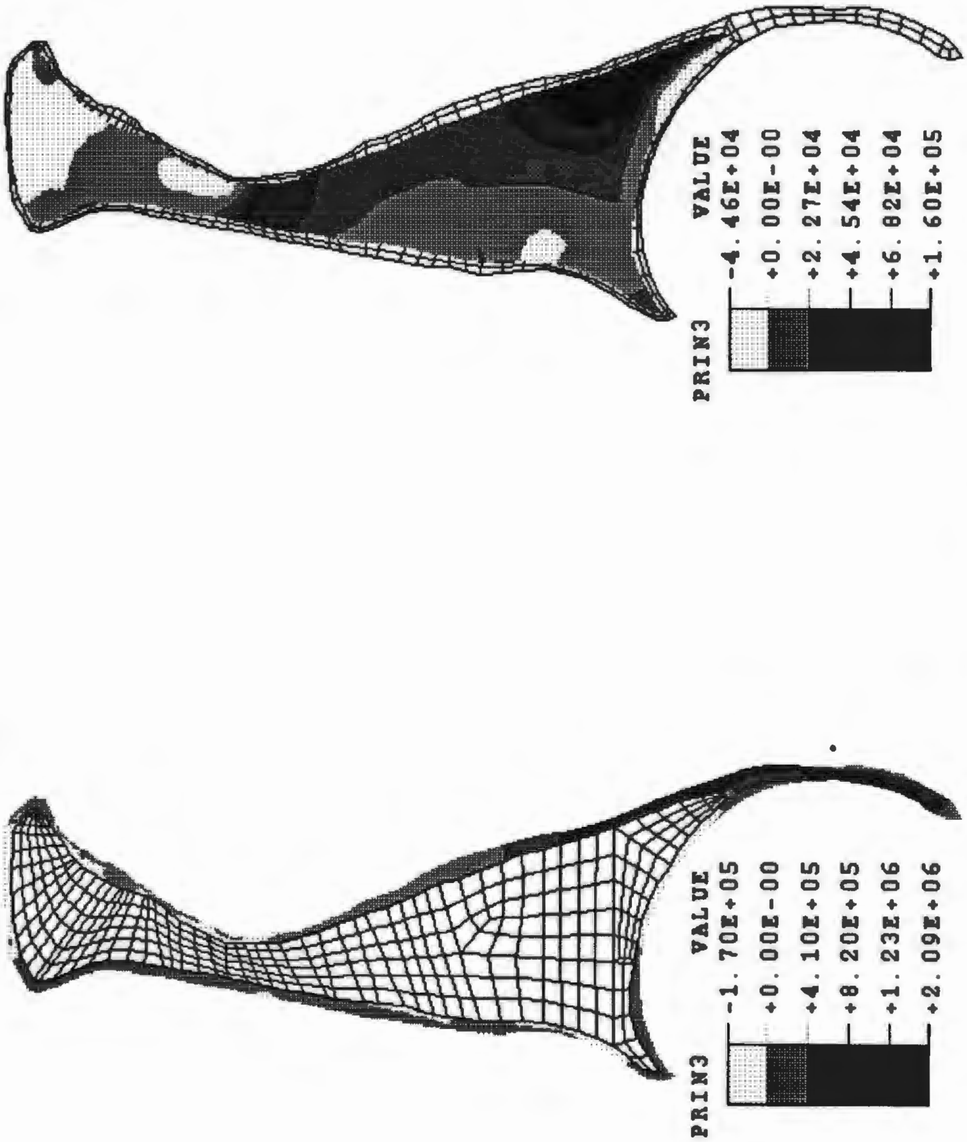

Figure 3.8: MAXIMUM PRINCIPAL CORTICAL AND CANCELLOUS STRESSES IN THE INTACT HEMIPELVIS SECTION

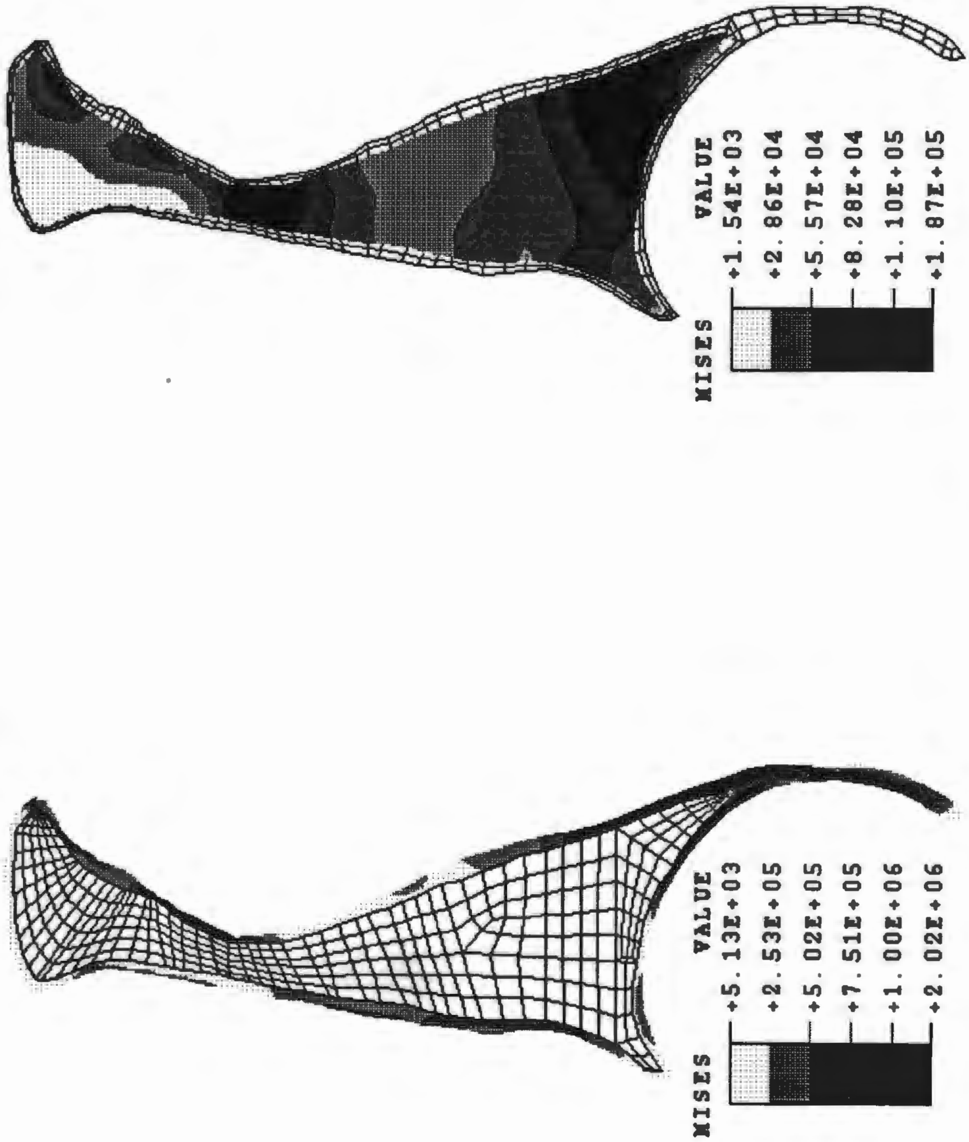

Figure 3.9: VON MISES CORTICAL AND CANCELLOUS STRESSES IN THE INTACT HEMIPELVIS SECTION

The Von Mises equivalent stresses (scalar quantities) are shown in Figure 3.9. The maximum equivalent stresses in the cortical and cancellous bone are predicted to be 2.02 MPa and 0.187 MPa respectively. These stress patterns follow similar trends to those indicated for the maximum principal stress (Figure 3.8). All the subsequent THA analyses confirmed this similarity - between maximum principal and Von Mises stresses - and it was therefore decided to present only the maximum principal stress results for all the analyses.

3.5.2. Cup orientation and metal backing

A series of analyses were performed to investigate the influence of cup orientation and metal backing material on the stress state of the bone, assuming a fully bonded cup/bone interface. Figures 3.10 and 3.11 present the maximum principal stresses in the cortical bone for the Titanium and Co-Cr backed cups. It is evident that, irrespective of material used as metal backing, the maximum lateral compressive stresses in the cortical bone tend to decrease in magnitude with an increase in cup angle from 30 to 60 degrees. The reverse is true for the medial cortical tensile stresses. The tensile stresses in the cortical bone are slightly higher in the Titanium-backed THA model when compared to the Co-Cr counterpart, by amounts of 6%, 8% and 5% for the 30, 45 and 60 degree cups respectively.

Although the maximum values of the stress approach those in the intact hemipelvis (Figure 3.8), especially in the 60^{o} cup models, stress "shielding" in the infero-medial region of the cortical bone occurs for both material types and all cup angles analysed. This is most marked in the Co-Cr backed cups. This same stress shielding effect is seen in the plots of the cancellous bone for these models (Figures 3.12 and 3.13). It is more marked here, since the maximum stress values reached in the Titanium-backed THA models are only 59% (for the 30 and 45 degree cups) and 64% for the 60 degree cup of that in the intact hip, while values for the Co-Cr models are 51%, 52% and 57% respectively. The tensile stress contour patterns in the medial cancellous bone are not markedly affected by the cup orientation.

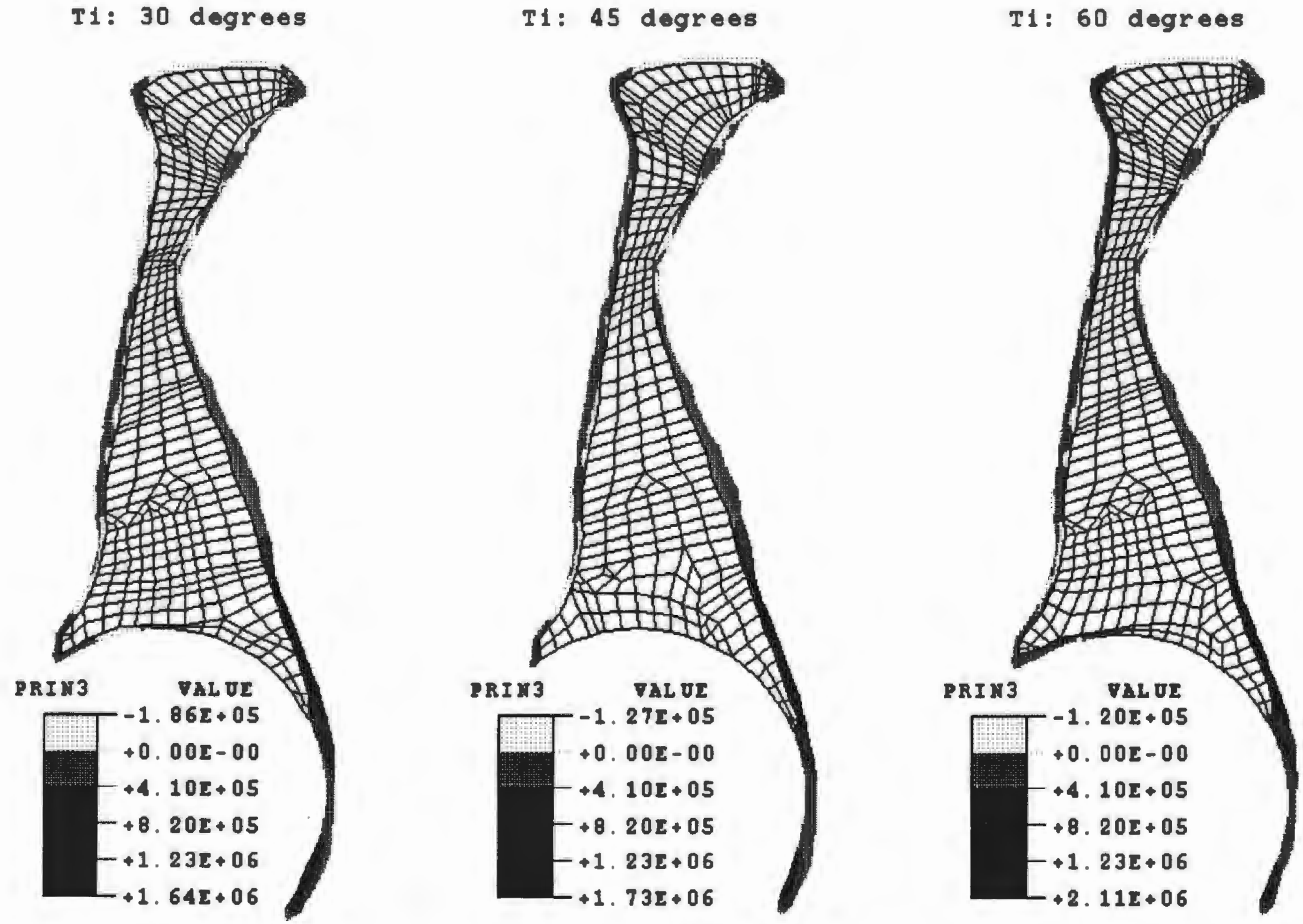

Figure 3.10: MAXIMUM PRINCIPAL STRESSES IN THE CORTICAL BONE WITH A FULLY BONDED CUP/BONE INTERFACE

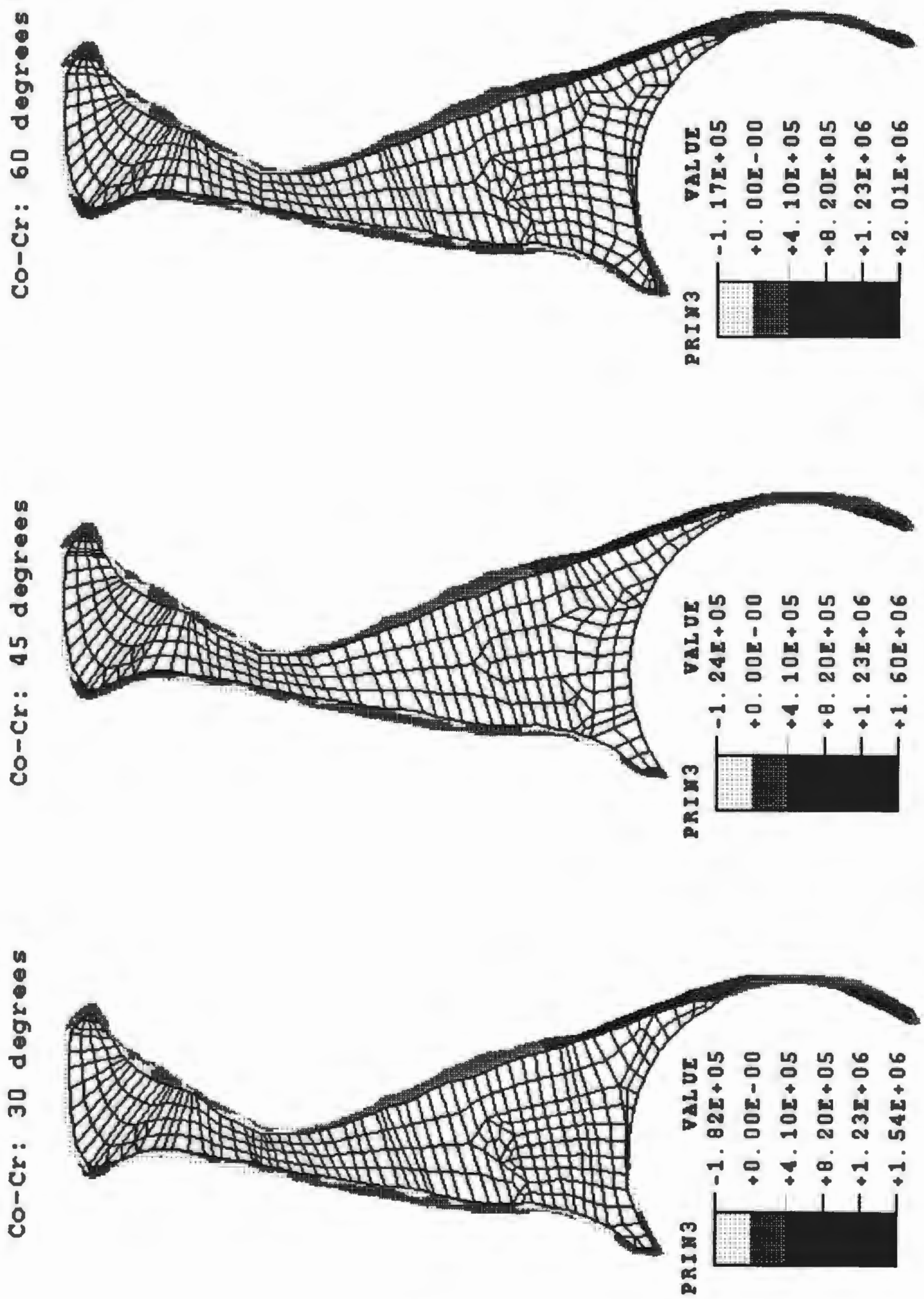

Figure 3.11: MAXIMUM PRINCIPAL STRESSES IN THE CORTICAL BONE WITH A FULLY BONDED CUP/BONE INTERFACE

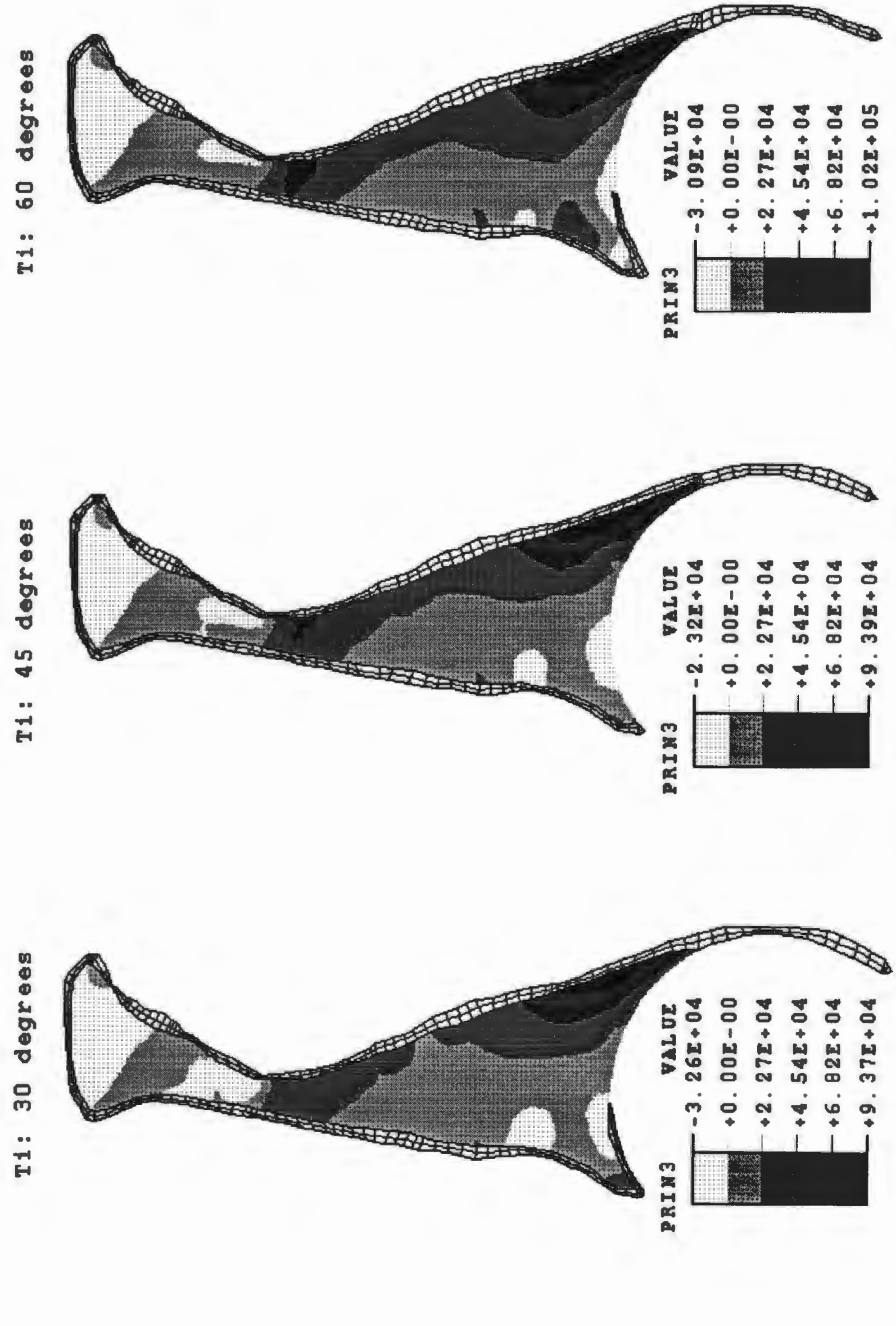

Figure 3.12: MAXIMUM PRINCIPAL STRESSES IN THE CANCELLOUS BONE WITH A FULLY BONDED CUP/BONE INTERFACE

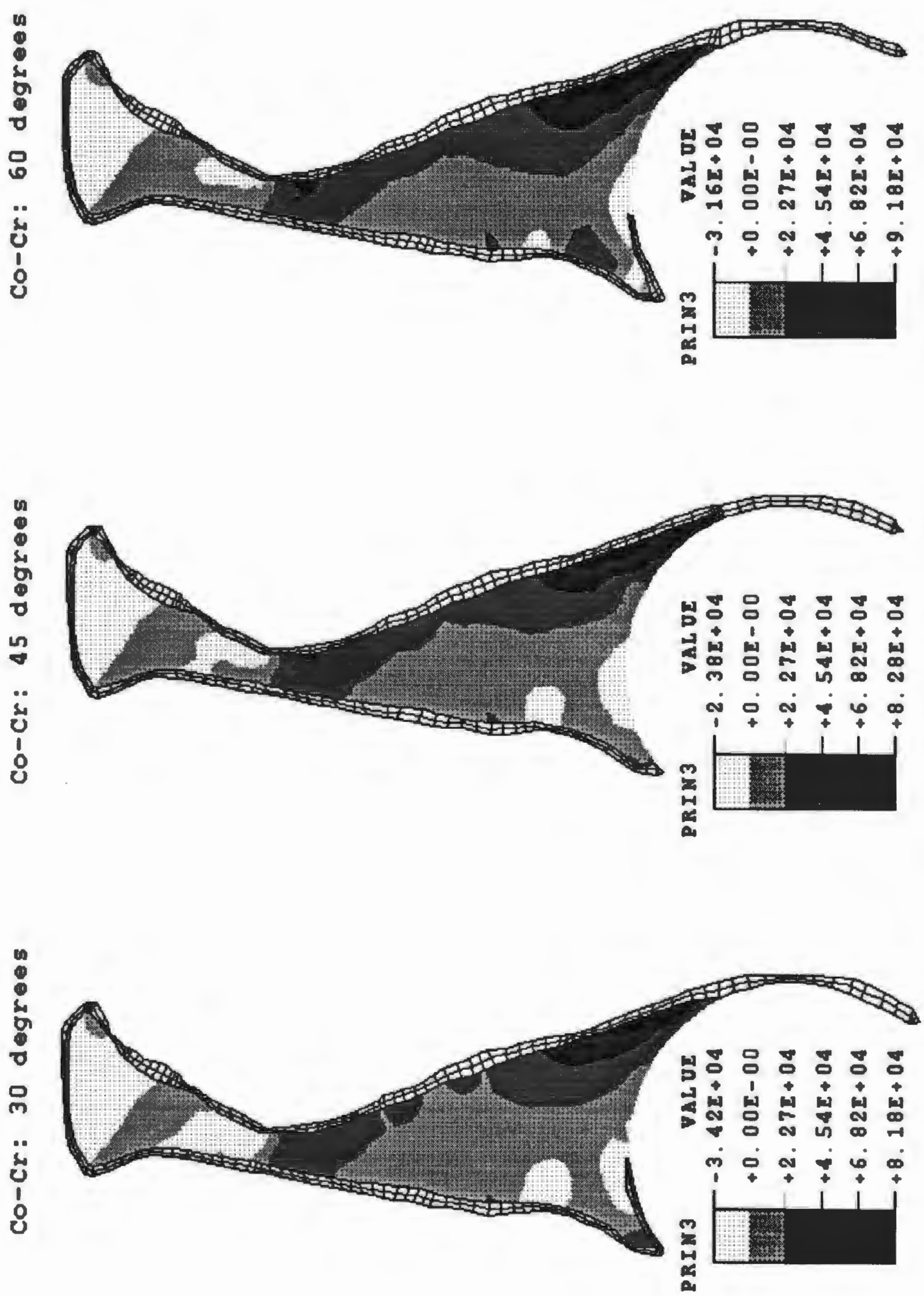

Figure 3.13: MAXIMUM PRINCIPAL STRESSES IN THE CANCELLOUS BONE WITH A FULLY BONDED CUP/BONE INTERFACE

The compressive stress in the infero-medial area of cancellous bone, immediately adjacent to the subchondral bone, of the intact hemipelvis has shifted towards the supero-lateral acetabular border in all the THA models. For a specific cup angle, this region of compressive stress is very similar for the two materials used. The effect of the different material can be seen, however, in the values that these compressive stresses attain. Again, the Co-Cr backed THA models exhibit greater stress shielding than those with Titanium as metal backing.

3.5.3. Cup/bone interface conditions

This section describes the results obtained for two different cup/bone interfaces, for a Co-Cr backed cup. Figures 3.14 and 3.15 indicate the stress magnitudes in the cortical bone with a fully bonded and unbonded interface respectively. The same trend in the tensile stress magnitudes exists under both interface conditions: stress increases with an increase in cup angle. The fully bonded interface results in a decrease in maximum compressive stress for an increasing cup angle, while the unbonded interface indicates that the least compressive stress occurs in the 45^{o} cup. The tensile stresses in the cancellous bone follow the same trend as those in the cortical bone, while the 45 degree cup has the lowest compressive stress in each case (Figures 3.16 and 3.17).

It is clear from Figures 3.14 through 3.17 that there is a large difference in the stress magnitudes of the cancellous and cortical bone for the two interface conditions. The most important changes in the stress state of the models are evident in the compressive stress in the cancellous bone. This compressive stress is increased almost fourfold with the assumed unbonded models when compared with the fully bonded case.

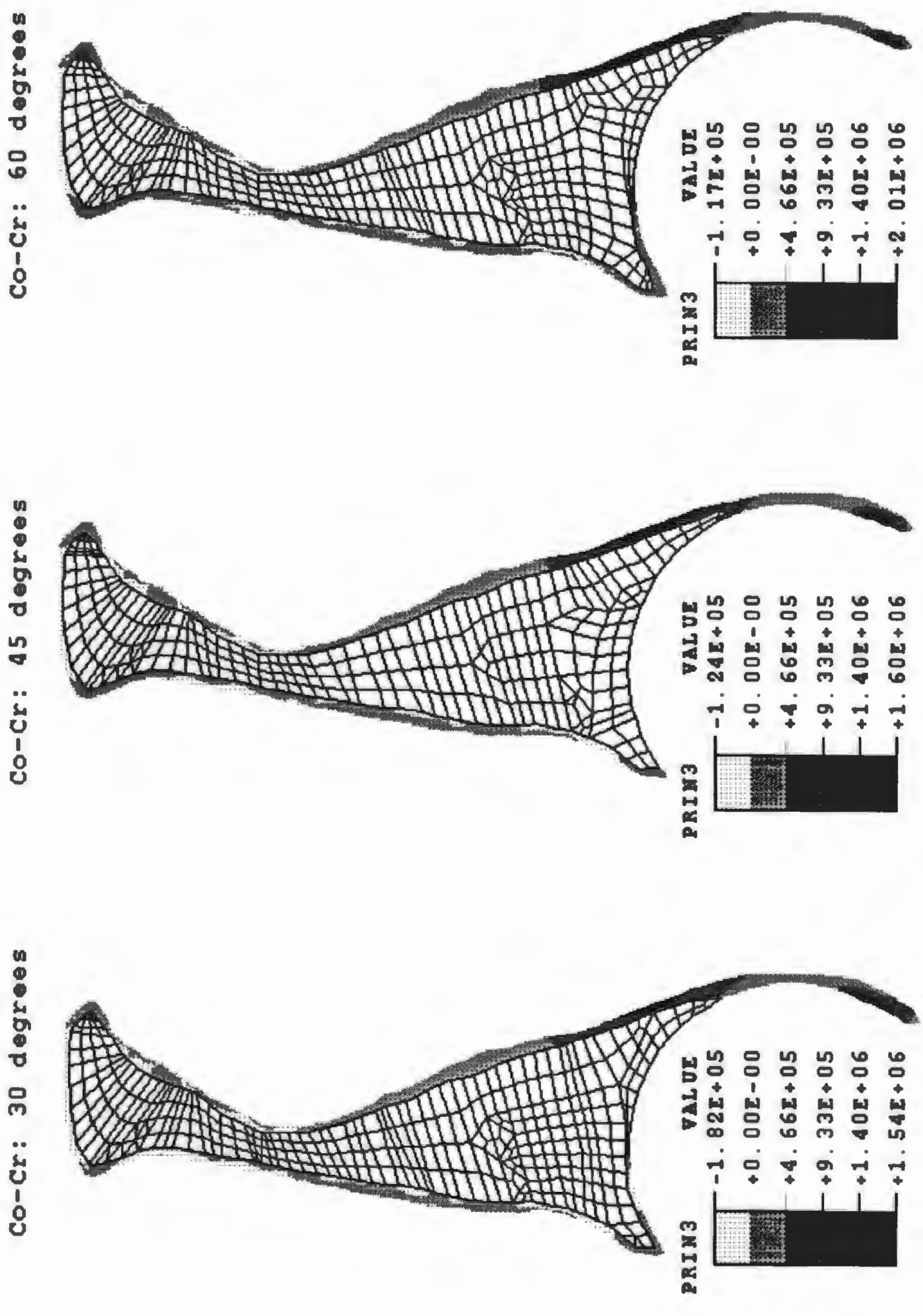

Figure 3.14: MAXIMUM PRINCIPAL STRESSES IN THE CORTICAL BONE WITH A FULLY BONDED CUP/BONE INTERFACE

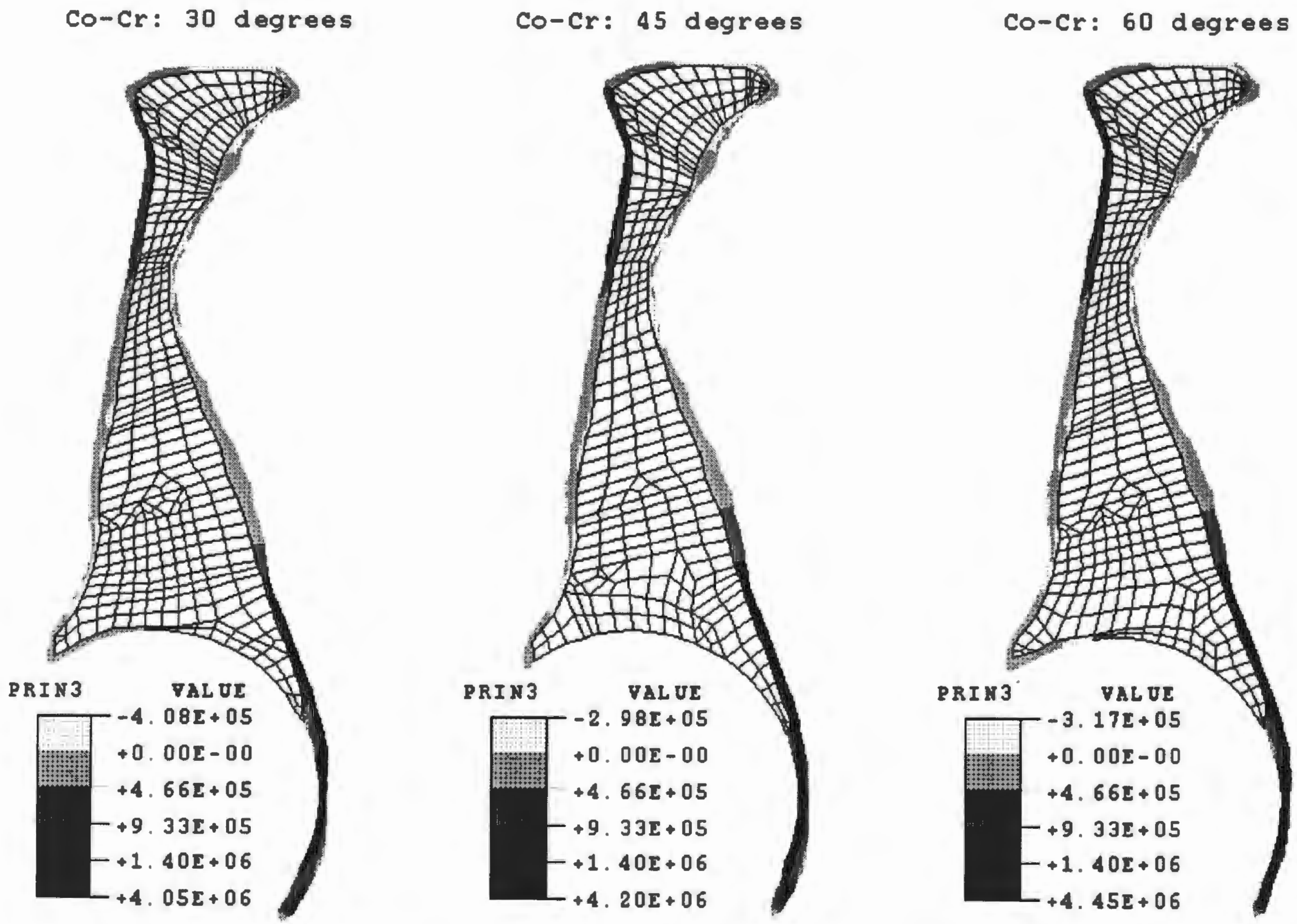

Figure 3.15: MAXIMUM PRINCIPAL STRESSES IN THE CORTICAL BONE WITH AN UNBONDED CUP/BONE INTERFACE

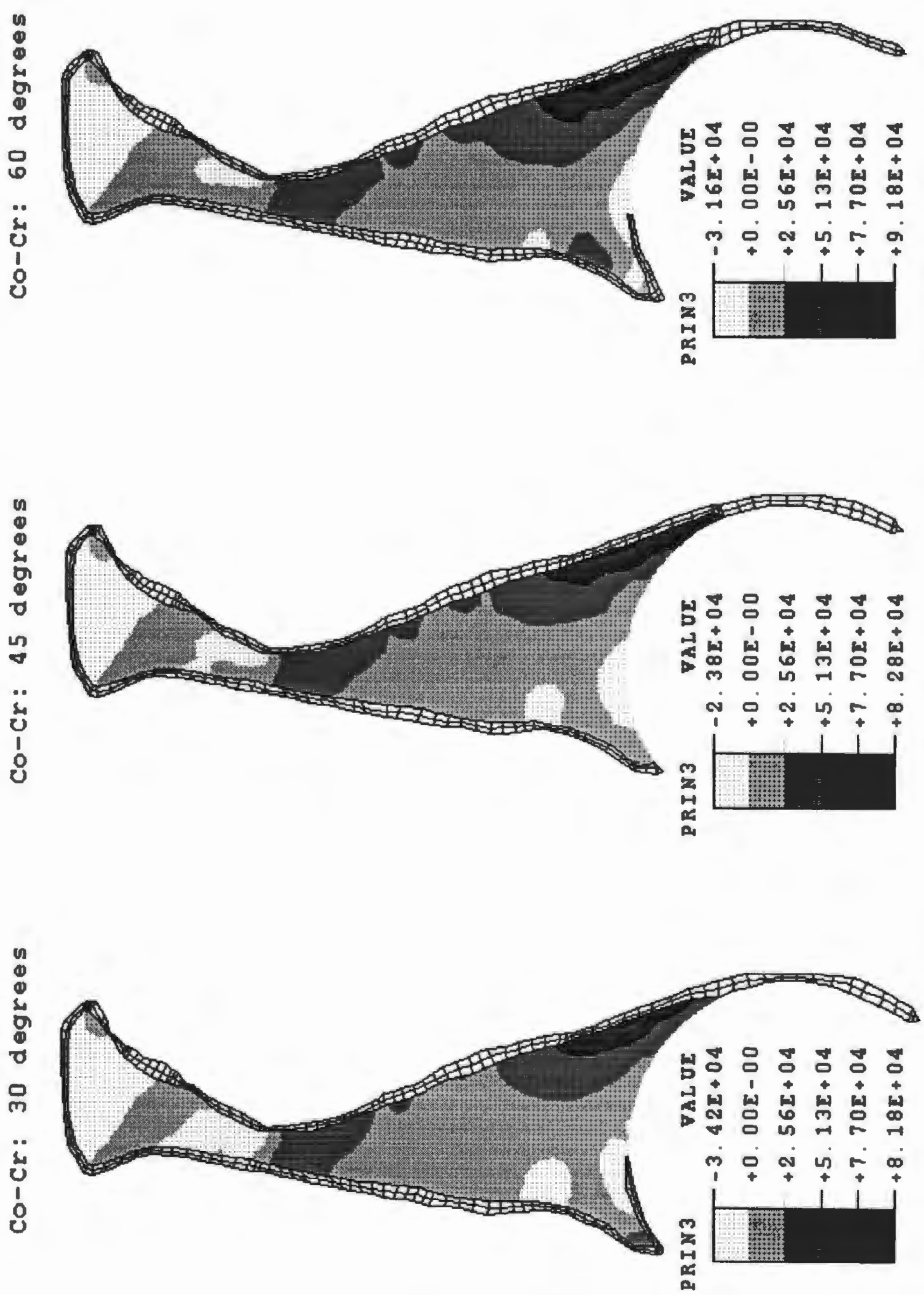

Figure 3.16: MAXIMUM PRINCIPAL STRESSES IN THE CANCELLOUS BONE WITH A FULLY BONDED CUP/BONE INTERFACE

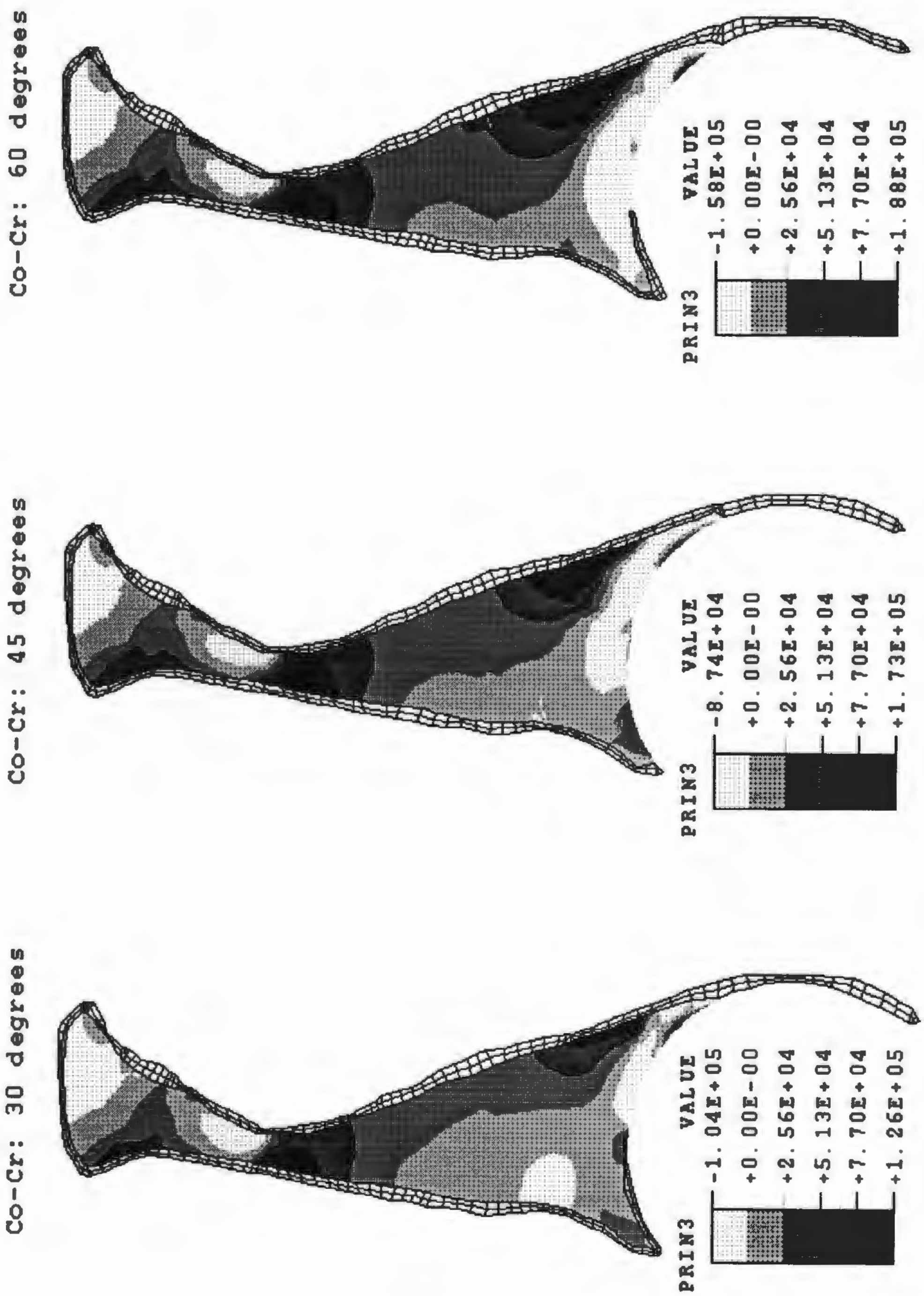

Figure 3.17: MAXIMUM PRINCIPAL STRESSES IN THE CANCELLOUS BONE WITH AN UNBONDED CUP/BONE INTERFACE

Besides for the difference in compressive stress magnitudes, there are two other important observations to be made: firstly, the region in which this compressive stress occurs is shifted from a supero-lateral position in the fully bonded models to a more medial position in the unbonded cases; and secondly, the area over which the compressive stress acts is greatly increased in the unbonded models, particularly in the 60 degree cup model. A similar difference is noted in the medial cortical bone tensile stress, which also undergoes an increase in stress magnitude of a factor of approximately four. Thus the assumed cup/bone interface conditions play an important role in the outcome of FEA analyses in THA.

3.5.4. Stresses at the unbonded cup/bone interface

This section reports the normal stresses only at the unbonded cup/bone interface, for different materials and cup orientations. This is done because the results for this stress output variable are not available for the fully bonded interface, since these latter models did not make use of elements to simulate the interface.

Figures 3.18 and 3.19 depict the normal stress distribution, for the abovementioned conditions. It is evident that the distribution of these normal stresses, while very similar for the two materials, varies according to the orientation of the cup. The "45 degree" cup appears to best transmit the loading pressure distribution of the femoral head onto the acetabulum.

There is a difference in the range of normal stress values predicted for the different cup orientations. For example, the Co-Cr "45 degree" cup (3.35 - 82.9 kPa) has a reduced range in these stress values relative to both the "30 degree" and "60 degree" cups, which have values ranging between 1.78 - 94.1 kPa and 1.27 - 99.0 kPa respectively (Figure 3.18).

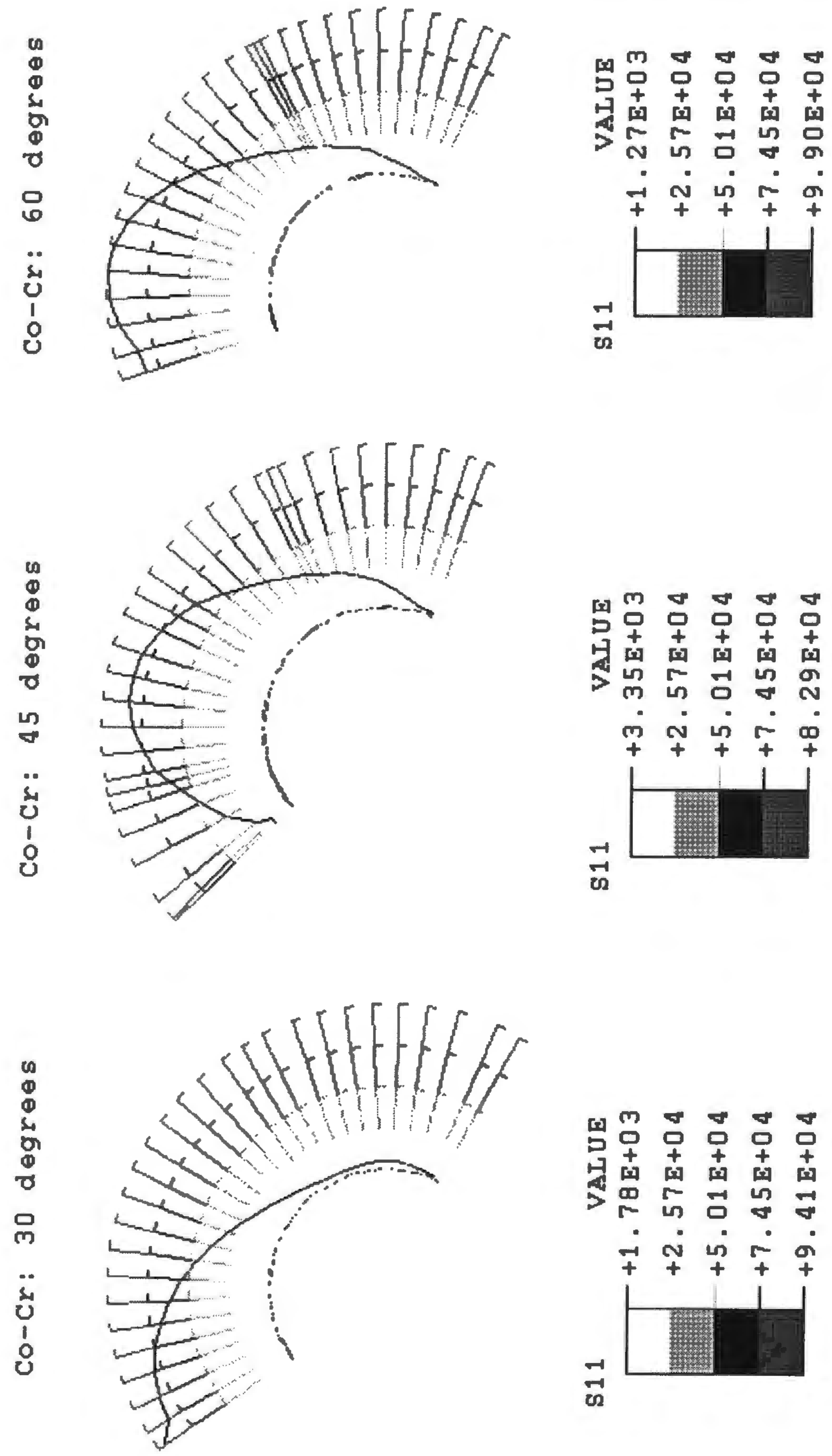

Figure 3.18: CUP/BONE INTERFACE NORMAL STRESSES WITH AN UNBONDED CUP/BONE INTERFACE

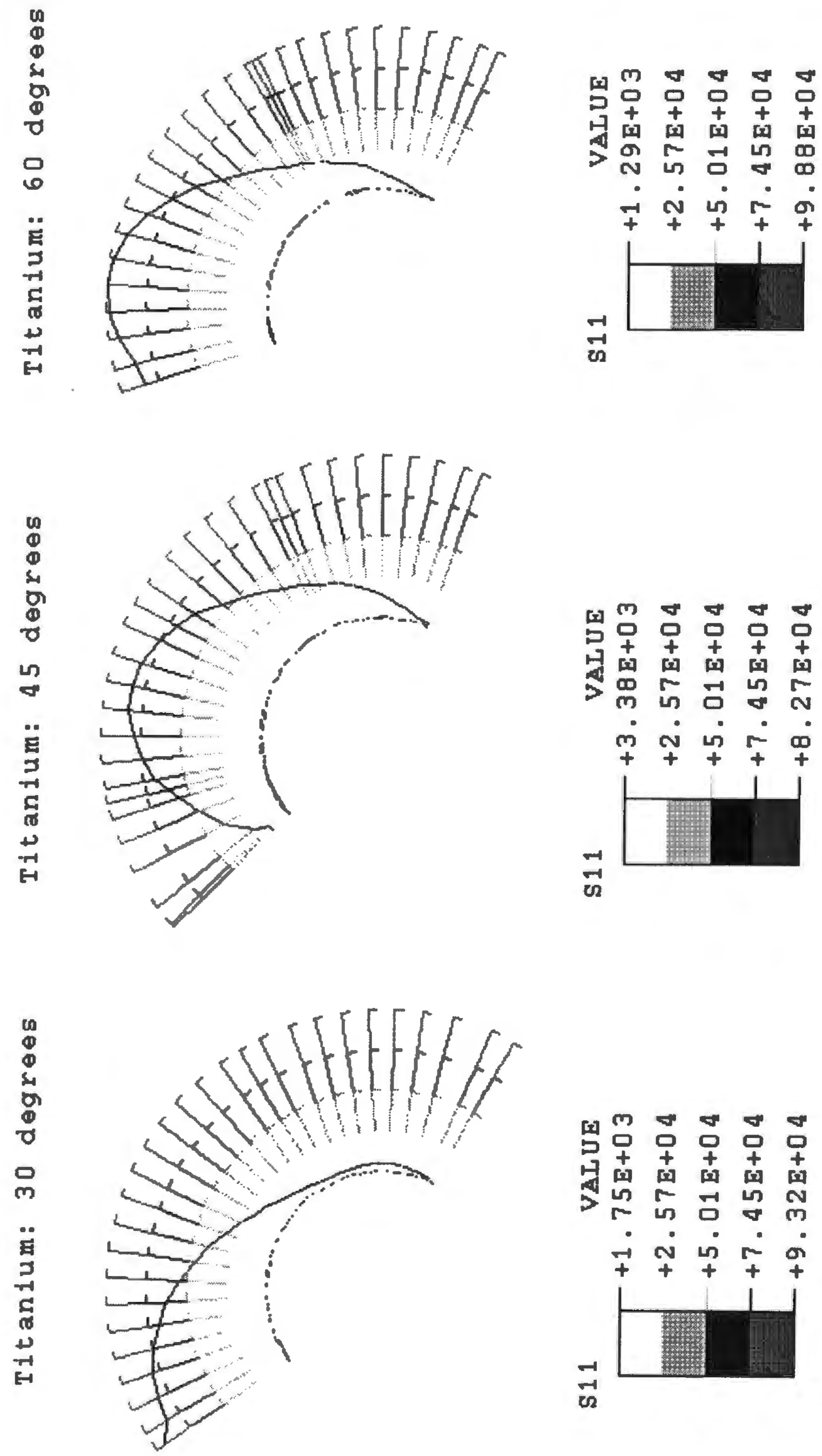

Figure 3.19: CUP/BONE INTERFACE NORMAL STRESSES WITH AN UNBONDED CUP/BONE INTERFACE

3.5.5. Cup stresses

Figures 3.20 and 3.21 show the maximum principal stresses in the Titanium and Co-Cr backed cups, for three cup orientations, assuming a fully bonded cup/bone interface. The tensile stresses recorded in the Co-Cr alloy are 59% higher than in the Titanium alloy for the 30^{o} and 45^{o} cups, and 70% for the 60^{o} cups. The compressive stresses, which occur primarily in the polyethylene liner, remain essentially the same for both material types and all three cup orientations.

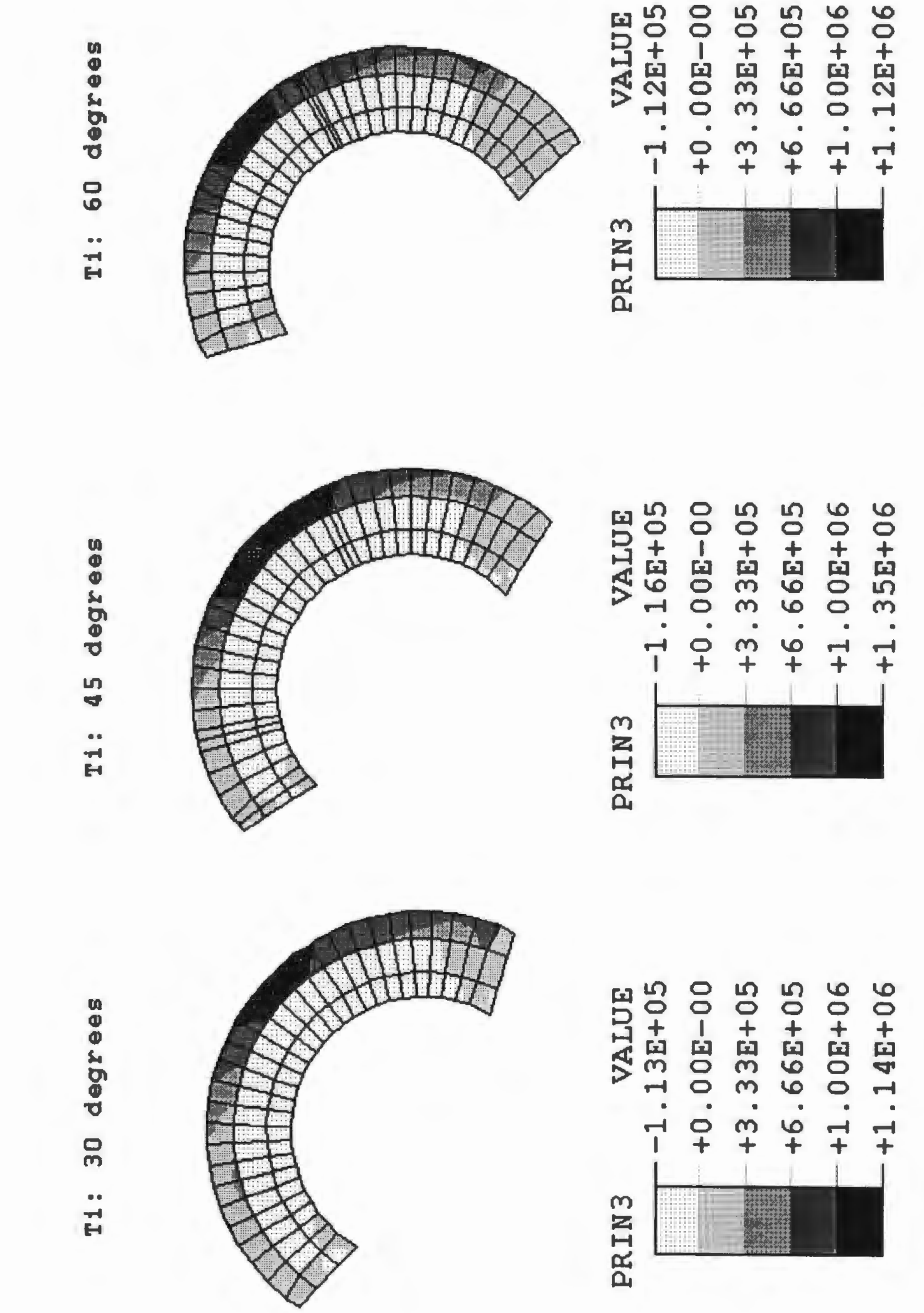

Figure 3.20: MAXIMUM PRINCIPAL STRESSES IN THE CUP WITH A FULLY BONDED CUP/BONE INTERFACE

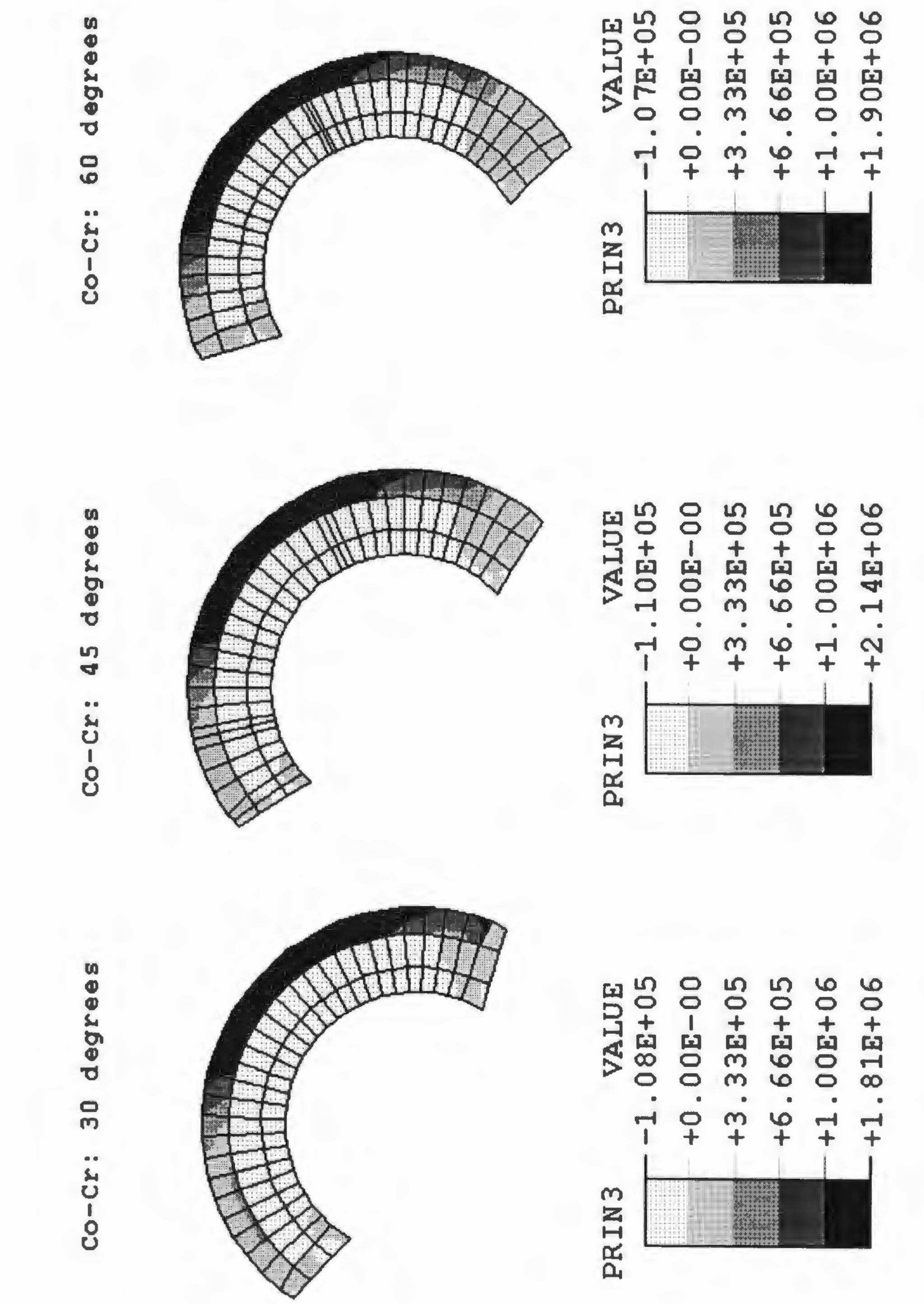

Figure 3.21: MAXIMUM PRINCIPAL STRESSES IN THE CUP WITH A FULLY BONDED CUP/BONE INTERFACE

3.6. DISCUSSION

Finite element studies are limited by their ability to fully represent the complexities of biological structures. Interpretation of the results of such analyses requires an appreciation and understanding of the model's inherent limitations, particularly when modelling a three-dimensional structure in two dimensions. The primary limitation of these 2D models is their increased flexibility relative to the actual hemipelvis, owing to out-of-plane stiffness present in the three-dimensional structure. As a consequence, the results of such models are to be interpreted with caution. However, it is felt that the results from such analyses are very beneficial for a qualitative understanding of the load transfer mechanism in the acetabular region of the hemipelvis.

The objectives of this first part of the study were to investigate the effect of the orientation of the acetabular component in THA on the post-operative stress state in the hemipelvis. At the same time, the effects of material backing and different assumed implant/bone interfaces were investigated. This was accomplished by parametric examination of two-dimensional plane strain models. The 2D section used was chosen over other alternative sections through the hemipelvic bone because it represents the plane of high loading and therefore allows the results to be interpreted more easily in terms of the 3D nature of the structure. An axisymmetric model was not used because it was felt that too many assumptions are made regarding the geometry of the hemipelvis away from the acetabulum.

Another limitation of the 2D model is its capacity for modelling the acetabular cup. Cementless cups are initially fixed into the bone by means of screws, and are provided with pegs or fins to provide them with anti-rotational stability. In 2D plane strain models such as these it is not possible to simulate these screws or pegs, nor the degree of anteversion at which the cup is inserted in to the acetabulum. As a result the cups can only be analysed for the general impact that they have on the bone, and not for their local effect.

The analyses included a refinement only introduced in recent FEA studies. Both the intact and artificial femoral heads, contact-coupled to the acetabulum/polyethylene liner respectively, were included in the analyses, similar to the first models of this type by Brown & DiGioia (1984), and later by Rapperport *et al* (1987) and Huiskes (1987). In the case of the THA models, the femoral prosthetic head presents an important deformation restraint to the relatively flexible polyethylene cup's inner surface. This implies that the application of a presumed external load at the inner socket surface results in considerable overestimations of the cup deformations and the bone stresses. This constraint on the deformation of the cup is more realistic than other studies (Vasu *et al*, 1982; Carter *et al*, 1982, Carter *et al*, 1983; Pedersen *et al*, 1982; Crowninshield *et al*, 1983), where the load distribution has been assumed and approximated as discrete loads on element edge nodes.

The use of the RIGID SURFACE to simulate the prosthetic femoral head in our analyses is essentially the same as including a whole meshed femoral head, and has the advantage of being cheaper for a computer workstation to perform due to the decrease in the number of finite elements. SOFTENED CONTACT ensures that the transmission of the load to the acetabulum occurs in a smooth manner. The prosthetic femoral head/cup interface conditions were assumed to be frictionless, since Brown and DiGioia (1984) reported that the co-efficient of friction at this contact surface had little effect on the overall stress state of the bone.

The stress distribution in the model of the intact hemipelvis confirms the suggestion by Jacob *et al* (1976) that it acts as a true sandwich structure, in which the cortical bone is highly stressed while the softer cancellous bone remains in a relatively unstressed condition, serving mainly to prevent collapse of the main load-bearing shell. Hence the predominant action of the cortical bone is to transfer the majority of the applied load away from the acetabulum superiorly over the surface of the ilium.

This cortical bone stress distribution is mostly tensile in the medial cortex with predominantly lower compressive stresses in the lateral cortex. This stress state represents bending in the ilium under the action of the hip abductor muscles, as reported by Vasu *et al* (1982). This situation is analogous to a beam supported at both ends with a central transverse point load applied normal to it, where the load is the hip joint reaction force and abductor muscles, and the supports are the sacro-iliac joint and the pubis symphysis.

The maximum principal stress distribution of the intact model is in agreement with the stress distribution reported by Vasu *et al* (1982), Carter *et al* (1982) and Carter *et al* (1983). However, where they report a maximum compressive and tensile stress in the lateral and medial cortices of approximately 10 MPa, our values are 0.17 and 2.1 MPa respectively. These results are nevertheless consistent with those reported elsewhere, particularly in the axisymmetric models that have been analysed (Pedersen *et al*, 1982; Huiskes, 1987). Huiskes (1987) concluded that the pure two-dimensional model overestimates the stresses approximately fourfold compared with the axisymmetric one, but this difference is not evident in the results of this study. It is felt that the large discrepancy between our results and those of Vasu *et al* (1982), Carter *et al* (1982) and Carter *et al* (1983) could be largely due to their seemingly incorrect placement of the cup, orientation of their section and their modelling of the loading by means of an assumed pressure distribution.

The results indicate that when any uncemented porous-ingrowth cup is implanted into the acetabulum, the stress patterns and magnitudes are significantly different from those of the intact hip. After THA the contact force at the cup/bone interface tends to push the cup into the bone between the medial and lateral walls off the ilium. This generalised conclusion is greatly affected by the angle of cup insertion and the assumed cup/bone interface conditions.

The "30 degree" cup has been shown, in almost all cases, to offer the worst stress results for the three cup orientations. In terms of minimising the stresses in the different bone regions, the "45 degree" cup has been found to give the best results. Sarmiento *et al* (1990) and Russotti *et al* (1988) reported an increased incidence of acetabular lucency in more horizontally inclined cups. Contradictory reports by Hierton *et al* (1983), Callaghan (1985) and Agins *et al* (1988) indicate that the polyethylene wear and loosening of the cup increase with more vertically inclined cups. These results suggest that a "neutral" angle of 45 degrees is the safest option for the surgeon when implanting the acetabular cup. It should be noted that we were unable to model the cup's anteversion because this occurs out of the plane of our model.

This study indicated that the subchondral bone experiences large tensile and compressive stresses in the single-legged stance phase of gait. This manifested itself as bending in this bony region, since the area in the direction of loading was in compression while the tensile stresses were evident in the infero-medial and supero-lateral regions of the acetabulum. The compressive stresses in the subchondral bone are transferred through the adjacent cancellous bone to the stiffer cortical bone in the medial wall.

As shown in the stress plots for the different cups used, a varied amount of subchondral bone was reamed to provide a suitably congruent surface for cup implantation. This bone reaming resulted in an increase in the peak stresses in the underlying cancellous bone. Thus the metal backing of the cup might serve the same purpose as the subchondral bone in the intact hemipelvis by reproducing the stiffening effect that this type of bone has in the acetabulum. Similar results were reported by Carter *et al* (1982) and Crowninshield *et al* (1983). In a comparison of the two materials, the results indicate that the Co-Cr alloy is a more efficient "absorber" of the induced stress compared to the Titanium alloy. This is due primarily to their ratios of Young's moduli: Co-Cr has a stiffness 1.9 times that of Titanium. However, the Titanium-alloy is slightly more effective in duplicating the role of subchondral bone, since it appears that the Co-Cr promotes greater stress shielding of the bone than its Titanium counterpart. This stress shielding is most evident in the infero-medial region of the subchondral bone, which could be a contributory factor in bone resorption and subsequent cup loosening.

A fully bonded cup/bone interface simulates the idealised - often hypothetical - 100 % osseointegration of the bone into the cup's porous coating, where no micromotion occurs at the interface. This bony ingrowth is the ultimate aim of all THA's performed using cementless porous-coated cups. However, the initial post-operative condition is one of an imperfect bond at this cup/bone interface. This is essentially an unbonded interface with friction.

The assumed interface conditions have been shown to play an important role in the stresses generated in the hemipelvis. The difference in stress states seen is explained by the fact that the fully bonded models behave as a continuum, which by its nature is a relatively stiff structure. On the other hand, the unbonded cup/bone interface has the cup attempting to drive its way through the acetabulum into the underlying cancellous bone, thereby resulting in a much larger bending effect in the acetabular rim. Hence the tensile stresses set up in the medial cortical wall far exceed those seen in the fully bonded case.

In order to create a better understanding of the load transfer mechanism in the replaced hemipelvis, this interface has to be examined in great detail. In reality, the immediately post-operative acetabulum should have initial fixation, by means of cancellous screws and pegs, that will promote bony ingrowth into the porous coating of the cup. The cups can then be considered as having interface conditions somewhere between the two extents amounts of ingrowth that have been modelled here. Rapperport *et al* (1987) found that different interface conditions result in markedly different periacetabular stress fields, a result which has been verified in these 2D analyses.

The "45 degree" cup has been shown to best transmit the load applied to the acetabular cup to the surrounding bone. Both the "30 degree" and the "60 degree" cups tend to "skew" the normal stress distribution at the implant/bone interface to the supero-medial border, this effect being more noticeable in the "30 degree" cup. This uneven distribution might promote subchondral and/or cancellous bone stress concentrations in the vicinity of these peak stresses, and could ultimately lead to the initiation of loosening of the implant.

It emerges that the "45 degree" cup almost always appears to be a good compromise between the two other extremes.

CHAPTER 4
THREE-DIMENSIONAL FEA MODELS

4.1. MODEL DEVELOPMENT

The mapping of the hemipelvis was performed by means of CT scans. The same hemipelvis used for the 2D models was scanned for the development of the three-dimensional FEA model. Initially, the hemipelvis was scanned as it lay in the casting box, from one end of the box to the other. These scans were then processed as described in Section 3.1, and an attempt was made to construct the 3D model from these scans. Superiorly to the acetabulum and in the area of the greater sciatic notch, large changes in the shape of the bone occur. In fact, it is in this area that the bone twists through approximately 60^{o} while also changing from an essentially planar structure to a quadrilateral-hemispherical one. As a result of these geometry changes the 3D subregions that were created in this area using PATRAN were 'illegal', and would have resulted in extremely skew and warped finite elements. Numerous attempts to overcome this problem did not resolve it, and it was decided to rescan the hemipelvis, having obtained a greater knowledge of both the geometry of the bone and the limitations of the PATRAN package.

The hemipelvis was rescanned in such a way that one of the scans passed through the greater sciatic notch and above the level of the acetabulum, and that the ilium was approximately normal to the plane of the scans. This strategy would then allow the transition area described above to be reasonably modelled. A total of 32 layers were scanned. The density of these layers varied according to the position on the bone: the ilium, ischium and pubis were scanned at 8 mm intervals, while the acetabular region was scanned at 4 mm intervals as this was the area of primary interest. Similarly to the 2D case, each layer was digitised and translated into one PATRAN input file. Hence 32 PATRAN input files were created for the complete hemipelvis.

These 32 files were input into PATRAN individually, and patched cortical and cancellous (2D) bone regions were created. PATRAN has a number of options by means of which 3D objects can be created. This involves combining the 2D patches, in various ways, so that they form hyperpatches, which are 3D geometric objects. The ideal situation is that where the hyperpatches are as cuboidal as possible, since this shape results in the best FEA mesh.

Adjacent layers were hyperpatched in a supero-inferior direction from the iliac crest as far as the inferior rim of the acetabulum. A similar approach to hyperpatching the ischial and pubic bone around the obturator foramen would have resulted in many extremely skew elements. To avoid this, a line through the centre of the obturator foramen was used as the common intersection line of a number of planes rotated through these bony regions. As a result, the ischial and pubic bone around the obturator foramen was mapped so that patches could be created in planes normal to the tangent of the bone's curvature at a particular point. These patches were in turn then hyperpatched. This approach resulted in a far better mesh design for this region, compared to the design that would have resulted had the parallel layered approach been used throughout the hemipelvis. The total number of hyperpatches used was approximately 350.

Figure 4.1 shows the mesh plot of the final 3D model. The figure (a) on the left, as in all future plots of this nature, is the hemipelvis viewed from the lateral aspect, but tilted through an angle of 20° to the horizontal. This results in a better view of the roof of the acetabulum. The plot on the right hand side (b) is the medial aspect of the hemipelvis, viewed parallel to the horizontal plane.

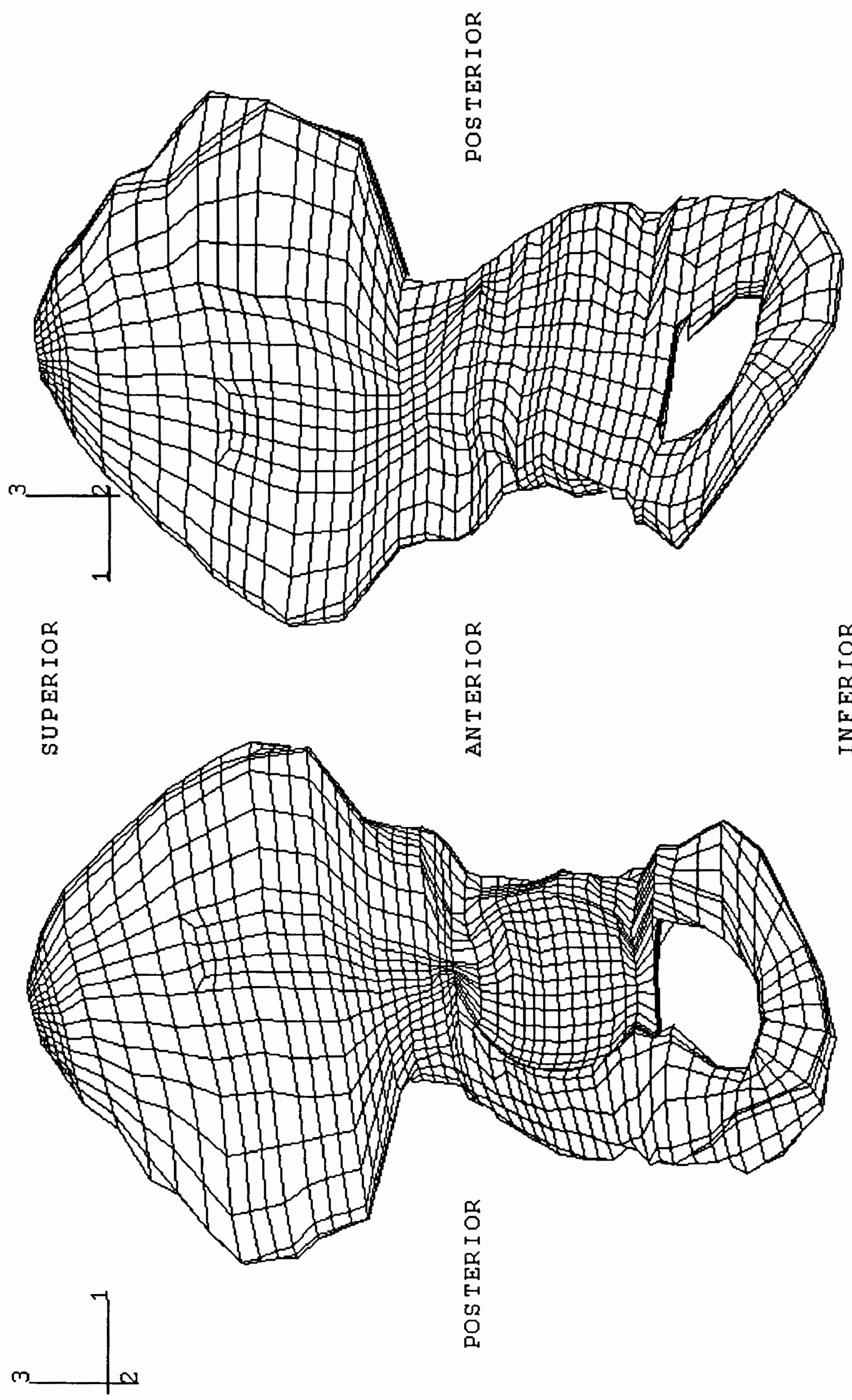

Figure 4.1: MESH PLOT OF THE THREE-DIMENSIONAL HEMIPELVIS MODEL

Only two changes were made regarding the geometry of the hemipelvis. Firstly, the surface of the acetabulum was modelled as being perfectly spherical in order to match the contour of the femoral head, which was assumed completely round. Secondly, the cartilage at the pubis symphysis was added so that the boundary conditions at this point would be realistically simulated (boundary conditions applied directly to the bony margin of the pubis symphysis would make the behaviour here stiffer than is the physical case).

In addition to these modifications, six muscles were modelled: gluteus medius, gluteus minimus, the anterior fibres of gluteus maximus, tensor fasciae latae, iliopsoas and rectus femoris. The implementation of the muscles is described in the section on Numerical Modelling.

A total of 4154 elements was used to construct the FEA model, this number being comprised of eight-noded hexagonal (ABAQUS type C3D8) elements, four-noded interface (ABAQUS type INTER4) elements and two-noded spring (ABAQUS type SPRINGA) elements. These were connected by 4985 nodes. The eight-noded hexagonal elements were made up of 1810 cortical bone elements, 1530 cancellous bone elements, 182 subchondral bone elements and 6 pubis cartilage elements. The two-noded spring elements were used exclusively to model the muscles, and comprised of the following: 9 gluteus maximus, 97 gluteus medius, 96 gluteus minimus, 24 tensor fasciae latae, 160 iliopsoas and 16 rectus femoris. 224 four-noded interface elements made up the remainder of the total elements used.

4.2. BOUNDARY AND LOADING CONDITIONS

Although a large amount of research has been undertaken in the investigation of the load transmission through the pelvis, the influence of the boundary conditions on the 3D biomechanical system of forces has been sparsely and inadequately reported. As a result, this aspect of the hemipelvic mechanics is another aim of this thesis.

The boundary conditions of our model included a fully constrained pubis symphysis and two different sacro-iliac joint constraints: the joint was allowed to move firstly in a supero-inferior direction and secondly antero-posteriorly. In order to model both the cartilage (elastic) and the ligament (stiff) at the pubis symphysis, the cartilage of the pubis symphysis was stiffened to incorporate the mechanical constraints imposed by the ligament. Initially the cartilage was assigned a stiffness of 50 MPa; thereafter this value was included as a variable in the analyses. This approach meant that the actual modelling of the ligament could be avoided, thus allowing for greater flexibility in the development of the optimum constraint conditions.

With these bony constraints applied to the model, a preliminary biomechanical analysis of the hip joint, which included the simulated muscles, was undertaken. From this it was apparent that the muscle tension values reported by other FEA research groups for the single-legged stance are static 'passive' tensions viz. tensions that arise in the muscles as a result of the body weight. In other words, with a specific set of boundary conditions on the hemipelvis, *either* the hip joint reaction load *or* the muscles forces must be included to re-create the loading pattern around the joint. Taking this approach, the muscle insertion points were fully constrained, and the reaction forces at these points should correspond to the muscle forces reported in the literature.

MUSCLE NAME	FORCE (N)
Gluteus medius	640 (500)
Gluteus minimus	320 (330)
Gluteus maximus	45 *
Tensor fasciae latae	135
Iliopsoas	290 (150)
Rectus femoris	580

Table 4.1: Muscle forces from Goel *et al,* 1978. Values in brackets taken from Jacob *et al,* 1976. *This value has been approximated, since the force gluteus maximus exerts is 135N but only the anterior (one third) fibres act as abductors.

Muscle force values for the six muscles that were modelled (gluteus medius, gluteus minimus, anterior fibres of gluteus maximus, iliopsoas, rectus femoris and tensor fasciae latae are taken from Goel *et al* (1978), and are as shown in Table 4.1. The pelvic attachment sites were identified from standard anatomy textbooks and atlases (McMinn & Hutchings, 1977; Grant & Basmajian, 1965; Clemente, 1981); all nodes of the FEA models that fell within an attachment site were assigned to that muscle.

Insertion points for these muscles on the femoral side were taken from the work of Dostal & Andrews (1981), who described the 3D pelvic and femoral attachment sites for 27 muscles acting around the hip. The co-ordinates of the insertion points for the six muscles modelled, were transformed into our reference frame and are shown in Table 4.2. The 'fan-shaped' muscle arrangement that resulted was simulated by the use of spring elements, which are described in Section 4.5. Our hemipelvis is defined as having its origin (co-ordinates (0,0,0)) at the centre of the femoral head, with the positive x-, y- and z-axes pointing anteriorly, medially and superiorly respectively (Figure 4.1). In this, and subsequent figures, 1, 2 and 3 represent x, y and z respectively.

McLeish & Charnley (1970), in their investigation of the abduction forces in one-legged stance, report a resultant hip reaction force of between 1.8 and 2.7 times body weight at an angle to the vertical varying between 7° and 10°. Goel *et al* (1978) describe this reaction force as being distributed uniformly over the acetabular articular surface, with a value of 3.43 times body weight.

MUSCLE NAME	X co-ordinate (mm)	Y co-ordinate (mm)	Z co-ordinate (mm)
Gluteus medius	21.659	-114.329	-6.118
Gluteus minimus	43.659	-110.329	-7.118
Gluteus maximus	30.659	-88.329	-83.118
Tensor fasciae latae	37.659	-56.329	-41.118
Iliopsoas	61.659	-74.329	-416.118
Rectus femoris	82.659	-43.329	-395.118

Table 4.2: Co-ordinates of muscle insertion points extrapolated from Dostal & Andrews, 1981. Distances are relative to the origin at the centre of the femoral head

For the purposes of this study Goel *et al*'s (1978) value was used (2550 N) since their muscle forces were adopted in our analyses. The reaction force was applied in the coronal plane, at an angle of 20° to the vertical.

4.3. MATERIAL MODELS

The material properties used in the 3D models that assumed a purely elastic material are the same as those used in the 2D analyses. The values are as shown in Table 3.1.

In order to gain some insight into the adaptive bone remodelling (ABR) that occurs in the pelvis, use has been made of an algorithm that is based on the remodelling hypotheses reported by Huiskes *et al* (1987). The specific algorithm used is explained below, while some of the remodelling theories that are currently in use are discussed in Appendix B.

The remodelling process is written as a density rate of change equation, while the tissue strain energy density (SED), and not the apparent strain energy density (Huiskes *et al*, 1987), is used as the driving factor in the process (Starke *et al*, 1993).

The governing equation for the remodelling of the bony material is:

$$\frac{\partial \rho}{\partial t} = K(U_b - U_n) \tag{1}$$

where:

density $\rho = \gamma\phi$ (trabecular density x volume fraction of solids)

actual bone SED $U_b = \frac{U_0}{\phi^m}$ (apparent bone SED / volume fraction of solids to the power of m)

apparent bone SED $U_o = \frac{1}{2}\,\sigma(\varepsilon, E)\,\varepsilon$ (half stress x strain)

isotropic Young's modulus $E_i = A\rho^B$ (A, B are constants) t = time

K = a time integration constant

The values for the constants and integration factors used in these analyses are as follows:

K = 0.03#

U_n = 1125 N/m^5 *

γ = 1900 kg/m^3

m = 4.5 †

A = 2.572-06 ‡

B = 3 ‡

#: The time integration constant is a model dependant parameter; this value gave the smoothest convergence for the model.

*: This value was calculated from Goel *et al*, 1978. The values for the principal stresses for each section of the pelvis were summed and then averaged over the volume of the bone.

†: If m=1, then one obtains the situation where the relationship between σ and ε is hyperbolic viz. as the strain increases, so the Young's modulus decreases. Clearly this does not reflect the physiologic condition. However, the choice of m, such that it is greater than B, results in an 'optimal' σ/ε relationship which is exponential in nature. In this way the remodelling routine is more stable numerically (Harrigan and Hamilton, 1992). The value used here (4.5) was obtained by choosing the 'best' curve obtained for this σ/ε relation for a number of differing m-values (the 'best' range of values was 3.5 to 4.5). (Starke *et al*, 1993).

‡: These values obtained from Carter and Hayes, 1977. The value for 'A' has been converted into S.I. units, assuming a strain rate of 1.56E-03.

The analysis takes place over three time steps: first a relaxation step, followed by a load step and finally a remodelling step. During the load step, the load is applied in increments until a fully converged, full-load condition is reached. At first, the initial density is passed into the program (submitted by the user) and E_i is then also computed, using the user-defined constants A and B. During the remainder of the load step, for a positive strain increment, the stress and strain (and hence the actual and apparent SED's) are updated, and the constitutive stress/strain relation is re-evaluated. During each increment of the following (remodelling) step the constitutive stress/strain relation is again re-evaluated, the new stress vector is calculated, the values for the actual and apparent SED's are calculated and the new Young's modulus is calculated, based on the new SED. At the end of each increment the state variables E_i, bone density, apparent SED and actual SED are then updated. The remodelling process continues until the density throughout the bone reaches a fully converged state, according to equation (1) above.

The remodelling algorithm also checks to ensure that the bone densities do not exceed physiologic limits. In these analyses, the upper and lower limits for the bone densities have been set at different limits. The cortical bone, subchondral bone and cancellous bone all had a lower density limit of 200 kg/m^3, and an upper limit of 1850, 1600 and 1000 kg/m^3 respectively. The lower and upper bone densities translate to stiffness values of 23.2 MPa, 18.3 GPa, 11.9 GPa and 2.9 GPa. It should be noted that the theory applied in these analyses deals specifically with changes in SED as a feedback to the density change, and any geometric variations in the bone is not included in the feedback path viz. surface remodelling of the bone is not taken into account in this algorithm. The Poisson's ratio used by the analysis program is assumed to be independent of bone material property changes, and is therefore constant.

4.4. NUMERICAL MODELLING AND IMPLEMENTATION

4.4.1. Hemipelvis and muscles

The FEA mesh that was generated within PATRAN was converted into ABAQUS format. Since the hemipelvis had been scanned so that the mesh development was the best possible, it was not necessarily in a physiologic position. Measurements were taken of bony landmarks on the hemipelves of two skeletons in order to obtain the angles that were required for the physiologic position to be found in the numerical model. These angles were then calculated on the numerical model so that a measure of the difference between the two could be obtained. The nodal co-ordinates defining the model were then simply transformed (translated and rotated) within ABAQUS, by means of the SYSTEM card (Appendix D). This process ensured that the resultant hip joint reaction force could be correctly applied to the hemipelvis.

This system specification is set up by giving the global co-ordinates of three points in the local system: the origin of the local system, a point on the local x-axis and a point in the (x,y) plane of the local system, on (or near) the local y-axis. This transformation affects only the input of nodal co-ordinates entered after the SYSTEM card - it has no effect on output, boundary conditions or load specifications. The transformations are switched off by inserting a data-free SYSTEM card. Appendix D illustrates these ABAQUS cards. It also shows the definition of the six muscle insertion point nodes as being input before the SYSTEM card; this is so since these nodes are already in the local system and have been input manually viz. were not converted from PATRAN.

As in the 2D models, the femoral head was included in the analysis, thereby avoiding the problem of applying an assumed load distribution on the acetabulum. It was modelled by means of a RIGID SURFACE, with SOFTENED CONTACT at the interface. The femoral head was assumed to be perfectly spherical which made it perfectly congruent with the rearranged surface of the acetabulum. Since the 3D spherical rigid surface had to be modelled, a different approach was required. A perfect sphere of diameter 54 mm was generated in PATRAN, and then meshed with triangular stress-displacement shell elements, ABAQUS type STRI3 (1998 elements made up of 1001 nodes). PATABA converted this information into nodal co-ordinates and element connectivities. This information was then read into the analysis as part of the rigid surface definition. ABAQUS now reads the nodal co-ordinates as vertices on the surface of the sphere, with the element connectivities defining the surface outward normals, which all point in the same direction. A Bezier surface is then fitted to the surface vertices. Figure 4.2 illustrates a simple example of a Bezier surface, which is analogous to a spline in two dimensions. Appendix D shows how this RIGID SURFACE was used within ABAQUS.

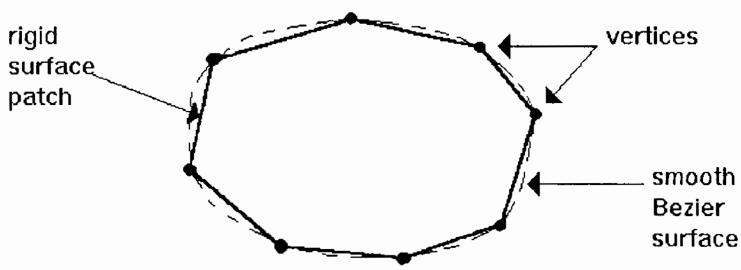

Figure 4.2: Diagram illustrating the development of a Bezier surface

The interface between the femoral head and the acetabulum was modelled using ABAQUS type INTER4 elements, which are analogous to the INTER2 elements used in the 2D analyses in that they allow small relative sliding to occur between the contacting surfaces. They are specific for use in a 3D analysis, where the contacting surfaces are eight-noded hexagonal elements. Figure 4.3 indicates how these elements are used, with the numerical integration being performed midway between the element nodes. This interface was assumed to be frictionless, as in the 2D analyses.

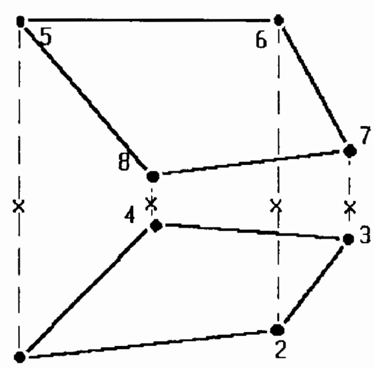

Figure 4.3: Diagram illustrating the ABAQUS INTER4 element. *x* represents the integration points for each of the nodes.

SOFTENED CONTACT - as described in Chapter 3 - was used between the femoral head and the acetabulum to simulate the conditions that exist at that interface.

SPRINGA elements were used to model the six muscles (Appendix D). A SPRINGA element is defined as an axial spring between two nodes, whose line of action is the line joining the two nodes. This line of action is free to rotate in a large displacement analysis. When the area of the muscle attachment was decided upon, the nodes that fell within that area became one of the two nodes that defined each SPRINGA element. The second node defining the element is the node representing the insertion point of the muscle on the femur, as explained in Section 4.2. Thus a large muscle such as the gluteus medius has a much larger number of SPRINGA elements assigned to it than a smaller one, such as tensor fasciae latae. Figure 4.4 shows the areas of attachments of these muscles on the surface of the hemipelvis. Unfortunately the post-processing application used (ABAQUS POST) represents each individual spring element in a three-dimensional manner which makes for a confusing image that virtually obscures the hemipelvis itself; hence these elements are not graphically recorded.

The static analysis, with an assumed elastic material, is performed in two time steps. The first step, the relaxation step, has all constraint areas completely fixed which enables the interface between the acetabulum and the femoral head (rigid surface) to establish favourable contact. This step takes place with no load being applied. Following the successful completion of the relaxation step, the full load is applied to the model. At the same time, the constraints on the model are altered to those required. This is performed by specifying that the old boundary conditions are no longer relevant and that new ones are now being imposed.

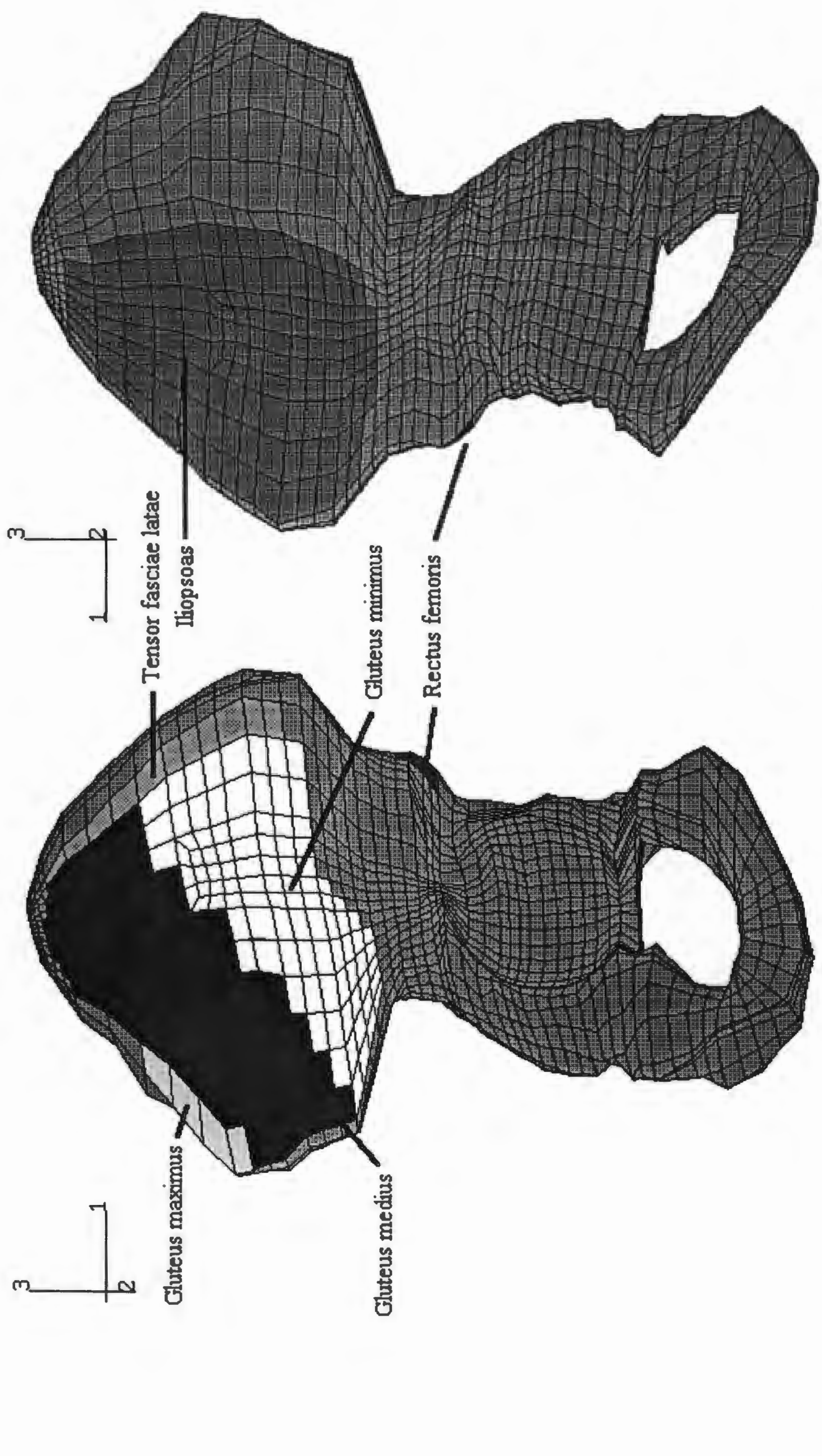

Figure 4.4: MUSCLE ATTACHMENT SITES ON THE HEMIPELVIS

The necessary fine adjustments required in the development of a good working model of the hemipelvis were then started. These adjustments included the spring k-values used for the muscles and the boundary conditions imposed on the hemipelvis. As mentioned earlier (Section 4.2), the muscle insertion nodes were fully constrained, the rationale here being that the reaction force measured at these nodes would correspond to each of the muscle forces reported in the literature. According to this approach, no specific spring k-value could then be deemed to be either right or wrong, but could only be said to be correct for the purposes of this study when the correct nodal reaction force was obtained.

An integral part of the boundary condition problems posed by the hemipelvis are the bony constraints themselves. As a result, a change in a muscle k-value would result in a changed reaction force at both the sacro-iliac joint and the pubis symphysis. Conversely, a change in the boundary condition at, say, the sacro-iliac joint would result in a change in the reaction forces registered at all of the muscle insertion nodes.

This system of balanced and counterbalanced constraints was examined over a series of "runs", which totalled approximately 100. The pertinent results from this study into the boundary conditions of the hemipelvis are presented in the following section.

Once the constraints of the problem had been finalised for the purely elastic model, the same model was used with the bone remodelling algorithm discussed in Section 4.3. The algorithm is implemented in ABAQUS by replacing the ELASTIC card by a USER MATERIAL card, which specifies that a user algorithm must be used as input for the material behaviour. The user constants required for this algorithm (12) are input in the first step, the relaxation step, of the analysis, as part of the USER MATERIAL definition. The remodelling occurs after a full load situation has been reached, and thus the bone remodelling itself occurs as the third step in the analysis.

4.4.2. Cup implantation

The modelling of the implanted (3D) cup into this intact model of the hemipelvis posed a variety of problems. Initially, the Duraloc porous-coated cup was measured and a geometric model was created in PATRAN (Figure 4.5 (a) and (b)). Some alterations were made to the exterior surface of the cup, in the form of radii that were created between the three pegs and the hemispherical dome of the main cup surface. This was done in order to create a smooth transition between the pegs and the hemisphere so that the Bezier surface defining the outer backing of the cup would not present numerical problems at sharp corners. However, in order to mesh this surface accurately enough, approximately 17000 elements with over 10000 nodes were required. The number of problems that this type of surface would create, not to mention the vast amount of computer time needed to analyse it, meant that an alternative was needed.

As a consequence of the above, a new approach was taken towards creating an "artificial" up. The basis of the new idea being pursued is that the three pegs of the cup act as beams fixed at one end (the hemispherical cup) and inserted into a soft material (bone). By simulating only the hemispherical part of the cup as a rigid surface, the question posed was whether beam elements, with their nodes numerically tied to this rigid surface, could reasonably approximate the effect of the cup pegs. This approach was taken and it was found to be a reasonably easy one to implement. The pegs were defined as ABAQUS type B31 beam elements, which are two-noded beams in 3D space. It is possible to specify various cross-sections of the beam elements, one of these cross-section options being a solid circular one. Thus the actual dimensions of the peg can be modelled by specifying the radius of the pegs as the radius of the beam elements. This ensures that the I-values are the same in both cases.

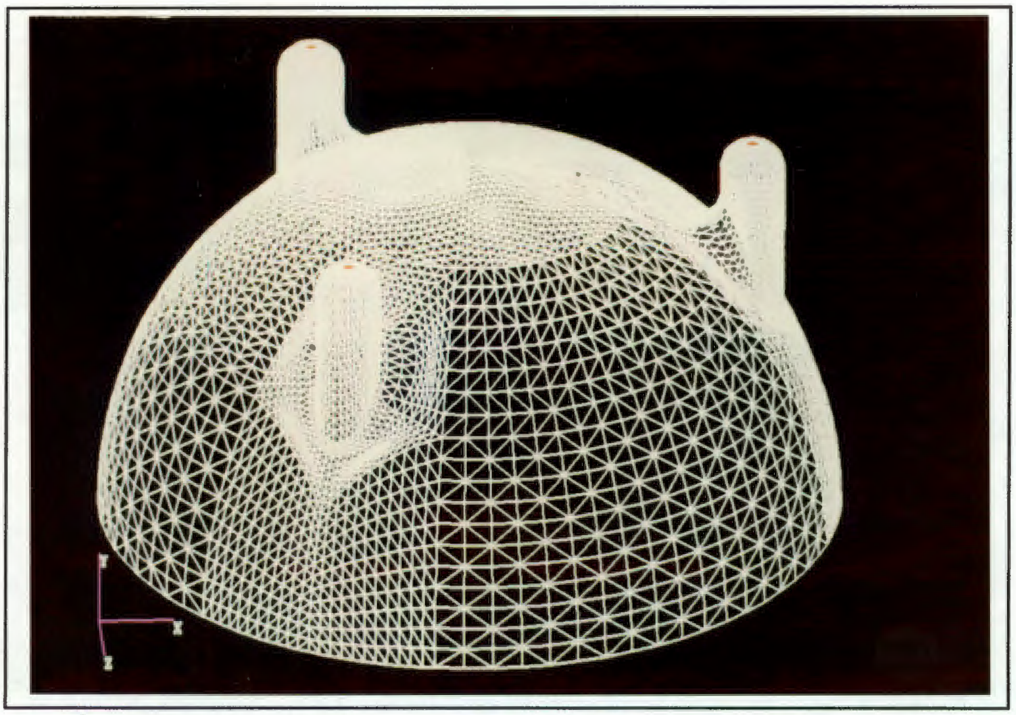

Figure 4.5 (a): Mesh plot of the pegged cup developed in PATRAN (hidden lines removed). Note the radii at the top of the pegs and at the junction between the pegs and the hemispherical dome of the cup, which were included to avoid sharp corners for the optimum Bezier fit.

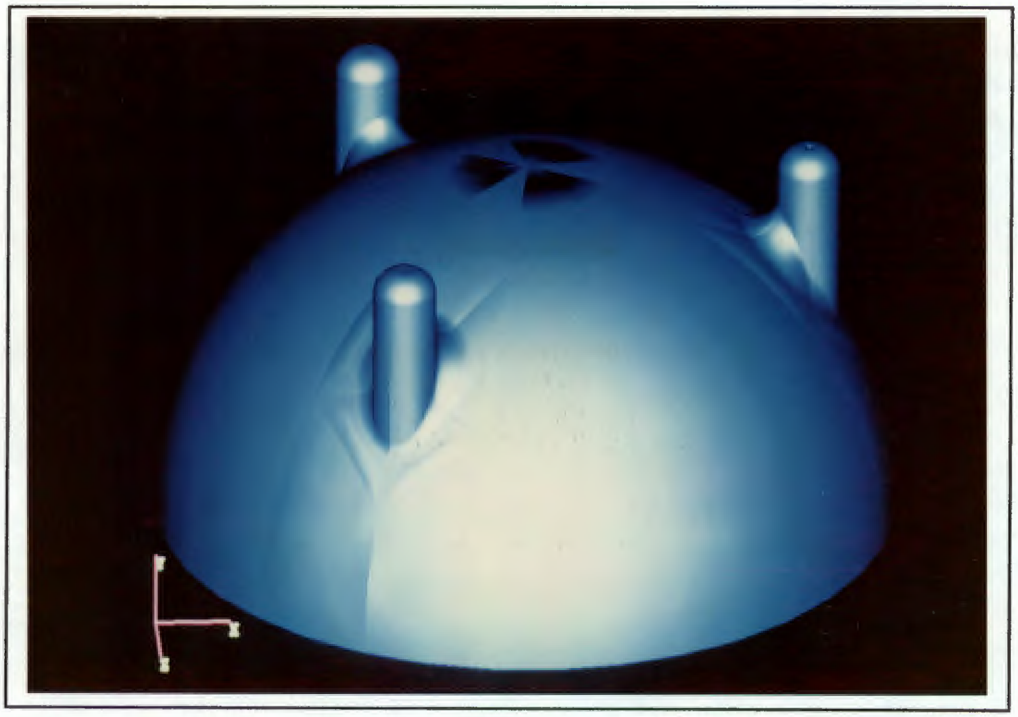

Figure 4.5 (b): The same view of the cup as in Figure 4.5 (a), seen as a shaded image here.

The final part of the modelling is that of tying the beam elements to the rigid surface of the cup. This is possible by using the MPC (Multi-Point Constraint) option in ABAQUS. This option allows constraints to be imposed between different degrees of freedom of the model. One of the specific sub-options of this option is the TIE option, which makes all active degrees of freedom equal at two nodes, or between a group of nodes and one other node. The latter was used, and hence all of the beam nodes were tied to the rigid surface reference node. Physically, this means that if the rigid surface (and therefore its reference node) translates by an amount (x,y,z), all of the beam nodes attempt to move through the bone by an amount (x,y,z).

This modelling approach was attempted on a 3D test model of dimensions 100 x 100 x 100 mm, together with another model of same dimensions which included a base-peg arrangement similar to that seen in the prosthetic cup. The latter model consisted of a metal plate, representing the metal backing of the cup, with a peg protruding into the bone. No attempt was made in either model to scale the cancellous and cortical bone region depths. In order to ensure that exactly the same loading was applied to both models, a rigid surface was applied to the underside of the metal plate in the second model, and the loading applied to this rigid surface. Both models are constrained along the top edge of the cancellous bone, while the loading is applied vertically to the rigid surface reference nodes.

4.5. RESULTS

In this section the results from three main areas of investigation are presented: 1) the model constraints; 2) adaptive bone remodelling; and 3) pegged cup modelling method.

4.5.1. Model constraints

An initial analysis was performed that modelled both the pubis symphysis and the sacro-iliac joint as being completely fixed, and without any of the muscles included in the analysis. It was found that the hemipelvis as a whole was very much over constrained, with most of the stress concentrations occurring in the sacro-iliac joint region.

A series of runs was then performed that retained the same bony constraints, but also included the muscle elements in the analyses. Although this constraint definition is not in accordance with those discussed Goel & Svensson (1978) concerning the investigations by Weisl (1954a,b; 1955) (Section 4.2.1), they were again performed to create a better understanding of the model constraints. As stated in earlier, the objective of these runs is to create the necessary amount of loading at the muscle insertion nodes in order to properly simulate the overall loading pattern of the hemipelvis. The resultant reaction forces at the muscle insertion nodes are plotted for the varying spring k-values for each individual analysis in Figure 4.6. Table 4.3 presents the exact values of these reaction forces and the corresponding spring stiffnesses. The reference muscle forces indicated in the Key of Figure 4.6 are those from Goel *et al* (1978), and represent the reaction force that should be present at the insertion node for that particular muscle. It should be noted that the stiffness assigned to the pubis symphysis cartilage for this series of runs was 50 MPa.

Figure 4.6: Graph of reaction force at the six muscle insertion nodes for different muscle spring k-values used, with the sacro-iliac joint free to displace vertically.

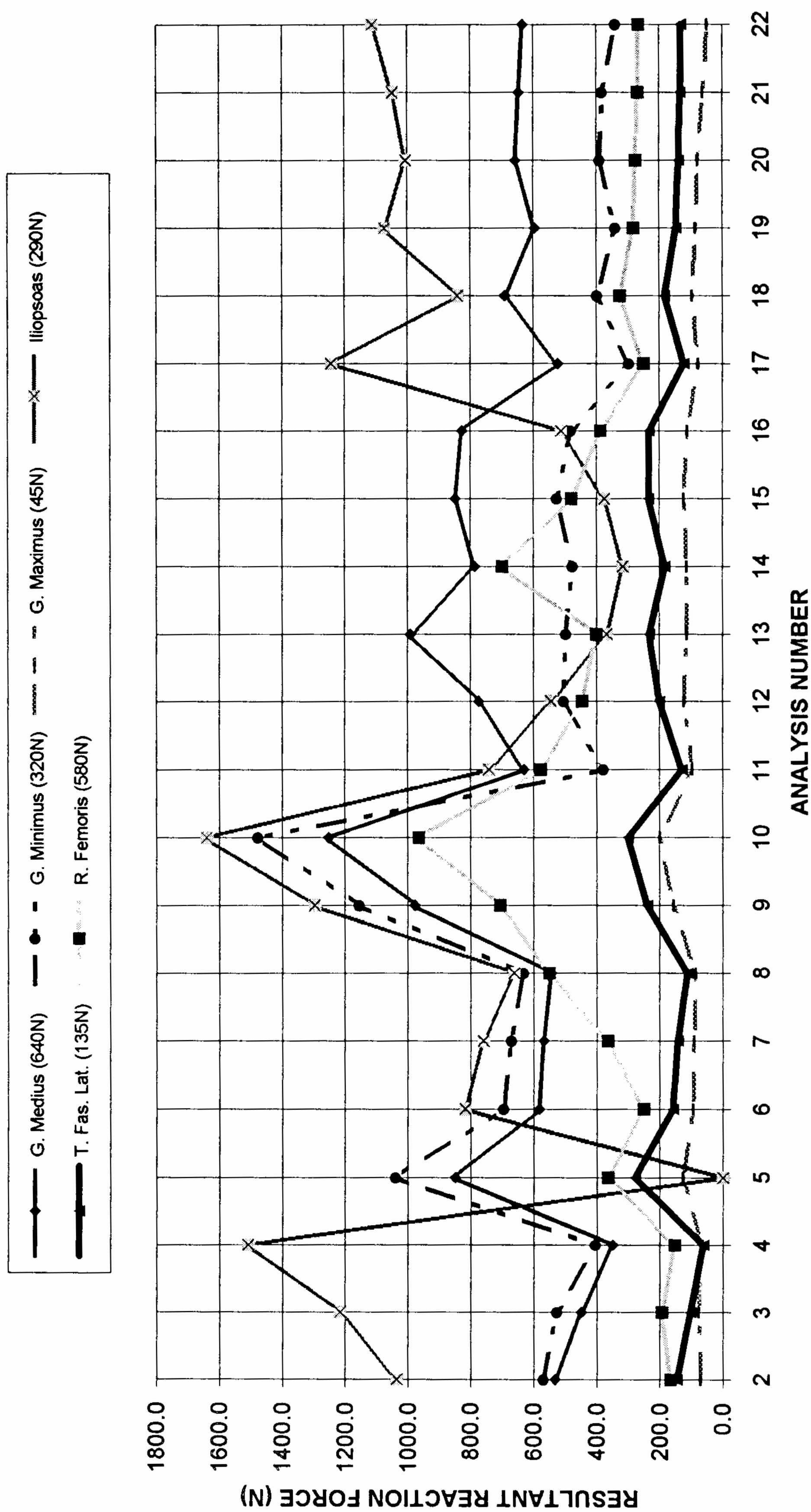

Muscle	R-force	k-values		Muscle	R-force	k-values		Muscle	R-force	k-values
	(N)	(N/m)			(N)	(N/m)			(N)	(N/m)
	RUN2				**RUN9**				**RUN16**	
G. Medius	533.1	60000		G. Medius	341.2	75000		G. Medius	827.5	100000
G. Minimus	569.8	60000		G. Minimus	707.6	150000		G. Minimus	480.1	50000
G. Maximus	70.6	60000		G. Maximus	98.7	150000		G. Maximus	111.2	100000
Iliopsoas	1035.9	50000		Iliopsoas	723.8	75000		Iliopsoas	510.4	25000
T. Fas. Lat.	145.6	60000		T. Fas. Lat.	126.2	150000		T. Fas. Lat.	233.2	100000
R. Femoris	166.0	60000		R. Femoris	567.7	500000		R. Femoris	386.8	150000
	RUN3				**RUN10**				**RUN17**	
G. Medius	448.8	150000		G. Medius	462.6	150000		G. Medius	521.9	100000
G. Minimus	527.3	150000		G. Minimus	870.7	200000		G. Minimus	296.6	50000
G. Maximus	76.6	150000		G. Maximus	75.6	150000		G. Maximus	76.9	100000
Iliopsoas	1216.0	150000		Iliopsoas	587.8	75000		Iliopsoas	1243.2	100000
T. Fas. Lat.	102.3	150000		T. Fas. Lat.	98.5	150000		T. Fas. Lat.	122.6	100000
R. Femoris	194.3	150000		R. Femoris	526.6	500000		R. Femoris	250.3	150000
	RUN4				**RUN11**				**RUN18**	
G. Medius	349.0	150000		G. Medius	629.2	150000		G. Medius	690.2	100000
G. Minimus	403.8	150000		G. Minimus	377.9	75000		G. Minimus	397.3	50000
G. Maximus	63.6	150000		G. Maximus	95.2	150000		G. Maximus	95.9	100000
Iliopsoas	1509.5	250000		Iliopsoas	741.2	75000		Iliopsoas	840.7	50000
T. Fas. Lat.	62.8	150000		T. Fas. Lat.	129.2	150000		T. Fas. Lat.	182.9	100000
R. Femoris	153.2	150000		R. Femoris	576.3	500000		R. Femoris	325.3	150000
	RUN5				**RUN12**				**RUN19**	
G. Medius	849.0	150000		G. Medius	773.2	200000		G. Medius	593.7	100000
G. Minimus	1039.7	150000		G. Minimus	503.8	100000		G. Minimus	339.3	50000
G. Maximus	126.0	150000		G. Maximus	122.3	200000		G. Maximus	85.0	100000
Iliopsoas	0	0		Iliopsoas	544.4	50000		Iliopsoas	1072.5	75000
T. Fas. Lat.	278.7	150000		T. Fas. Lat.	201.3	200000		T. Fas. Lat.	148.0	100000
R. Femoris	363.1	150000		R. Femoris	445.3	300000		R. Femoris	282.2	150000
	RUN6				**RUN13**				**RUN20**	
G. Medius	581.3	150000		G. Medius	990.9	200000		G. Medius	656.4	125000
G. Minimus	694.7	150000		G. Minimus	497.4	75000		G. Minimus	388.6	62500
G. Maximus	93.3	150000		G. Maximus	113.1	150000		G. Maximus	78.1	100000
Iliopsoas	818.1	75000		Iliopsoas	366.7	25000		Iliopsoas	1005.4	75000
T. Fas. Lat.	158.5	150000		T. Fas. Lat.	232.1	150000		T. Fas. Lat.	137.8	100000
R. Femoris	249.5	150000		R. Femoris	401.2	200000		R. Femoris	274.2	150000
	RUN7				**RUN14**				**RUN21**	
G. Medius	566.8	150000		G. Medius	785.9	150000		G. Medius	646.0	125000
G. Minimus	671.2	150000		G. Minimus	475.7	75000		G. Minimus	380.6	62500
G. Maximus	90.3	150000		G. Maximus	113.3	150000		G. Maximus	62.0	80000
Iliopsoas	758.9	75000		Iliopsoas	316.0	25000		Iliopsoas	1047.5	80000
T. Fas. Lat.	141.2	150000		T. Fas. Lat.	183.5	150000		T. Fas. Lat.	133.2	100000
R. Femoris	363.0	250000		R. Femoris	698.3	500000		R. Femoris	268.4	150000
	RUN8				**RUN15**				**RUN22**	
G. Medius	542.9	150000		G. Medius	847.7	150000		G. Medius	632.9	120000
G. Minimus	632.5	150000		G. Minimus	524.5	75000		G. Minimus	338.5	55000
G. Maximus	85.3	150000		G. Maximus	123.1	150000		G. Maximus	47.3	60000
Iliopsoas	660.7	75000		Iliopsoas	374.1	25000		Iliopsoas	1112.1	85000
T. Fas. Lat.	112.6	150000		T. Fas. Lat.	233.6	150000		T. Fas. Lat.	132.0	100000
R. Femoris	550.8	500000		R. Femoris	479.2	250000		R. Femoris	265.3	150000

Table 4.3: Muscle stiffness values for the series of analyses where the sacro-iliac joint is allowed to displace vertically.

The initial observation to be made concerning these results is that the force measured in iliopsoas muscle is far above that derived experimentally. In fact, the reaction forces shown are completely unrealistic, since this muscle is primarily a flexor of the hip joint and only a secondary adductor. In the phase of gait when the active muscles are primarily the abductors one would expect reduced activity from the flexors, extensors and adductors. Thus this muscle force, in the single-legged stance phase of gait, should be, intuitively, within an order of magnitude of the reference force described in Table 4.1 and shown in Figure 4.6 viz. approximately 290 N. Due to the balance of forces acting around the hip joint this elevated iliopsoas force brings about a reduction in other flexor forces, as can be seen for the values in rectus femoris.

It can be seen from Figure 4.6 that this problem could not be overcome throughout this first series of runs, no matter what muscle spring stiffnesses were used (Table 4.3). At this stage it was felt that obvious problems existed with the bony constraints as they had been applied to the hemipelvis. A new series of runs was started, in which the sacro-iliac joint was constrained now in the vertical direction, but allowed to displace in the antero-posterior direction. The stiffness (Young's modulus) of the pubis symphysis cartilage was also introduced as a variable. The reaction forces for this new series are shown in Figure 4.7, while the muscle spring stiffnesses and pubis symphysis cartilage stiffness are indicated in Table 4.4.

Up to RUN38 it was never quite clear whether the proposed reaction force of 640 N could be reached for the gluteus medius muscle. What was clear, however, from RUN38 itself was that this reaction force was easily decreased by a decrease in spring stiffness, while a large increase in the spring stiffness did not result in a correspondingly large increase in the reaction force. In all the runs up to this point it had been hoped that the actual spring stiffness value would be reflected in the reaction forces i.e. that the springs would, in a limited manner, reflect the physiologic behaviour of the muscles themselves. As this was not the case, the spring stiffness was increased up to a value of 1000000 N/m in RUN39.

Figure 4.7: Graph of reaction force at the six muscle insertion nodes for different spring k-values used, with the sacro-iliac joint allowed to displace in the antero-posterior direction.

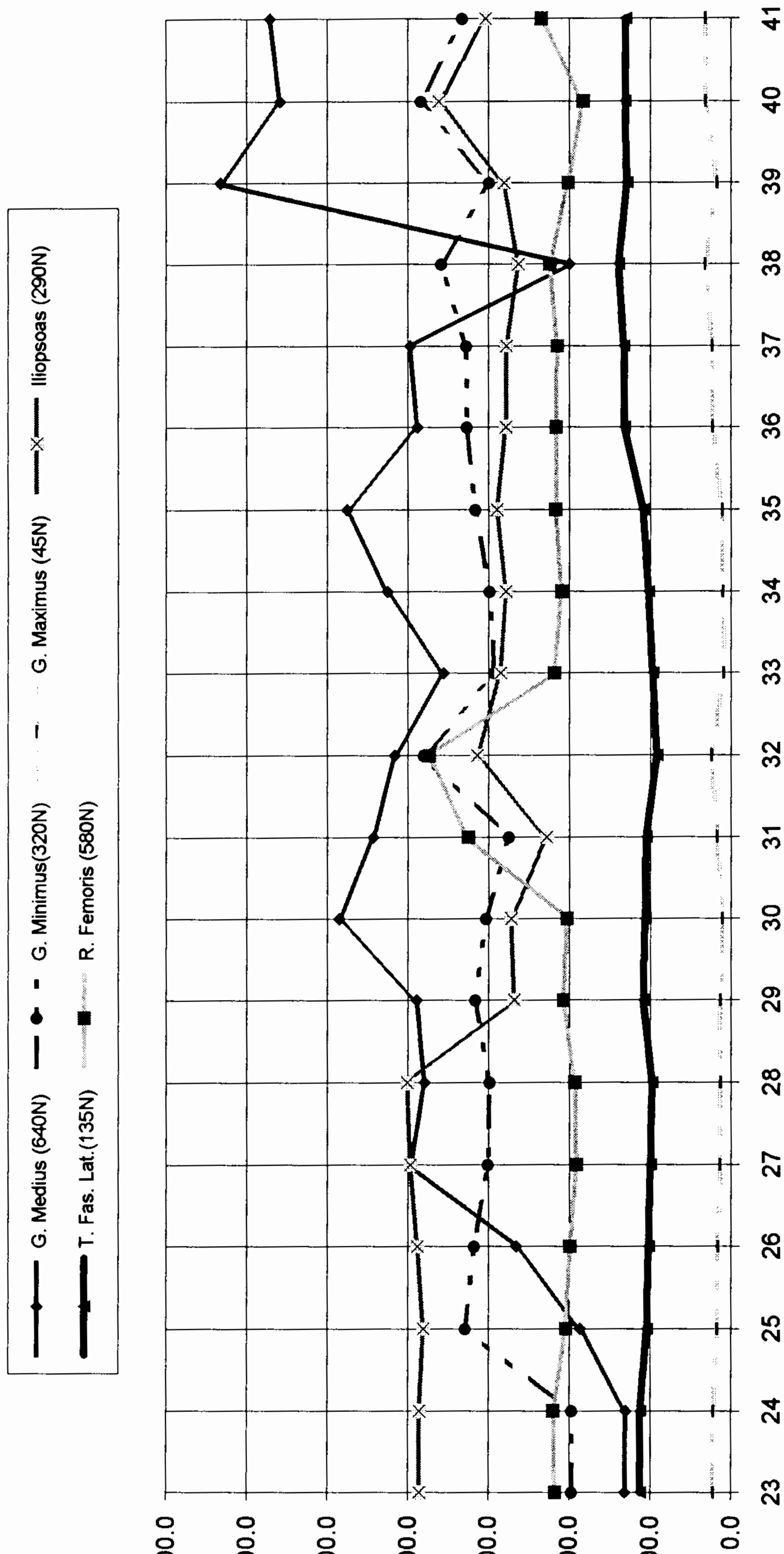

Muscle	**R-force**	**k-values**	**Muscle**	**R-force**	**k-values**	**Muscle**	**R-force**	**k-values**
	(N)	**(N/m)**		**(N)**	**(N/m)**		**(N)**	**(N/m)**
	RUN23	(1000)		**RUN30**	(250)		**RUN37**	(200)
G. Medius	131.88	119000	G. Medius	485.29	700000	G. Medius	396.84	500000
G. Minimus	196.48	52000	G. Minimus	303.25	100000	G. Minimus	327.32	100000
G. Maximus	21.87	56000	G. Maximus	10.96	56000	G. Maximus	23.24	100000
Iliopsoas	385.69	85000	Iliopsoas	271.83	50000	Iliopsoas	277.58	50000
T. Fas. Lat.	112.68	102000	T. Fas. Lat.	106.38	102000	T. Fas. Lat.	132.60	125000
R. Femoris	217.61	150000	R. Femoris	202.71	150000	R. Femoris	214.91	150000
	RUN24	(500)		**RUN31**	(250)		**RUN38**	(250)
G. Medius	130.49	119000	G. Medius	442.70	700000	G. Medius	199.78	200000
G. Minimus	197.12	52000	G. Minimus	274.80	100000	G. Minimus	358.67	100000
G. Maximus	21.99	56000	G. Maximus	17.52	100000	G. Maximus	32.03	100000
Iliopsoas	386.25	85000	Iliopsoas	228.40	50000	Iliopsoas	263.02	50000
T. Fas. Lat.	112.18	102000	T. Fas. Lat.	105.18	125000	T. Fas. Lat.	139.20	125000
R. Femoris	219.61	150000	R. Femoris	325.32	300000	R. Femoris	224.51	150000
	RUN25	(500)		**RUN32**	(250)		**RUN39**	(500)
G. Medius	186.23	200000	G. Medius	416.34	1000000	G. Medius	633.00	1000000
G. Minimus	328.96	100000	G. Minimus	380.08	200000	G. Minimus	299.42	100000
G. Maximus	17.89	56000	G. Maximus	24.44	200000	G. Maximus	17.15	100000
Iliopsoas	380.74	85000	Iliopsoas	313.73	100000	Iliopsoas	280.99	50000
T. Fas. Lat.	103.88	102000	T. Fas. Lat.	91.48	175000	T. Fas. Lat.	128.90	125000
R. Femoris	204.31	150000	R. Femoris	373.62	500000	R. Femoris	201.71	150000
	RUN26	(500)		**RUN33**	(250)		**RUN40**	(500)
G. Medius	265.84	300000	G. Medius	355.26	700000	G. Medius	558.70	1000000
G. Minimus	318.09	100000	G. Minimus	292.38	100000	G. Minimus	383.53	150000
G. Maximus	16.10	56000	G. Maximus	9.13	56000	G. Maximus	31.92	200000
Iliopsoas	388.35	85000	Iliopsoas	285.28	50000	Iliopsoas	361.23	75000
T. Fas. Lat.	102.38	102000	T. Fas. Lat.	97.08	102000	T. Fas. Lat.	130.90	150000
R. Femoris	198.91	150000	R. Femoris	218.11	150000	R. Femoris	182.61	150000
	RUN27	(500)		**RUN34**	(50)		**RUN41**	(500)
G. Medius	396.28	500000	G. Medius	425.13	700000	G. Medius	571.23	1000000
G. Minimus	300.59	100000	G. Minimus	298.16	100000	G. Minimus	332.26	125000
G. Maximus	13.52	56000	G. Maximus	10.08	56000	G. Maximus	31.40	200000
Iliopsoas	397.38	85000	Iliopsoas	278.11	50000	Iliopsoas	303.85	62500
T. Fas. Lat.	99.61	102000	T. Fas. Lat.	102.09	102000	T. Fas. Lat.	130.40	150000
R. Femoris	191.11	150000	R. Femoris	209.41	150000	R. Femoris	234.32	200000
	RUN28	(250)		**RUN35**	(100)			
G. Medius	379.31	500000	G. Medius	475.62	700000			
G. Minimus	298.83	100000	G. Minimus	316.44	100000			
G. Maximus	13.20	56000	G. Maximus	11.00	56000			
Iliopsoas	400.69	85000	Iliopsoas	289.91	50000			
T. Fas. Lat.	97.83	102000	T. Fas. Lat.	108.39	102000			
R. Femoris	193.51	150000	R. Femoris	216.71	150000			
	RUN29	(250)		**RUN36**	(150)			
G. Medius	388.84	500000	G. Medius	388.39	500000			
G. Minimus	316.41	100000	G. Minimus	326.29	100000			
G. Maximus	12.72	56000	G. Maximus	22.93	100000			
Iliopsoas	268.35	50000	Iliopsoas	278.75	50000			
T. Fas. Lat.	108.38	102000	T. Fas. Lat.	131.60	125000			
R. Femoris	207.31	150000	R. Femoris	216.11	150000			

Table 4.4: Muscle stiffness values for the series of analyses that have the sacro-iliac joint able to displace in the antero-posterior direction. It is important to note the extra variable in this data, the stiffness of the pubis symphysis cartilage, which is shown (in MPa) in brackets after the run name.

The final reaction forces for the six muscles, in Newtons (N), were as follows: gluteus medius, 571.2; gluteus minimus, 332.2; anterior fibres of gluteus maximus, 31.4; iliopsoas, 303.9; tensor fasciae latae, 130.4; and rectus femoris 234.3. Figures 4.8 and 4.9 show the maximum principal stress concentrations in the cortical and cancellous bone respectively, for these muscle reaction forces. The maximum principal tensile stresses in the cortical and cancellous bone were 9.29 and 1.29 MPa respectively. These values correspond to a percentage of the ultimate tensile strengths for the bone regions of 5 and 48% respectively. The corresponding compressive stresses are 1.43 and 0.105 MPa respectively. The tensile stress peaks occur in the superior acetabular region, while the compressive stresses occur primarily superiorly to the acetabular rim itself.

Components of the reaction force at the pubis symphysis were measured as being -105.94, -372.03 and 31.92 N in x, y and z directions. The resultant of these three components is 386.82 N. The components of the reaction force mean that this area of the hemipelvis is physically attempting to move anteriorly with a force of 106 N, laterally with a force of 372 N and inferiorly with a force of 32 N.

Components of the reaction force at the sacro-iliac joint were measured as being 72.29 and -1020.08 N in y and z respectively (this joint was allowed to displace in the x-direction, hence no reaction force). Physically this means that the joint was attempting to move medially with a force of 72 N and superiorly with a force of 1020 N. The resultant force vector on this joint is calculated as being 1022.6 N.

Displacements of the hemipelvis occurred in two manners, as can be seen in Figure 4.10. Firstly, the hemipelvis, when viewed from the lateral aspect, tended to rotate about the acetabulum in an anti-clockwise direction (Figure 4.10 (a)). As a result, the ilium displaced posteriorly and the ischium and pubis rotated anteriorly. Secondly, the supero-medial displacement of the acetabular and inferior iliac regions (Figure 4.10 (b)) occurs in the direction of principle loading of the hip joint resultant reaction force.

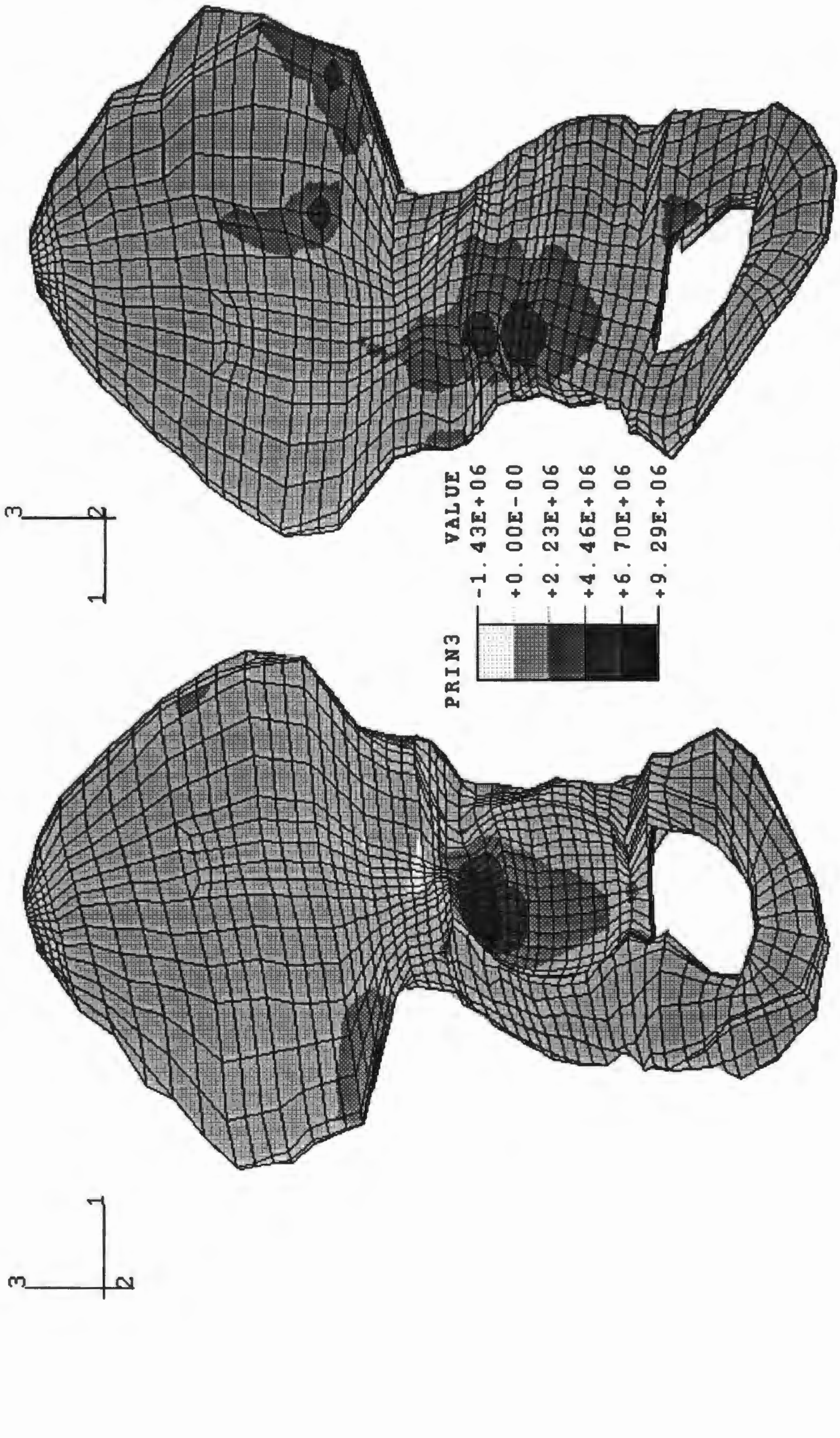

Figure 4.8: MAXIMUM PRINCIPAL STRESSES IN THE CORTICAL BONE

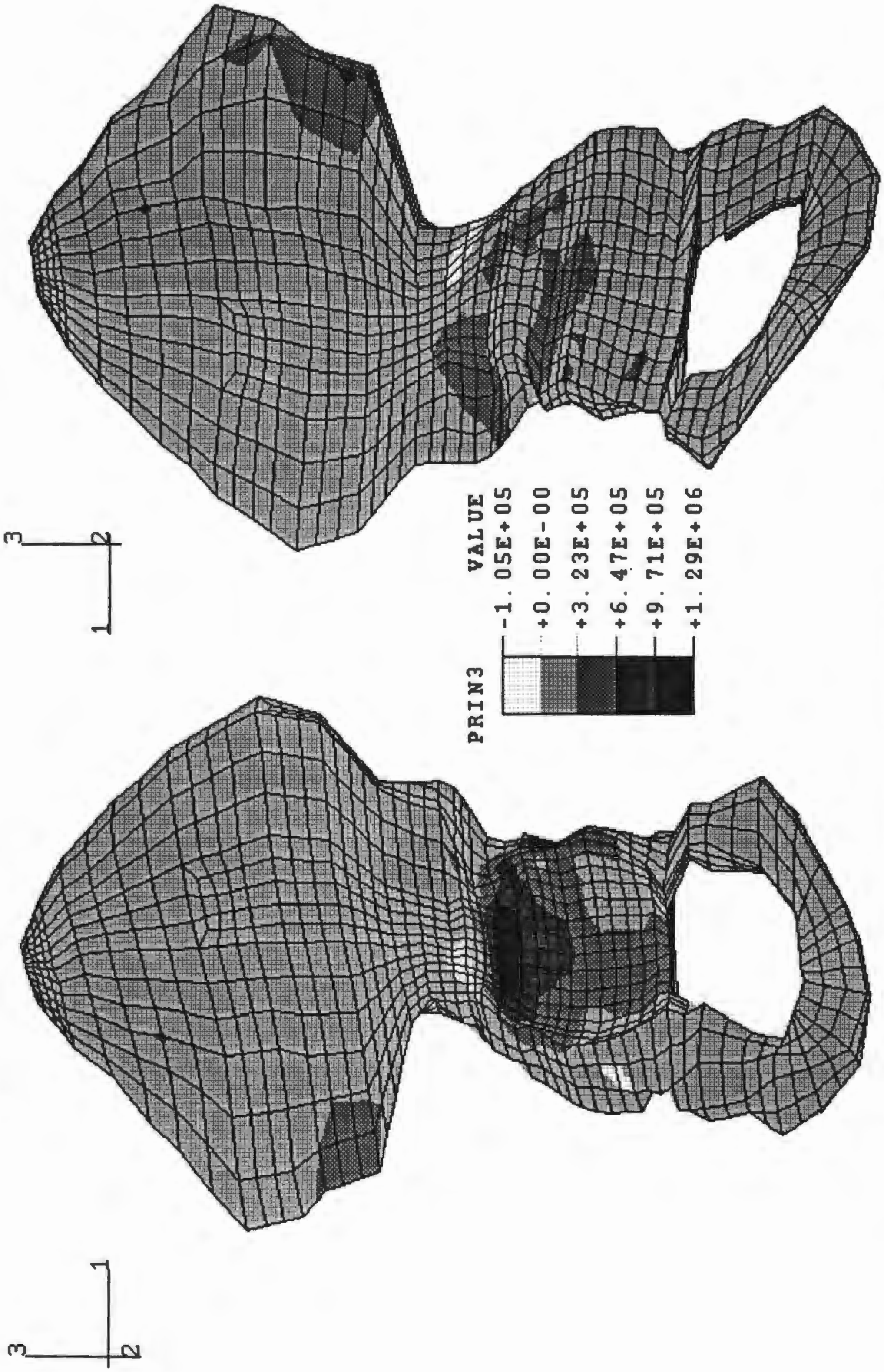

Figure 4.9: MAXIMUM PRINCIPAL STRESSES IN THE CANCELLOUS BONE

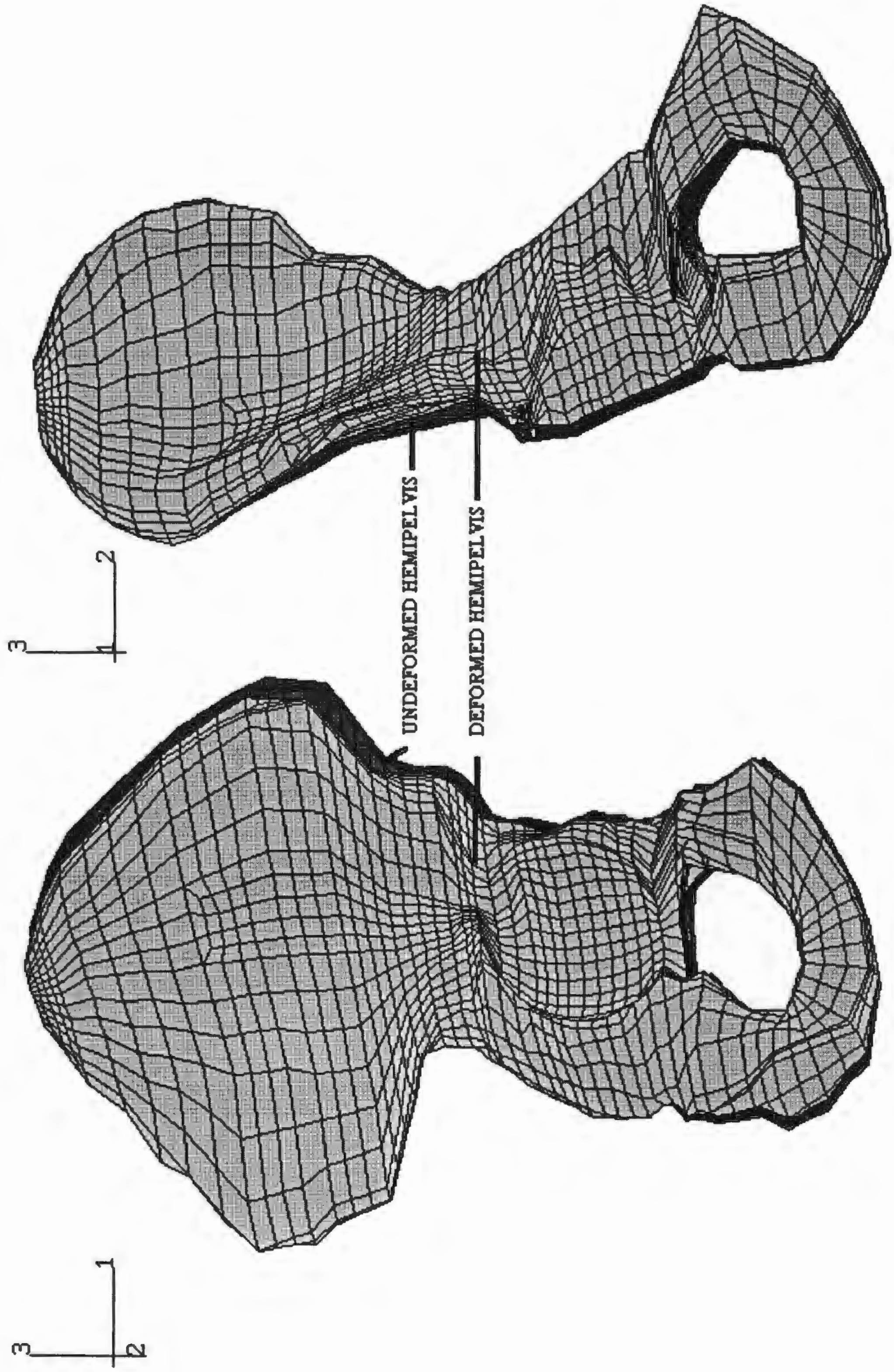

(a) (b)

Figure 4.10: DISPLACED SHAPE OF THE HEMIPELVIS
(magnification = 75)

4.5.2. Adaptive bone remodelling

The elastic material properties for the bone were substituted by a bone remodelling algorithm as described in Section 4.3. Figure 4.11 illustrates the convergence behaviour of eleven randomly chosen cortical bone elements. These were selected over the entire surface of the hemipelvis, and are representative of elements that undergo both increase and decreases in bone density. The graph indicates the change in bone density over time for these 11 elements. It should be noted that element number 4 remains at the maximum density, 1850 kg/m^3, for the duration of the analysis and element number 9 stiffens up slightly to approach 1800 kg/m^3. The remainder of the element bone densities converge to a final value of between 1600 and 900 kg/m^3. The convergence curve for element 10 shows that the density decreases quite rapidly to approximately 1450 kg/m^3, and then stiffens again to a maximum value of approximately 1500 kg/m^3. From this diagram it is clear that the results obtained are indicative of the final bone densities.

Figure 4.12 shows these final bone densities in the cortical bone. The cortical bone density distribution corresponds with the overall stresses seen in the hemipelvis, since the expected increase in densities can be observed in and above the superior region of the acetabulum, and also on the medial arch that leads from the quadrilateral acetabular surface to the sacro-iliac joint. The two main areas of decreasing density in the cortical bone, relative to the input starting density of 1730 kg/m^3, are the superior iliac region and almost all of the posterior aspect of the ischium.

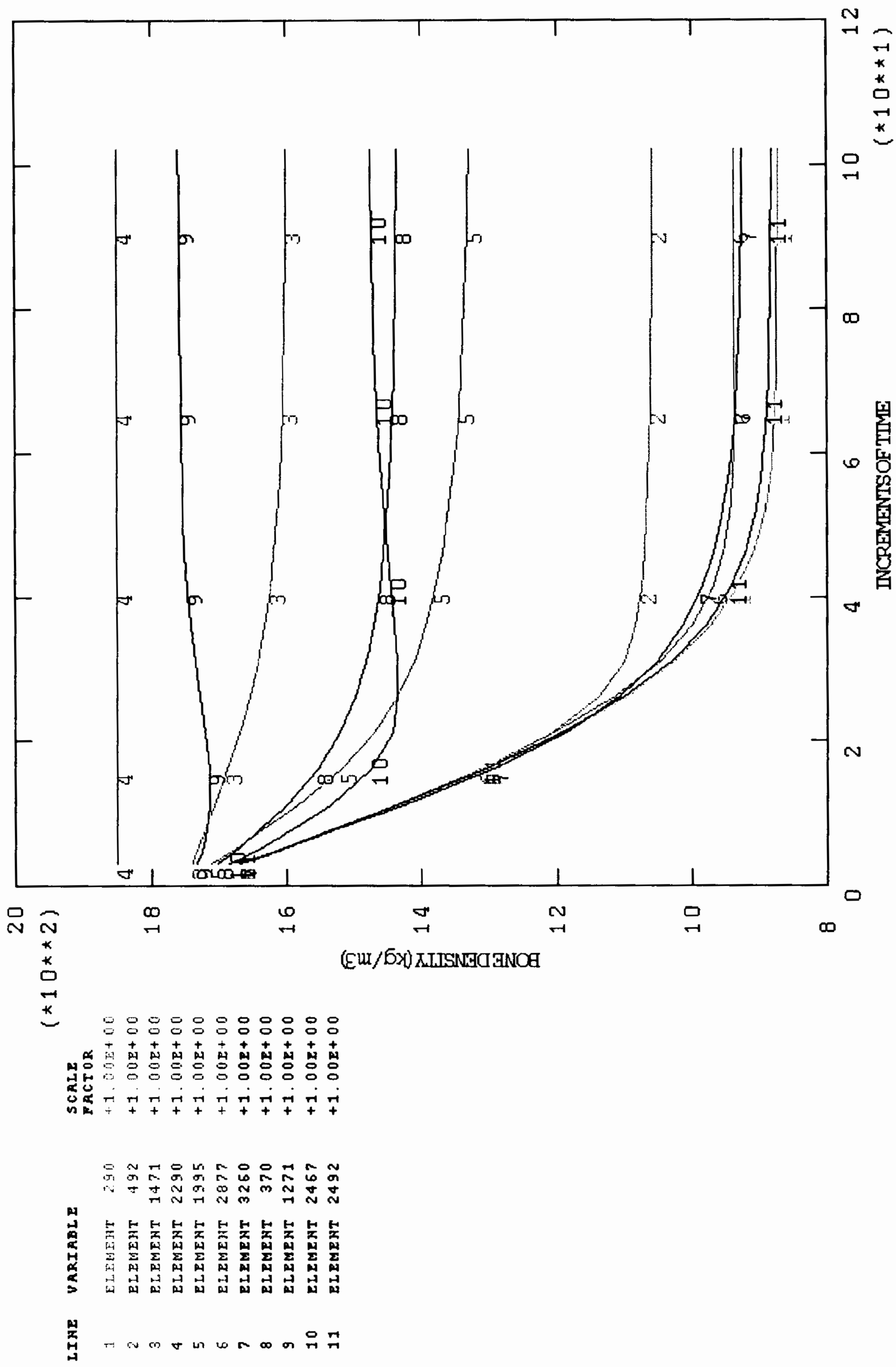

Figure 4.11: CORTICAL BONE DENSITY CONVERGENCE

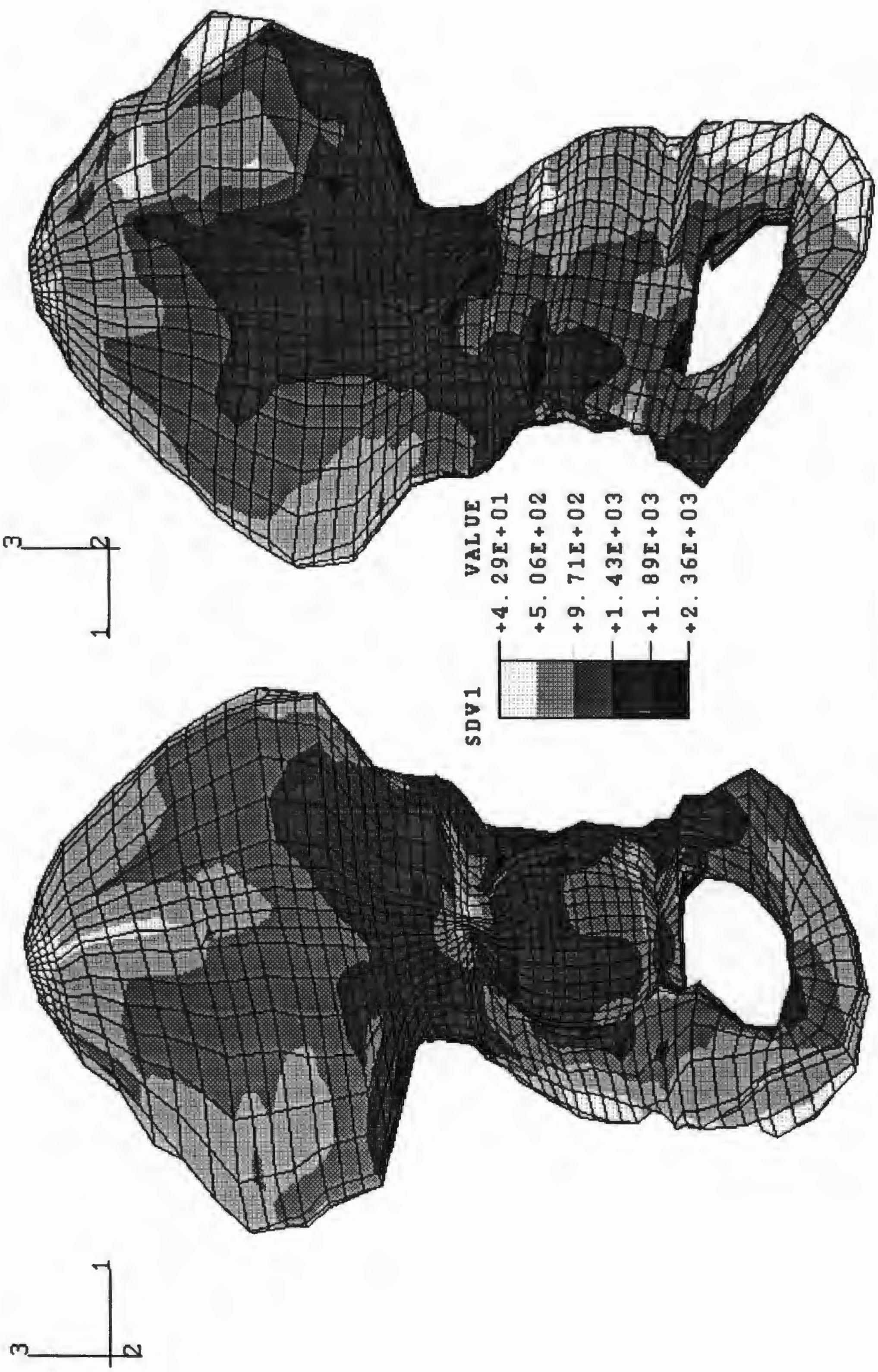

Figure 4.12: BONE DENSITY DISTRIBUTION IN THE CORTICAL BONE

Figure 4.13 indicates the convergence of the bone densities for different elements over the surface of the cancellous and subchondral bone. Both of the upper bone density limits are clearly identifiable as 1000 and 1600 kg/m^3 respectively. The cancellous bone densities (Figure 4.14) shows similar behaviour to the cortical bone, especially around the acetabulum. It can be seen that most of this bone stiffens to the upper bound of 1000 kg/m^3 except in the upper iliac region and the posterior ischium, which correspond to the least dense areas of the cortical bone. This plot also shows the bone densities for the subchondral bone. The superior half of the acetabulum, which bears most of the immediate load, has its corresponding subchondral bone stiffening to the upper bound of 1600 kg/m^3, while the lower half has a gradual decrease in bone density to that of the maximum found in the cancellous bone, 1000 kg/m^3.

Figures 4.12 and 4.14 indicate the increased density of the bone under the main load-bearing areas, which are essentially the roof/superior rim of the acetabulum, and the inferior section of the ilium immediately adjacent to the acetabulum. In particular, the anterior rim of the acetabulum has remodelled to the maximum prescribed density, which is illustrated very well in the X-ray of the dry hemipelvic bone (Figure 4.15). Furthermore, the cancellous bone in this area assumes a very uniform bone density distribution, which becomes less dense towards the superior aspect. Comparison with the X-ray again is very favourable.

The region of the ilium immediately superior and adjacent to the greater sciatic notch has remodelled to the maximum density value as well. The predicted increase in bone density of the medial cortical bone along the arcuate line (the ridge extending from the medial quadrilateral surface superiorly towards the sacro-iliac joint) extends superiorly to the vertical border of the sacro-iliac joint, which corresponds well with the radiographic appearance of the hemipelvic bone (Figure 4.15).

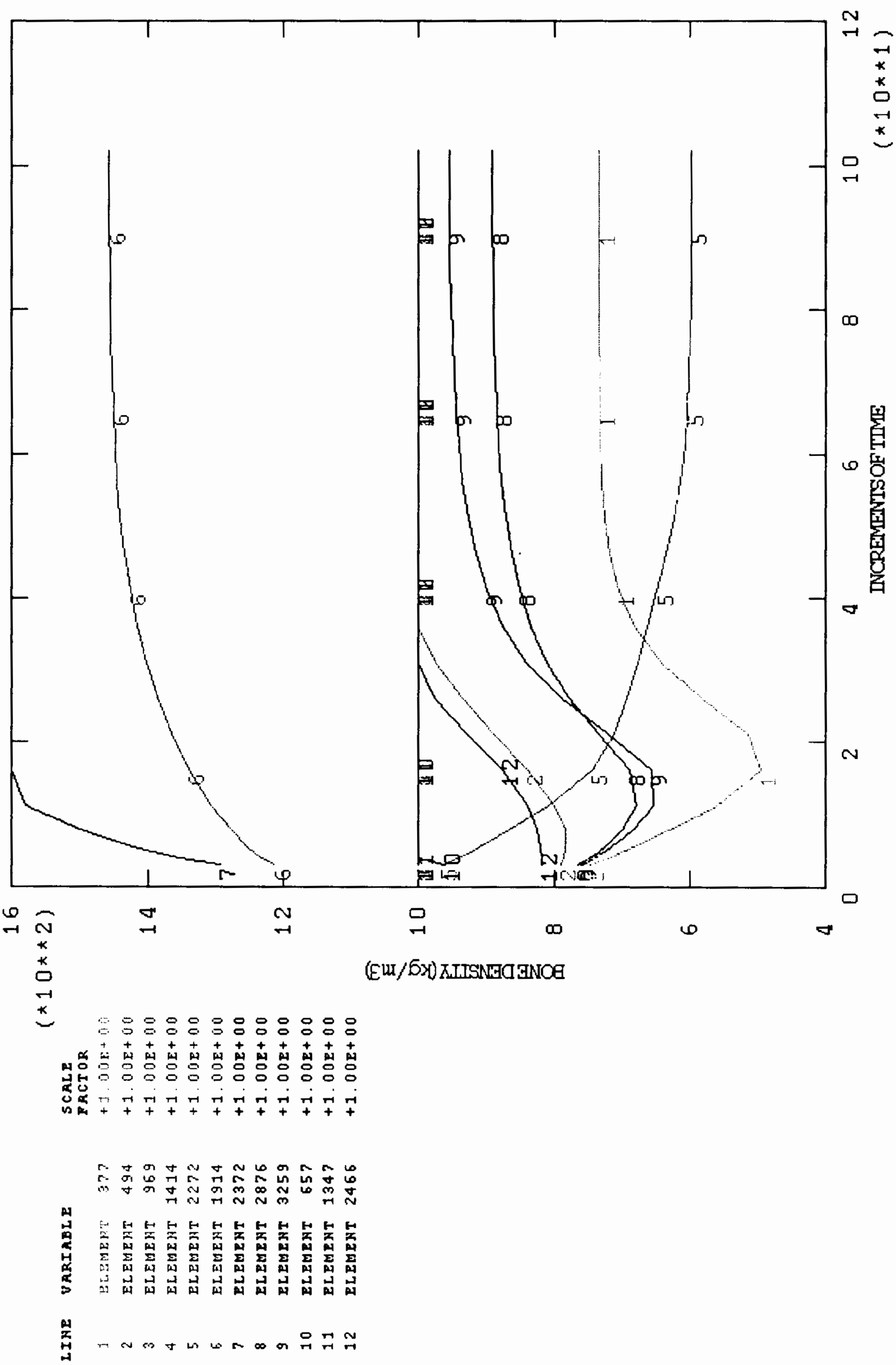

Figure 4.13: CANCELLOUS BONE DENSITY CONVERGENCE

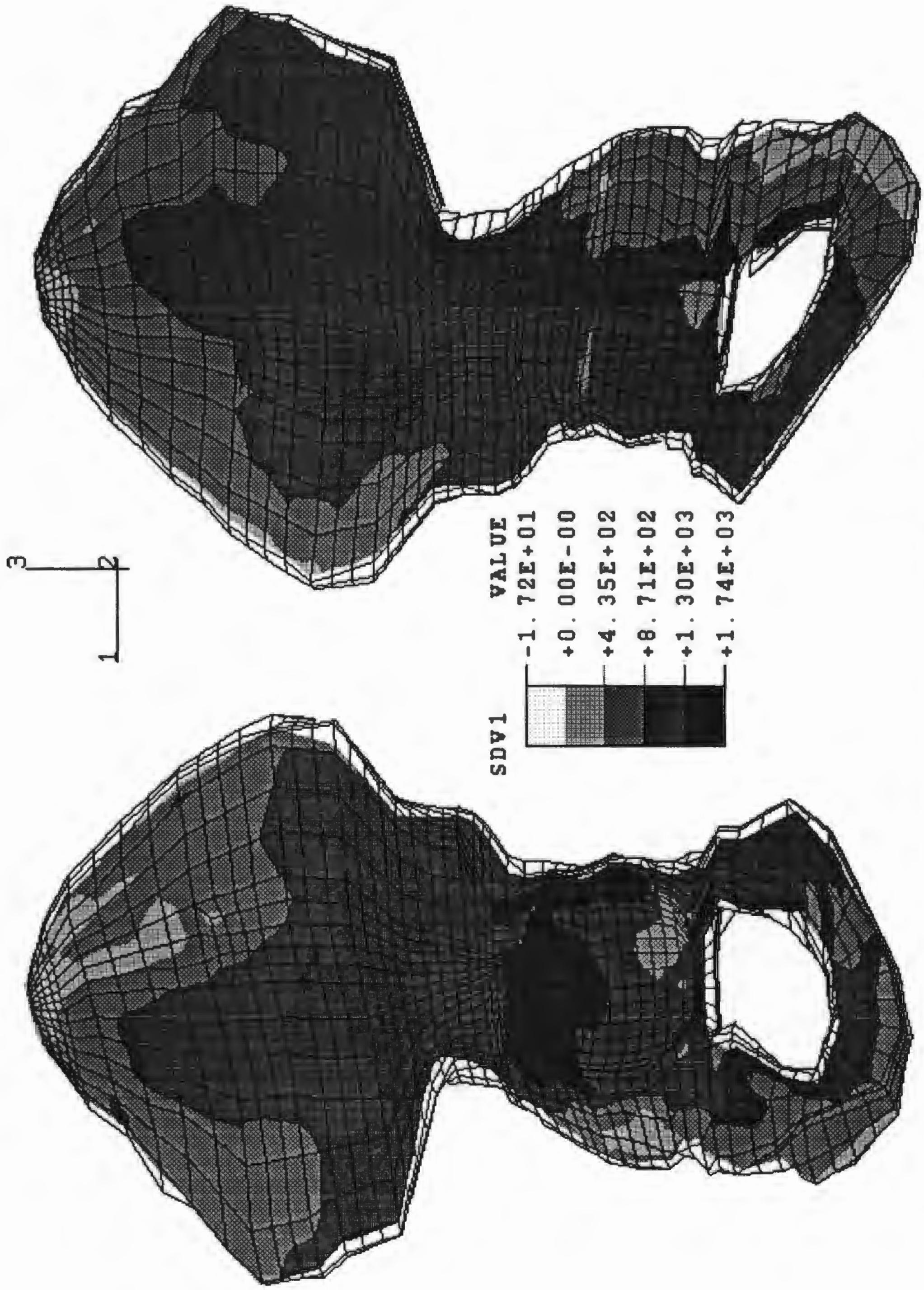

Figure 4.14: BONE DENSITY DISTRIBUTION IN THE CANCELLOUS BONE

Figure 4.15: X-ray of dry right hemipelvis showing bone density distribution

4.5.3. Cup implantation

The results for the two 3D test models that were developed are shown in Figure 4.16. The models are both viewed from the cup side of the bone, looking up through a section through the cortical and the cancellous bone, in the x - z plane. The features representing the cup and peg have themselves been omitted from these diagrams so the bone stresses could be more easily compared. Figure 4.16 (a) is the test model of the pegged cup, and Figure 4.16 (b) is a diagram of the test model simulating the cup and peg arrangement by means of beam elements and a rigid surface.

The stress contours shown indicate that the overall difference in tensile and compressive stress magnitudes are reasonably similar (15.6 % and 16.3 % difference respectively) and that a direct comparison between the two models is favourable. However, the effect of the beam element, when compared to the proper peg model, shows poor correlation in the local stress distribution around the peg.

It is evident from the plots that the degree of complexity of the two models is markedly different, even in these two relatively simple models. As an example of this, the peg model (Figure 4.16(a)), by necessity, consisted of 602 elements, while the beam simulation model (Figure 4.16(b)) consisted of only 44 elements.

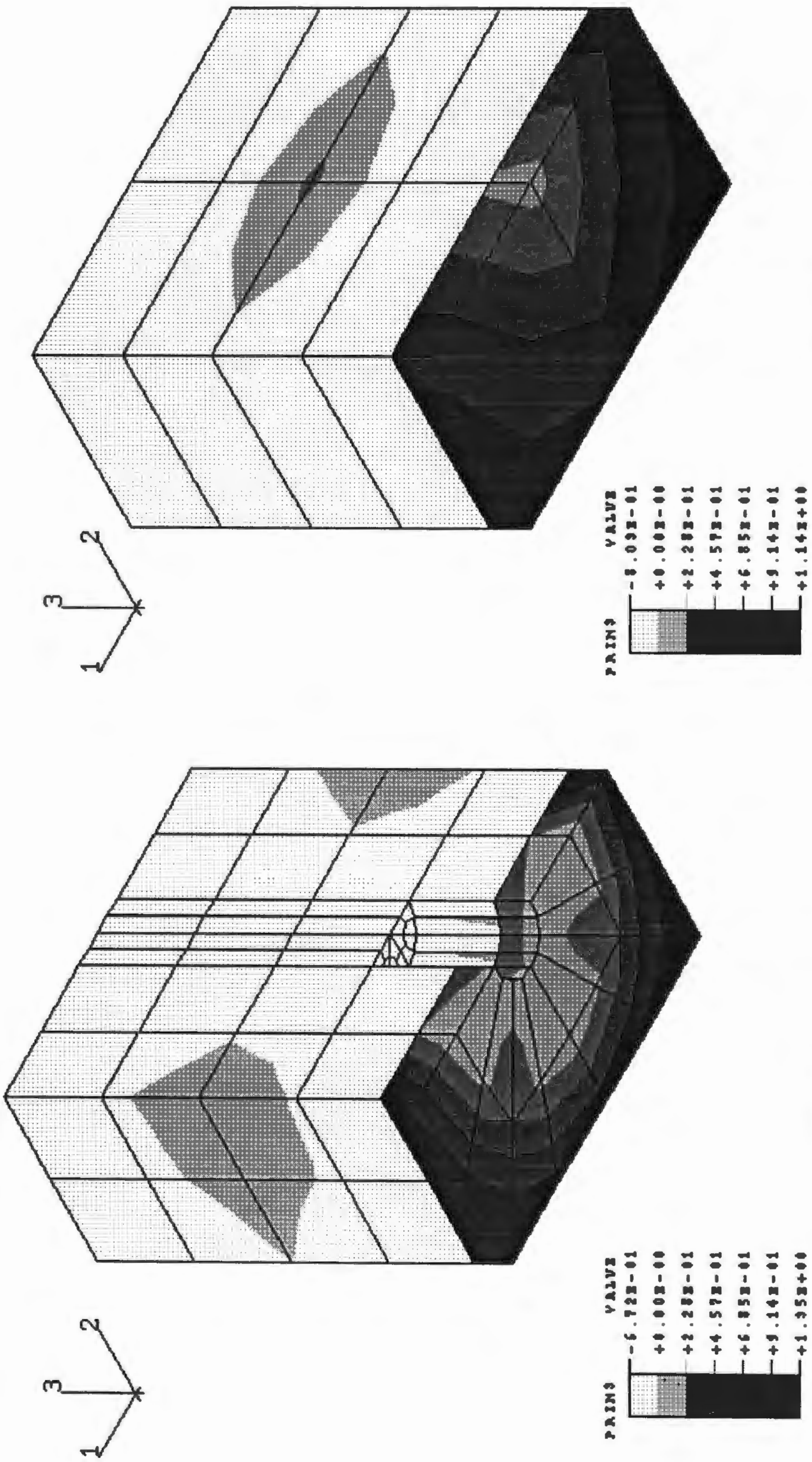

peg model

(a)

beam model

(b)

Figure 4.16: MAXIMUM PRINCIPAL STRESSES IN THE 3D PEG AND BEAM TEST MODELS

4.6. DISCUSSION

The modelling of a complex 3D object such as the human hemipelvis often entails a number of assumptions. Some of these assumptions, such as the modification of the acetabular surface and the addition of the pubis symphysis, have already been mentioned. At the outset, it is important to note that a fundamental aim of FEA analysis is to minimise the number of elements in the model being analysed, without compromising the accuracy of the results. The choice of which muscles acting around the hip joint to include in the bone modelling will obviously have a bearing on the predicted results. In this type of biomechanical analysis the greater number of muscles that are simulated will result in a closer approximation of the real structure. However, the assigning of accurate values of the individual muscle forces is of paramount importance, yet this information is unfortunately not always available. In this study six muscles were modelled, for two reasons. Firstly, the four abductor muscles (gluteus medius & minimus, the anterior fibres of gluteus maximus and tensor fasciae latae) are central to a representative model of the forces acting around the hip joint, since without these muscles single-legged stance would be difficult if not impossible. The other two muscles (iliopsoas: primarily a flexor and a secondary adductor, and rectus femoris: purely a flexor) were included because quantitative information regarding the forces that they exert is available.

From the biomechanics of the whole pelvis during single-legged stance it is known that the centre of gravity shifts away from the supporting leg, accompanied by a slight tilting of the pelvis due to the action of the abductor muscles. In so doing, the mechanics of the pelvis change from being a symmetrical system of forces (normal, or two-legged stance) to an asymmetrical one (single-legged stance). Simulating the behaviour of the whole pelvis by means of a model which only represents half of the system being analysed, as is the case in our model, presents a modelling problem.

The problem can be attempted by modelling both the symmetric and asymmetric conditions, and then reaching the final result by superposition of the two stress values at each integration point. This is in itself problematic since it is nigh impossible to conclude from each of the individual results whether the modelling approach is correct, and hence there is no way of rectifying any errors that may exist with the model. Another method would involve the inclusion of the sacrum into the model, so that the body weight, and not the hip reaction force, could be used as the primary load condition. Again, major problems were foreseen with this approach since not only would the interface at the sacro-iliac joint have to be numerically modelled but the constraints on the opposite side of the sacrum would have to be applied.

Having acknowledged that while the simulation of this asymmetric problem as a symmetric one is an oversimplification, it is clear that there is no easy compromise to be found in terms of the modelling approach. Either the hemipelvis is modelled as a symmetric problem, or it becomes necessary to model the entire pelvis. In terms of the most accurate simulation, this latter option is the ideal. However, it would also involve a great deal of detailed knowledge of the sacro-iliac joint micromotion and hence detailed modelling of this region. It would also be numerically very expensive. For the above reasons the hemipelvis was modelled as a symmetric problem and the results are discussed in terms of this condition.

It has been shown that the constraints on the hemipelvis can be divided into two groups. The primary constraints are those applied to the bony surface of the hemipelvis, and the secondary constraints are those applied to the muscle insertion nodes. Goel *et al* (1978), Hansen & Koeneman (1991), Dalstra & Huiskes (1990, 1992) and Schüller *et al* (1993) describe their hemipelvic models as being fully constrained at the pubis symphysis. Grant & Basmajian (1965) described the pubis symphysis as being two opposed bony surfaces which are coated with hyaline cartilage and joined both by fibrocartilage and by the strong inferior pubic ligament which provides further stability. As a result of this consensus between anatomists and biomechanists on the constraints at the pubis symphysis, these previously applied constraints were used in our model.

Hansen & Koeneman (1991), Dalstra & Huiskes (1990, 1992) and Schüller *et al* (1993) report having constrained the sacro-iliac joint from all possible movement. However, Goel and Svensson (1978) report on the findings of Weisl (1954a,b;1955) regarding the behaviour of the sacro-iliac joint, and stated that there is a small antero-posterior movement between the sacrum and the ilium. This movement is not one of rotation about a fixed horizontal axis but rather one where the cranial part of the joint moves a greater distance than the caudal part. Also, Grant & Basmajian (1965) demonstrated this antero-posterior movement of the sacrum on a fresh pelvic specimen. Thus there is a discrepancy between the manner in which previous researchers have modelled the constraints at this joint and the mechanical behaviour of this joint as described by anatomists. In our study a large difference in the overall behaviour of the hemipelvis was observed when the allowable movement of the sacro-iliac joint was changed from a supero-inferior direction to an antero-posterior direction. The latter constraint resulted in the predicted muscle forces, thus confirming the behaviour of the joint as reported by Weisl (1954a,b; 1955) and Grant & Basmajian (1965).

Note that while some researchers have attempted to model ligaments in their studies (e.g. Goel *et al*, 1978), no attempt has been made to do so here. Similarly, Crowninshield *et al* (1978), in their investigation of the hip biomechanics, ignored the hip ligaments since they constrain joint motion (and therefore transmit load) only near the limits of the range of joint motion.

The modelling of the muscle insertion points as reported facilitated in solving the boundary condition problem of the hemipelvis. In the first series of analyses performed, the forces in iliopsoas and rectus femoris muscles were found to be very disproportionate to the *in vivo* condition, since the force in the former was much greater than that expected while that in latter muscle was lower. This anomaly in the muscle forces instituted a change in the boundary conditions at the sacro-iliac joint.

Over the second series of analyses this reaction force at the iliopsoas insertion node was very responsive to a change in spring stiffness for this muscle, which meant that the reported value of load in the muscle could be easily attained. This solution to one problem, however, seemed to create another, different problem. The area on the ilium which bears the origin of gluteus medius is largely prevented from displacing because of the vertical constraint applied to the nearby sacro-iliac joint. This had the effect of markedly reducing the reaction force at this muscle's insertion node, and hence in the muscle itself. This was observed in the reduction of the gluteus medius force by more than a factor of four purely by the change in the boundary conditions at the sacro-iliac joint.

The only other irregularity that existed in the results for the this series of analyses were those of the reaction force for rectus femoris. Why was this reaction force consistently around 200 N? This value is almost one third of that reported in the literature. From data presented by Crowninshield *et al* (1978), it is clear that rectus femoris does indeed reach a peak value of about 600 N. However, this maximum load only occurs after the single-legged stance, and not simultaneously with the peak loads of the abductor muscles, since this muscle is purely a flexor. Thus the value of 234 N predicted by our study appears to be perfectly acceptable.

Attempts at applying both the resultant hip joint reaction force and muscle loads to the hemipelvis resulted in stresses and displacements that were far greater than the expected range of values. Further analysis of the biomechanics at the hip joint indicated that the muscle tensions measured by research workers are static 'passive' tensions viz. tensions that develop in the muscles as a result of the person's body weight. In other words, with a specific set of boundary conditions on the hemipelvis, *either* the hip joint reaction load *or* the muscles forces must be included to re-create the loading pattern around the joint. Taking this approach, the use of both these load types is patently incorrect.

Our working hypothesis is that the reaction force at each of the six insertion points of the muscles, when fully constrained, should correspond to the measured muscle forces for the analysis to have any practical meaning. As a result the six insertion points on the femur were rigidly fixed to represent the static nature of the muscles at this point while the full hip resultant reaction force was applied to the acetabulum. It should be noted that muscles do not insert at a particular point on a bone. However, the muscle insertion points used in this study are from the reported work of Dostal & Andrews (1981). Their work is based on an assumed straight line action of muscles, and hence these muscle insertion sites are reported as single points on the femur.

Eight-noded solid hexagonal elements were used throughout the hemipelvic model. Goel *et al* (1978), Oonishi *et al* (1983), Hansen & Koeneman (1991), Dalstra & Huiskes (1990, 1992) and Schüller *et al* (1993) made use of both solid elements (for cancellous bone) and shell elements (for cortical bone) in the development of their models. This approach to modelling the cortical bone was not used in our model because it limits the model to an assumed cortical bone thickness. In contrast, our model's cortical bone thickness varied according to the CT scans made of the hemipelvis. Also, to investigate the bone remodelling in the whole of the hemipelvis necessitates that both the cortical and cancellous bone be modelled as solid elements.

These elements are standard linear interpolation elements which are perfectly adequate for general stress-displacement problems. However, a possible shortcoming of these elements is the potential 'locking' which occurs when subjected to a bending moment (Hibbitt, 1993). This means that the element stiffness can increase by up to 10 times for a severe case of bending. At great expense this potential problem can be avoided by refining the

FEA mesh in the problem area, by utilising 20-noded quadratic interpolation elements, or by making use of incompatible mode elements.

To guard against the occurrence of this 'locking' occurring in our model, the hemipelvis was examined for signs of bending. The ilium of the hemipelvis lies approximately in the x - z plane, thereby making it possible to investigate any bending that may occur in this plane. For the σ_{zz} stresses (acting in the superior direction) no bending was evident across the ilium, while for the σ_{xx} stresses (acting in the anterior direction) two small areas showed signs of carrying a bending load. This occurred over a relatively small area and therefore did not warrant any further investigation.

The maximum principal tensile stresses in the cortical and cancellous bone of our model are predicted to be 9.29 and 1.29 MPa respectively. This in itself confirms the fact that the hemipelvis behaves as a "sandwich" structure: the cortical bone is the main load bearing structure, while the cancellous is both a "vehicle" for the transmission of the load to the cortices and a supporting structure for the outer stiffer walls. It should be noted that altering the assigned elastic material properties of the bony regions did not have a significant effect on the overall load transfer to the hemipelvis, thus confirming the true "sandwich" nature of this bone. This is a similar finding to that of Dalstra & Huiskes (1992).

Goel *et al* (1978) reported a maximum tensile and compressive stress of 40 MPa each in the cortical bone of their model. This is a large discrepancy between these values and the values for this study, which were 9.29 and 1.43 MPa respectively. However, a study by Schreiber *et al* (1976) found the maximum tensile stress in the cortical bone to reach a value of 8.2 MPa, which does correspond very well with the value found here. Nevertheless, general trends in the "Goel" model are confirmed by the model reported here. They found that the maximum stresses occur in the acetabulum, while the lowest stresses occur in the region where the sacrospinous ligament attaches to the ischium viz. on the postero-inferior region of the hemipelvis. The reported stress distribution of their model is almost identical to that seen in our hemipelvis.

Compressive stresses predicted in the hemipelvis occur predominantly superior to the acetabular rim, with a peak value of 1.43 and 0.105 MPa in the cortical and cancellous bone respectively. It is noteworthy that this is the same region of compressive stress as predicted in the 2D analysis.

The stress plots for the 3D model indicate that, although the load has been applied in the coronal plane, the maximum stress appears to be directed towards the sacro-iliac joint. This is a consistent finding for all our results. Holm (1980) reported that in the standing position the hip is loaded through an axis which is directed from the sacro-iliac joint distally-anteriorly to the top of the acetabulum. Although this "loading vector" is sure to vary by a certain amount in one-legged stance the overall loading effect on the hemipelvis remains the same.

The fundamental assumption in all strain-related adaptive bone remodelling theories and algorithms is that the biological processes occurring within the bone matrix do not play a role in the regulation of such processes. The stimulus for remodelling is a difference between the current strain state of the bone and some optimum value. The algorithm used in our analyses is based on the fact that experimental studies have shown a linear relationship between the elastic modulus and the strength of trabecular bone (Goldstein, 1987), and that the strength of bone is proportional to the strain rate raised to the 0.06 power (Carter and Hayes, 1977).

The predicted densities using the adaptive bone remodelling algorithm correlates very well with those seen on an X-rayed dry hemipelvis. The correlation is so good that any deviation between the two can be blamed on characteristic individual differences in anatomic specimens. The results have shown very clearly that assuming the cortical bone to only have one material property throughout the hemipelvis is incorrect.

A possible explanation for the stiffening in the overhanging part of the ilium (posterior to the greater sciatic notch) is the analogous case of a cantilever beam supported at one end (the anterior part of the ilium, supported below by the acetabulum). This bone stiffens up to minimise any tendency of the ilium to bend about the fulcrum of the greater sciatic notch. The observed reduction in cortical bone density in the superior ilium can in part be attributed to the boundary conditions that are imposed on the nearby sacro-iliac joint. This density reduction in the posterior aspect of the ischium may be due to a modelling error, since the relatively large and strong sacrospinous ligament, which joins the ischial spine to the sacrum, has been omitted in this analysis.

The solution path for the adaptive bone remodelling process has no effect on the ultimate converged bone densities. The value for K (the time integration constant) does, however, play a large role in determining whether the solution actually converges or not. The bone densities in some regions of the hemipelvis did not reach a full converged state for a value of K equal to 0.04. However, a K value of 0.03 resulted in the final converged bone density distribution.

The convergence behaviour exhibited by some of the areas of the bone (especially the cancellous bone) shows a marked decrease in the bone density followed by a reversal of the density path so that it increases up to a converged value. The reason for this are not evident, but can be presumed to relate to the strain energy of that region of bone specifically, and the whole hemipelvis generally.

The results for the bone remodelling are perhaps more instructive than the elastic material model for validating that the model is in fact correct, notwithstanding the limitations already mentioned above. This is reflected in the very good correlation between the bone density distribution predicted in the hemipelvis, under one loading condition, and the X-rayed bone. It is felt that a dynamic analysis of the bone remodelling would be even more useful in achieving a greater understanding of the biomechanics of the pelvis.

It has been shown that the implantation of a pegged cup into the pelvis is not a readily achievable goal at this point in time. A method has been presented which shows potential as a numerical simulation of the actual peg, using beam-type elements. Although the models used to test this method are somewhat crude, the overall difference between the use of a solid peg and beam elements to represent that peg is about 15 %. It is probable that the percentage difference between the two models may not be as large as in this case if a more refined mesh was used in the beam model. However, while the peg simulation by means of beam elements may not provide a completely favourable correlation with the pegged model, this drawback is offset to a degree by the fact that it is inexpensive to both model and analyse.

It is felt that a better comparison could be made if a similar test model was used, but which modelled the hemispherical shape of the cup. This alteration alone would alter dramatically the stress distribution seen in the bone, and would be the next step before implantation into the fully 3D intact model.

Unfortunately, such a 3D model would almost certainly be of limited value if the observer required specific information regarding the local effect of the pegs. In this case, a smaller model - only of the acetabular area - would have to be developed in order to create a much finer FEA mesh that incorporates the peg into the bone.

CHAPTER 5
CONCLUSIONS & RECOMMENDATIONS

Conclusions

1 Two-dimensional versus three-dimensional modelling

A two-dimensional plane strain finite element analysis of the hemipelvis provides a qualitative indication of the stress distribution within the bone. It is not possible to obtain accurate predictions of the stress magnitudes in the bone from this type of analysis, and hence a three-dimensional model is necessary to provide such quantitative information. This difference is most evident by comparing the maximum principal stress values for the two intact models developed; the three-dimensional model predicts stresses five times those predicted in the two-dimensional analysis.

2 Plane strain versus axisymmetric analyses

There is no fundamental advantage to be gained from developing an axisymmetric as opposed to a plane strain model, since both model types predict similar stress magnitudes.

3 Outcome of the two-dimensional study

- the "neutral" angle of 45^{O} provides the best compromise, between 30^{O} and 60^{O}, as the angle of cup insertion;
- there is no obvious advantage to using either Co-Cr or Titanium alloys as the cup metal backing, except that the latter appears to be marginally better flexurally matched to bone;

- the assumed cup/bone interface conditions are a crucial factor in determining the correct results for such a stress analysis, since the two modelled in this study predict stress magnitudes that differ by a factor of two. It is imperative that conditions at this interface are fully understood and that the modelling of this interface is performed in a very careful manner.

4 **Three-dimensional modelling of the hemipelvis**

- provides the optimum simulation of the hemipelvis;
- indicates that there is essentially no movement at the pubis symphysis;
- indicates that displacement of the hemipelvis occurs primarily at the sacro-iliac joint, in an antero-posterior direction;
- is best modelled with the muscle insertion nodes completely constrained.

5 **Strain-related adaptive bone remodelling**

- is a good predictor of bone densities in the hemipelvis;
- indicates that a single assumed elastic modulus throughout a bone region is misrepresentative of the actual density distribution in the hemipelvis.

6 **Pegged cup model implantation**

- provides good prediction of the global bone stress magnitudes;
- provides a poor local correlation of stress magnitudes and distributions around the peg;

- this simulation, when implemented in a fully 3D model, may provide useful results.

Recommendations

1 The 2D models should be used for further investigation of the modelling and behaviour of the cup/bone interface.

2 A better 3D simulation of a complex structure such as the hemipelvis will be possible only when accurate quantitative data regarding the muscle loads of all the muscles acting around the hip joint are available.

3 All biomechanical analyses of this type should include a precise definition of the bone material properties in order to improve the accuracy of the results obtained.

4 The simulation of the pegged cups by means of beam elements and a rigid surface should be implemented, firstly in more representative test models, and finally in the complete 3D model of the hemipelvis.

5 The 3D model can be adapted to investigate the use of the cemented cup in Total Hip Arthroplasty. Implementation of this into the 3D model would be relatively easy to perform, and would able valuable comparisons to be made between the two fixation principles.

6 This 3D model can also be easily adapted to examine differences in surgical technique, such as orientation of the cup and extents of reaming, and different pathological conditions such as dysplasia and protrusio acetabulae.

APPENDIX A
REVIEW OF STRESS ANALYSIS METHODS

1 STRAIN GAUGES

Probably the most widely used device for strain gauge measurement is the electrical resistance strain gauge. They are very sensitive to the changes in the strain state of a material. Their ease of use is of great benefit for stress analysis: the strain gauge is simply cemented to the material in which it is required to measure the strain. The resistance of the strain gauge alters when it is subjected to stress, in a way that the electrical resistance measured across the gauge is proportional to the strain in the material. Strain gauges give displacements between two points defining a base taken as a reference. The electrical resistance strain gauges can be either single (uniaxial) or rosette (triaxial), foil or semiconductor.

The electrical resistance strain gauges do have some limitations: (1) the temperature must remain constant during measuring; (2) the strain should not be larger than 2%; (3) changes in moisture may affect the output; and (4) the positioning and the number of gauges is critical to the outcome. Special gauges are available that can overcome or avoid these inherent limiting factors in the use of strain gauges, except for point (4) mentioned above. Here the human factor plays a much greater role in the accuracy of the measurement (Durelli, 1977).

Mechanical strain gauges have longer base lengths (than the electrical resistance type), cannot be used for dynamic applications and their output has to be recorded visually. They are, however, not subjected to the temperature and humidity limitations of electrical resistance strain gauges (Durelli, 1977). In general, mechanical strain gauges do not enjoy as much use as the electrical resistance type.

The application of this method in examining the stress/strain behaviour of the human pelvis was employed by Jacob *et al* (1976), Petty *et al* (1980), Lionberger *et al* (1985) and Finlay *et al* (1986).

2 PHOTOELASTICITY

Photoelasticity is a very precise and sensitive stress analysis method. It determines both the magnitude and directions of the maximum shear stresses in the material. It is based on the double refracting properties of certain plastics, and measures the changes in indices of refraction (Fessler, 1953). The photoelastic material may be regarded as consisting of tiny spheres which, under stress, are deformed into ellipsoids, with different refractive indices along the two axes. The degree of deformation will depend on the magnitude of the force applied, whereas the orientation of the axes of the ellipsoid will depend on the direction of the force (Holm, 1981).

If a model is cut from a flat plate of such a material and then loaded in the plane of the plate, two types of optical interference patterns may be observed when examined in polarised light. By successive variation of the direction of polarisation it is possible to plot the isoclinics (lines of equal inclination of the principal stresses) for a number of directions. Then the lines of action of the principal stresses, called 'stress projectories', are derived from these isoclinics (Fessler, 1953). The other set of interference fringes, the isochromatic, provides information concerning the magnitude of the stresses (Post, 1979).

Both two- and three-dimensional photoelastic analyses can be performed, (Durelli, 1977) although the three-dimensional analysis is a lot more complex to perform and interpret (Bourgois and Wagner, 1985). Photoelasticity, when applied for maximum shear stresses, gives wholefield stress patterns, while photoelasticity for principal stress orientations is a semi-wholefield method because the isoclinics are recorded as lines. This is a definite advantage over strain gauges, which give point-by-point information. Nevertheless, although a deformed grid includes whole-field information, the evaluation has to be conducted point-by-point (Durelli, 1977).

In the field of biomedical research pelvic and acetabular stress analysis studies have been conducted using photoelasticity (Holm, 1981; Oonishi, 1981).

3 HOLOGRAPHIC INTERFEROMETRY

Holographic interferometry (HI) can also be used to study stresses and strains in cadaveric or moulded pelves. The principle of (HI) is that when wavefronts emerging from a laser-illuminated object are compared for two slightly different positions of the object (undeformed and deformed), an interference (fringe) pattern is formed (Spirakis *et al*, 1992a). HI stress analysis can be conducted using either a continuous wave (cw) or pulsed laser, using either double exposure or real-time methods. The fringes that are produced can be used to determine the direction of movement produced by stresses on the model, which is very useful in understanding the deformations due to the applied stresses (Miyanaga *et al*, 1980).

Although this method provides results which can be both qualitative or quantitative, the need for high stability and darkness during recording (when using a cw laser) limit its applicability. This method gives interference patterns with small deflections, and is very sensitive (Durelli, 1977; Spirakis *et al*, 1992a). It is being used increasingly in the field of biomedical research. Miyanaga *et al* (1980), Vukicevic *et al* (1982) and Spirakis *et al* (1992b) have reported on pelvic and acetabular deformations using this method.

4 THE FINITE ELEMENT METHOD

The most widely and commonly used computational stress analysis technique used today is the Finite Element Method (FEM). Finite Element Analysis (FEA) requires the development of a model which mimics the real structure in four essential ways: (1) geometry; (2) material properties; (3) interface and boundary conditions; and (4) loading conditions. Thereafter the model is mathematically divided into blocks or elements connected at nodal points. These elements are assigned elastic constants (material properties). The boundary conditions and loading configurations are numerically defined as displacements and forces, respectively, in boundary nodes (Huiskes *et al*, 1985; Huiskes and Chao, 1983; Zienkiewicz, 1977).

The mathematical descriptions of the model can be more or less accurate, depending on the level of refinement required, and are usually based on experimentally determined data. The FEM is suitable in principle for any structure: geometries, material properties and loading of any complexity can be accounted for (Huiskes and Chao, 1983). The method has found applications in many fields of mechanics and can be used when bodies have complicated boundaries and nonhomogeneous anisotropic nonelastic properties (Durelli, 1977).

The relationships between the forces in a structure (e.g. a spring) and the displacements at its end points are written in matrix form. The FEA program then calculates the stiffness characteristics of each element and assembles the element mesh through mutual forces and displacements in each node. Thus the continuous structure is replaced by a (large) number of small elements, to each of which equilibrium and compatibility equations are applied. The solution then obtained is approximate in that it converges to the exact solution for the model when the mesh density approximates infinity (Durelli, 1977; Huiskes and Chao, 1983).

Finite element analysis of the pelvis and acetabular component is complicated by (i) the irregular geometry of the bone; (ii) the non-homogeneous anisotropic properties of bone tissue; (iii) the dynamic character of the joint loading; (iv) the assumption of boundary conditions and (v) the validation of results. Despite these difficulties, FEA has the advantages that parametric studies are relatively easy to perform and whole-field stresses and strains can be analysed. In determining stresses and/or strains at hidden points (such as the bone/implant interface), this technique offers the advantage that it does not disturb the variable to be quantified, and does not require slices to be taken to expose hidden areas. Numerous 2D and 3D FEA analyses of the pelvis and acetabulum have been undertaken.

APPENDIX B
BONE REMODELLING

At present there are essentially two theories which attempt to explain the adaptive behaviour of bone under load. Both theories relate stress/strain in bone to ABR behaviour, while neglecting the biological mechanisms governing the relationship. Bone is also considered to be a continuum and therefore theories of linear elasticity are valid. The effects of loading rates, visco-elastic effects and inertial effects are not considered.

Fyhrie and Carter (1986a) developed a "theory of self-optimisation", which relates the apparent bone density (ρ) to the effective stress of the bone, according to the relationship

$$\rho = A\sigma_{eff}^{\alpha}$$

where: A, α = constants

= apparent density of bone

In two later publications (Carter *et al*, 1987; Fyhrie and Carter, 1986b) the value for the effective stress is derived from the equation

$$\sigma_{eff}^{2} = 2EU$$

where: E = Young's modulus

U = apparent strain energy density.

They assume α = 1/2 and the effective stress to be derived from the apparent strain energy density (SED = strain energy/bone volume) for the above equation.

The last part of the development of this theory comes from the work of Carter and Hayes (1977) who determined that

$$E = c\rho^3 .$$

where c = a constant.

In this way the density is directly proportional to the density:

$$\rho = c'U$$

where c' = 2Ac = constant.

It is noteworthy that their optimisation function can also be written in the form U_b = constant, where U_b is the 'true' or bulk SED in the bone (i.e. individual trabeculae) itself, since $U = \rho U_b / \rho_c$ provides that the cortical bone density, ρ_c, equals the 'true' or bulk density of the bone (trabeculae) itself (Huiskes *et al*, 1987).

The above formulation is only one of the possible ones in which the 'self optimisation' theory of Fyhrie and Carter (1986a) can be applied. This aspect presented above deals only with bone density, whereas the unifying theory as a whole incorporates the optimisation of the trabecular orientation.

Cowin and co-workers developed what they termed an adaptive 'theory of elasticity' (Cowin and Hegedus, 1976; Hegedus and Cowin, 1986; Cowin and Firoozbakhsh, 1982). This theory attempts to describe the adaptive remodelling behaviour of bone from one loading configuration to another, rather than predicting the optimal structure of normal bone, as in the above theory of self optimisation. They assumed that cortical bone tissue has a site-specific natural or homeostatic equilibrium strain state. Thus a change of load or an abnormal loading situation (and hence strain state) will stimulate the bone tissue to adapt its mass in such a way that the equilibrium strain state is again achieved. In the theory, then, the rate of adaptation of the bone is coupled to the difference between the equilibrium and the actual strain states.

They proposed that the remodelling takes two forms, after the suggestion by Frost (1964): (a) internal, where only the bone density can change, and (b) external, where only the surface geometry can change by the addition/removal of material to/from the periosteal and endosteal surfaces under stimulation by the local strain state.

The two cases are simply stated as follows:

(a) $$\frac{dE}{dt} = A(\varepsilon - \varepsilon^0)$$

where ε° = equilibrium strain tensor

A = matrix of remodelling co-efficients

(b) $$\frac{dX}{dt} = B(\varepsilon - \varepsilon^0)$$

where X = characteristic surface co-ordinate perpendicular to the surface

B = matrix of remodelling co-efficients

This theory of adaptive elasticity developed by Cowin and co-workers has been somewhat adapted by Huiskes et al (1987). This alternative algorithm does not use the strain tensor as the feedback control variable, but rather the strain energy density, SED. The difference between the actual SED, U, and a site-specific homeostatic equilibrium SED, U_n, is assumed as the driving force for adaptive activity, where the SED U is defined as

$$U = \frac{1}{2}\varepsilon\sigma.$$

Incorporated into this theory is Carter's suggestion (Carter, 1984) that bone is 'lazy' in its behaviour viz. the relation between adaptive rate and the SED is non-linear. This implies that a certain (unknown) threshold level in over- or underloading must be exceeded before the bone reacts to the stimulus.

Hence for internal remodelling

$$\frac{dE}{dt} = C_e(U - Un)$$

This equation is similar to the one used in this thesis (Chapter 4). The bone density used by Huiskes et al (1987) to determine E is the apparent bone density as defined by Carter and Hayes (1977). The bone density used in our study was the tissue strain energy density, the difference being that the latter accounts for the spaces between the trabeculae, especially in cancellous bone, and does not assume bone to be a continuum.

In 1992, Huiskes *et al* add that the ABR signal is based on the assumption that bone strives to normalise the <u>average elastic energy/unit of mass</u> for a particular loading history:

$$S = \frac{1}{n}\sum\left(\frac{U_i}{\rho}\right)$$

where ρ = apparent density.

The objective of the net bone remodelling process can then be described as

$$S - S_{ref} = 0.$$

APPENDIX C

SAMPLE 2D ABAQUS INPUT DECK

*HEADING *title*

THA 2D HIP, FULLY UNBONDED CUP/BONE INTERFACE, TITANIUM METAL BACKING

**

** NEUTRAL FILE GENERATED ON: 26-NOV-92 16:48:59 PATABA VERSION: 3.1A

**

****

** NODE DEFINITIONS

****

**

*NODE

1, -.181757522E+01, .631711884E+02, .000000000E+00 ***node number, x, y, z***

.

etc

**

****

** FOUR-NODED ELEMENT DEFINITIONS

****

**

*ELEMENT,TYPE=CPE4,ELSET=CORTICAL ***element definition, element type, element set***

1, 34, 42, 12, 10 ***element number, node #, node #, node #, node #***

2, 12, 10, 36, 44

.

etc

*ELEMENT,TYPE=CPE4,ELSET=CANCELLOUS

.

*ELEMENT,TYPE=CPE4,ELSET=TITANIUM

.

*ELEMENT,TYPE=CPE4,ELSET=UHMWPE

.

**

```
****************************************************************
** INTERFACE AND SOFTENED CONTACT DEFINITIONS
****************************************************************
**
*ELEMENT,TYPE=IRS21,ELSET=INTER
 2000, 416, 419, 9999                *element #, node #, node #, rigid surface reference node
        .
        etc
*INTERFACE, ELSET=INTER              *defines ELSET=INTER as femoral head/cup interface
*SURFACE CONTACT, SOFTENED           *softened contact
0.000125,100000                      *clearance (c), pressure at c=0 (pO)
*ELEMENT,TYPE=INTER2,ELSET=INTER2         *defines ELSET=INTER2 as cup/bone interface
 3000, 429, 431, 2000, 2001               *element #, node #, node #, node #, node #
        .
        etc
*INTERFACE, ELSET=INTER2
*FRICTION                            *friction definiton
0.3                                  *co-efficient of friction
*SURFACE CONTACT, SOFTENED           *softened contact
0.000125, 100000                     *clearance (c), pressure at c=0 (pO)
*RIGID SURFACE                       *circular rigid surface definition
START,3.0351,1.90659,3.0511,1.90659
CIRCL,3.0511,1.92259,3.0511,1.90659
CIRCL,3.0671,1.90659,3.0511,1.90659
CIRCL,3.0511,1.89059,3.0511,1.90659
CIRCL,3.0351,1.906590001,3.0511,1.90659
**
****************************************************************
** ELEMENT PROPERTIES
****************************************************************
**
*SOLID SECTION, ELSET=CORTICAL, MATERIAL=CORTICAL
 .100000000E+01
*SOLID SECTION, ELSET=CANCELLOUS, MATERIAL=CANCELLOUS
 .100000000E+01
*SOLID SECTION, ELSET=TITANIUM, MATERIAL=TITANIUM
 .100000000E+01
*SOLID SECTION, ELSET=UHMWPE, MATERIAL=UHMWPE
```

```
 .100000000E+01
************************************************************
** MATERIAL DEFINITIONS
************************************************************
**
*MATERIAL, NAME=CORTICAL              *material definition
*ELASTIC, TYPE=ISO                    *isotropic elastic material definition
 .150000000E+11, .300000000E+00       *Young's modulus, Poisson's ration
*MATERIAL, NAME=CANCELLOUS
*ELASTIC, TYPE=ISO
 .150000000E+10, .300000000E+00
*MATERIAL, NAME=TITANIUM
*ELASTIC, TYPE=ISO
 .110000000E+12, .360000000E+00
*MATERIAL, NAME=UHMWPE
*ELASTIC, TYPE=ISO
 .690000000E+09, .400000000E+00
**
************************************************************
 LOAD STEP
************************************************************
**
*STEP, AMP=RAMP               *start of load step, analysis begins
*STATIC                       *definition of static analysis
1.0, 1.0
*CLOAD                        *definition of concentrated load
  9999, 1, 1026.1             *x-component of hip resultant load to rigid surface reference node
  9999, 2, 2819.1             *y-component of hip resultant load to rigid surface reference node
*BOUNDARY, OP=NEW             *definition of boundary conditions
    1, 1,2 0.0                *node #, degrees of freedom constrained, zero displacement
    2, 1,2 0.0
      .
     etc
*END STEP                     *end of load step, analysis ends
```

APPENDIX D

SAMPLE 3D ABAQUS INPUT DECK

```
*HEADING                                              *title
        INTACT 3D HIP
**
** NEUTRAL FILE GENERATED ON: 11-MAR-93 19:25:06  PATABA VERSION: 3.1A
**
*************************************************************
**  NODE DEFINITIONS
*************************************************************
**
*NODE                                                 *muscle insertion point nodes
5000,0.021659,-0.114329,-0.006118
5100,0.043659,-0.110329,-0.007118
5200,0.030659,-0.088329,-0.083118
5300,0.037659,-0.056329,-0.041118
5400,0.061659,-0.074329,-0.416118
5500,0.082659,-0.043329,-0.395118
**
*************************************************************
**  SYSTEM TRANSFORMATION
*************************************************************
**
*SYSTEM                                               *transforms nodal co-ordinates
-0.119595,-0.0851525,0.154,8.66025,-5,0               *transforms nodal co-ordinates generated
5,8.66025,2.362373                                     in PATRAN into physiologic position
*NODE,INPUT=/j2/grega/3d/intact/intact.nod            *nodal co-ordinated input from file
**
*SYSTEM                                               *resets system co-ordinates
**
*************************************************************
**  EIGHT-NODED ELEMENT DEFINITIONS
*************************************************************
*ELEMENT,TYPE=C3D8,ELSET=CORTICAL,INPUT=/j2/grega/3d/intact/intact.el1
                                          *gets cortical hexagonal elements from file
```

*ELEMENT,TYPE=C3D8,ELSET=CANCELLOUS,INPUT=/j2/grega/3d/intact/intact.el2

****gets cancellous hexagonal elements from file***

*ELEMENT,TYPE=IRS4,ELSET=INTER,INPUT=/j2/grega/3d/intact/intact.el5

****gets femoral head/cup interface elements from file***

*ELEMENT,TYPE=C3D8,ELSET=CARTILAGE,INPUT=/j2/grega/3d/intact/intact.el6

****gets cartilage hexagonal elements from file***

*ELEMENT,TYPE=C3D8,ELSET=PID5,INPUT=/j2/grega/3d/intact/intact.el8

****gets subchondral hexagonal elements from file***

**

****

** SPRINGA (MUSCLE) ELEMENT DEFINITIONS

****

**

*ELEMENT,TYPE=SPRINGA,ELSET=GMAX,INPUT=/j2/grega/3d/intact/gmax.el

****gets SPRINGA elements for gluteus maximus from file***

*ELEMENT,TYPE=SPRINGA,ELSET=GMED,INPUT=/j2/grega/3d/intact/gmed.el

****gets SPRINGA elements for gluteus medius from file***

*ELEMENT,TYPE=SPRINGA,ELSET=GMIN,INPUT=/j2/grega/3d/intact/gmin.el

****gets SPRINGA elements for gluteus medius from file***

*ELEMENT,TYPE=SPRINGA,ELSET=TFL,INPUT=/j2/grega/3d/intact/tfl.el

****gets SPRINGA elements for tensor fasciae latae from file***

*ELEMENT,TYPE=SPRINGA,ELSET=IP,INPUT=/j2/grega/3d/intact/ip.el

****gets SPRINGA elements for iliopsoas from file***

*ELEMENT,TYPE=SPRINGA,ELSET=RECFEM,INPUT=/j2/grega/3d/intact/rfem.el

****gets SPRINGA elements for rectus femoris from file***

**

****

** ELEMENT PROPERTIES

****

**

*SOLID SECTION, ELSET=PID1, MATERIAL=MID1

*SOLID SECTION, ELSET=PID2, MATERIAL=MID2

*SOLID SECTION, ELSET=PID4, MATERIAL=MID4

*SOLID SECTION, ELSET=PID5, MATERIAL=MID5

*SPRING, ELSET=GMED

1000000 ****gluteus medius spring k-value***

*SPRING, ELSET=GMIN

125000 ****gluteus minimus spring k-value***

```
*SPRING, ELSET=GMAX
200000                              *gluteus maximus spring k-value
*SPRING, ELSET=IP
62500                               *iliopsoas spring k-value
*SPRING, ELSET=TFL
150000                              *tensor fasciae latae spring k-value
*SPRING, ELSET=RECFEM
200000                              *rectus femoris spring k-value
**
************************************************************
** INTERFACE AND SOFTENED CONTACT DEFINITIONS
************************************************************
**
*INTERFACE,NAME=INTER               *defines ELSET=INTER as femoral head/cup interface
*SURFACE CONTACT,SOFTENED           *softened contact
0.000125,100000                     *clearance (c), pressure at c=0 (pO)
**
*RIGID SURFACE,TYPE=BEZIER                   *Bezier rigid surface definition
*VERTEX, INPUT=/j2/grega/3d/intact/femhead.ver *vertices of rigid surface input from file
*PATCH, INPUT=/j2/grega/3d/intact/femhead.pat  *patches of rigid surface input from file
**
************************************************************
** MATERIAL DEFINITIONS
************************************************************
**
*MATERIAL,NAME=CORTICAL              *material definition
*ELASTIC,TYPE=ISO                    *isotropic elastic material definition
15E09,0.3                            *Young's modulus, Poisson's ratio
*MATERIAL,NAME=MID2
*ELASTIC,TYPE=ISO
1.5E09,0.3
*MATERIAL,NAME=MID4
*ELASTIC,TYPE=ISO
500E06,0.4
*MATERIAL,NAME=MID5
*ELASTIC,TYPE=ISO
3E09,0.2
**
```

```
************************************************************
** RELAXATION STEP          *no load applied, establishing contact conditions at interface
************************************************************
**
*STEP                       *start of relaxation step, analysis begins
*STATIC                     *definition of static analysis
1.0,1.0
*BOUNDARY                   *definition of boundary conditions
SACRUM,1,3                  *sacro-iliac joint completely fixed
PUBIS,1,3                   *pubis symphysis completely fixed
MUSCLES,1,3                 *muscle insertion nodes completely fixed
9999,1,6                    *rigid surface reference node completely fixed
*ENDSTEP                    *end of relaxation step
**
************************************************************
** LOAD STEP
************************************************************
**
*STEP                       *start of load step, analysis begins
*STATIC
1.0,1.0
*CLOAD
9999,2,872.2                *y-component of hip resultant load to rigid surface reference node
9999,3,2396.2               *z-component of hip resultant load to rigid surface reference node
*BOUNDARY,OP=NEW            *definition of new boundary conditions
SACRUM,2,3                  *sacro-iliac joint released in antero-posterior direction
PUBIS,1,3                   *pubis symphysis completely constrained
MUSCLES,1,3                 *muscle insertion nodes completely constrained
9999,4,6                    *rigid surface reference node released in translational D.O.F.'s
*ENDSTEP                    *end of load step, analysis ends
```

REFERENCES

Agins HJ, Alcock NW, Bansal M
1988
Metallic wear in failed titanium-alloy total hip replacements: a histological and quantitative analysis
Journal of Bone and Joint Surgery 70A: 347-356

Amstutz HC, Markoff KL, McNeice GM, Gruen TA
1976
Loosening of total hip prostheses
pp 102-116 Ed. E McCollister In: The Hip: Proceedings of the Fourth Open Scientific Meeting of The Hip Society
St Louis: C.V. Mosby

Amstutz HC, Ma SM, Jinnah RH, Mai L
1982
Revision of aseptic loose total hip arthroplasties
Clinical Orthopaedics and Related Research 170:21-33

Andrew TA, Flanagan JP, Gerundini M, Bombelli R
1986
The isoelastic, noncemented THA: preliminary experience with 400 cases
Clinical Orthopaedics and Related Research 206:127-138

Apel DM, Smith DG, Schwartz CM, Paprosky WG
1989
Threaded cup acetabuloplasty: early clinical experience
Clinical Orthopaedics and Related Research 241:183-189

Ashby MF, Jones DRF
1980
Engineering Materials I
Robert Maxwell, Oxford, U.K.

AutoCAD Release 11
1990
Software & reference manuals
Autodesk, Inc.

Basmajian JV
1981
Primary Anatomy
p 180, 8th ed. London: Williams and Wilkins Co.

Beckenbaugh RD, Ilstrup DM
1978
Total hip arthroplasty
Journal of Bone and Joint Surgery 60A:306-313

Bertin KC, Freeman MAR, Morscher E, Oeri A, Ring PA
1985
Cementless acetabular replacement using a pegged polyethylene prosthesis
Archives of Orthopaedic and Traumatic Surgery 104:251-261

Brand RA, Pedersen DR, Yoder SA
1986
How definition of "loosening " affects the incidence of loose total hip reconstructions
Clinical Orthopaedics and Related Research 210:185-191

Brown DB, DiGioia AM
1984
A contact-coupled finite element analysis of the natural adult hip
Journal of Biomechanics 17: 437-448

Bobyn JD, Engh CA, Glassman AH
1988
Radiography and histology of a threaded acetabular implant: one case studied at two years
Journal of Bone and Joint Surgery 70B:302-304

Bourgois R, Wagner J
1985
Advances in photoelasticity applied to biomechanical problems
pp 725-730 Eds. SM Perren & E Schneider In: Biomechanics: current interdisciplinary research.
Martinus Nijhoff Publishers.

Callaghan JJ, Salvati EA, Pellicci PM, Wilson PD, Ranawat CS
1985
Results of revision for mechanical failure after cemented total hip replacement, 1979 to 1982: a two to five year follow-up
Journal of Bone and Joint Surgery 67A: 1074-1085

Callaghan JJ
1990
Total hip arthroplasty: clinical perspective
Clinical Orthopaedics and Related Research 276: 33-40

Cameron HU
1982
The results of early clinical trials with a microporous coated metal hip prosthesis
Clinical Orthopaedics and Related Research 165: 188-195

Carlsson AS
1981
Total hip replacement according to Charnley. A review of complications and functions.
Acta Orthopaedica Scandinavica 52: 339-346

Carter DR
1984
Mechanical loading histories and cortical bone remodelling
Calcified Tissue International 36:S19-S24

Carter DR, Hayes WC
1976
Bone compressive strength: the influence of density and strain rate
Science 194:1174-1176

Carter DR, Hayes WC
1977
The compressive behaviour of bone as a two-phase porous structure
Journal of Bone and Joint Surgery 59A: 954-962

Carter DR, Vasu R, Harris WH
1982
Stress distributions in the acetabular region -II. Effects of cement thickness and metal backing of the total hip acetabular component
Journal of Biomechanics 15:165-170

Carter DR, Vasu R, Harris WH
1983
Periacetabular stress distributions after joint replacement with subchondral bone retention
Acta Orthopaedica Scandinavica 54: 29-35

Carter DR, Fyhrie DP, Whalen RT
1987
Trabecular bone density and loading history: regulation of connective tissue biology by mechanical energy
Journal of Biomechanics 20: 785-794

Carter DR, Orr TE, Fyhrie DP
1989
Relationships between loading history and femoral ccancellous bone architecture
Journal of Biomechanics 22: 231-244

Chandler HP, Reineck FT, Wixson RL, McCarthy JC
1981
Total hip replacement in patients younger than thirty years old
Journal of Bone and Joint Surgery 63A:1426-1434

Charnley J
1960
Anchorage of the femoral head prosthesis to the shaft of the femur
Journal of Bone and Joint Surgery 42B: 28-42

Charnley J
1970
Total hip replacement by low-friction arthroplasty
Clinical Orthopaedics and Related Research 72: 7-21

Charnley JC, Cupic Z
1973
The nine and ten year results of the low-friction arthroplasty of the hip
Clinical Orthopaedics and Related Research 95:9-25

Cheal EJ, Snyder BD, Nunamaker DM, Hayes WC
1987
Trabecular bone remodelling around smooth and porous implants in an equine patellar model
Journal of Biomechanics 20: 1121-1134

Clemente CD
1981
Anatomy: a regional atlas of the human body (2nd Ed)
Urban & Schwarzenburg, Baltimore-Munich

Cotterill P, Hunter GA, Tile M
1982
A radiographic analysis of 166 Charnley-Mueller total hip arthroplasties
Clinical Orthopaedics and Related Research 163:120-126

Cowin SC, Hegedus DH
1976
Bone remodelling I: theory of adaptive elasticity
Journal of Elasticity 6: 313-326

Cowin SC, Nachlinger RR
1978
Bone remodelling III: uniqueness and stability in adaptive elasticity theory
Journal of Elasticity 8: 285-295

Cowin SC, Firoozbakhsh K
1982
Bone remodelling of diaphysial surfaces under constant load: theoretical predictions
Journal of Biomechanics 7: 471-484

Crowninshield RD, Johnston RC, Andrews JG, Brand RA
1978
A biomechanical investigation of the human hip
Journal of Biomechanics 11:75-85

Cracchiolo A, Severt R, Moreland J
1992
Uncemented total hip arthroplasty in rheumatoid arthritis diseases
Clinical Orthopaedics and Related Research 277: 166-174

Crowninshield RD, Pedersen DR, Brand RA, Johnston RC
1983
Analytical support for acetabular component metal backing
pp 207-215 In: The Hip: Proceedings of the Eleventh Open Scientific Meeting of the Hip Society
St Louis, CV Mosby

Crowninshield RD
1987
Implant design in total hip arthroplasty
pp 41-49 Ed. WT Stillwell In: The art of total hip arthroplasty.
Grune & Stratton, Inc.

Dalstra M, Huiskes R
1990
The pelvic bone as a sandwich construction; a three dimensional finite element study
Proceedings of the 7th Meeting of the European Society of Biomechanics B32
Aarhus

Dalstra M, Huiskes R
1992
Development of a pelvic finite element model
Proceedings of the 8th Meeting of the European Society of Biomechanics 23
Rome

Davey JR, Harris WH
1989
A preliminary report of the use of a cementless acetabular component with a cemented femoral component
Clinical Orthopaedics and Related Research 245:150-155

DeLee JB, Charnley J
1976
Radiological demarcation of cemented sockets in total hip replacement
Clinical Orthopaedics and Related Research 121:20-32

Dobbs HS
1980
Survivorship of total hip replacements
Journal of Bone and Joint Surgery 62B:168-173

Dorr LD, Takei GK, Conaty JP
1983
Total hip arthroplasties in patients less than forty-five years old
Journal of Bone and Joint Surgery 65A:474-479

Dostal WF, Andrews JG
1981
A three-dimensional biomechanical model of hip musculature
Journal of Biomechanics 14: 803-812

Ducheyne P, Aernoudt E, De Meester P, Martens M, Mulier JC, Van Leeuwen D
1978
Factors governing the mechanical behaviour of the implant-porous coating-trabecular bone interface
Journal of Biomechanics 11:297-307

Durelli AJ
1977
The difficult choice: Evaluation of methods used to determine experimentally displacements, strains and stresses
Applied Mechanics Reviews 30:1167-1178

Eftekhar NS, Pawluk RJ
1980
Role of surgical preparation in acetabular cup fixation.
pp 308-328 Ed. LH Riley In: The Hip. Proceedings of the Eighth Open Scientific Meeting of the Hip Society
St. Louis, CV Mosby

Engh CA, Glassman AH, Griffin WL, Mayer JG
1988
Results of cementless revision for failed cemented total hip arthroplasty
Clinical Orthopaedics and Related Research 235:91-110

Engh CA, Griffin WL, Marx CL
1990
Cementless acetabular components
Journal of Bone and Joint Surgery 72B:53-59

Fessler H
1953
Load distribution in a model of a hip joint
Journal of Bone and Joint Surgery 39B:145-153

Finlay JB, Bourne RB, Landsberg RPD, Andreae P
1986
Pelvic stresses in vitro - I. Malsizing of endoprostheses
Journal of Biomechanics 19:703-714

Frost HM
1964
The Laws of Bone Structure
Charles C. Thomas, Springfield, Illinois

Fyhrie DP, Carter DR
1986a
A unifying principle relating stress to trabecular bone morphology
Journal of Orthopaedic Research 4:304-317

Fyhrie DP, Carter DR
1986b
Prediction of cancellous bone apparent density with 3-D stress analysis
Transactions 32nd Annual Orthopaedic Research Society p 331

Galante J, Rostoker W, Lueck R, Ray RD
1971
Sintered fibre metal composite as a basis for attachment of implants to bone
Journal of Bone and Joint Surgery 53A: 101-110

Grant JCB, Basmajian JV
1965
Grant's Method of Anatomy (7th Ed)
Waverly Press, Inc., Baltimore, U.S.A.

Goel VK, Svensson NL
1977
Forces on the pelvis
Journal of Biomechanics 10:195-200

Goel VK, Valliappan S, Svensson NL
1978
Stresses in the normal pelvis
Computers in Biology and Medicine 8: 91-104

Halley DK, Wroblewski BM
1986
Long-term results of low-friction arthroplasty in patients 30 years of age or younger
Clinical Orthopaedics and Related Research 211: 43-48

Hansen TM, Koeneman JB
1991
Biomechanical 3-D analysis of the human pelvis
Finite Element News 2: 30-37

Harrigan TP, Hamilton JJ
1992
An analytical and numerical study of the stability of bone remodelling theories: dependance on microstructural stimulus
Journal of Biomechanics 25: 477-488

Harris WH, Penenberg MD
1987
Further follow up on socket fixation using a metal-backed acetabular component for total hip replacement
Journal of Bone and Joint Surgery 69A:1140-1143

Harris WH, White RE
1982
Socket fixation using a metal-backed acetabular component for total hip replacement
Journal of Bone and Joint Surgery 64A:745-748

Hart RT, Davy DT, Heiple HG
1984
A computational method for stress analysis of adaptive elastic materials with a view toward applications in strain-induced bone remodelling
Journal of Biomechanical Engineering 106: 342-350

Hedley AK, Kabo M, Kim W, Coster I, Amstutz HC
1983
Bony ingrowth fixation of newly designed acetabular components in a canine model
Clinical Orthopaedics and Related Research 176:12-23

Hegedus DH, Cowin SC
1976
Bone remodelling II: small strain adaptive elasticity
Journal of Elasticity 6: 337-352

Hibbitt, Karlsson & Sorensen, Inc.
1992
ABAQUS User Manuals, Version 5.2
Providence, Rhode Island, USA

Hibbitt D
1993
Personal communication

Holm NJ
1980
The internal stress pattern of the os coxae
Acta Orthopaedica Scandinavica 51:421-428

Holm NJ
1981
The development of a two-dimensional stress-optical model of the os coxae
Acta Orthopaedica Scandinavica 52:135-143

Homsy CA, Cain TE, Kessler FB, Anderson MS, King JW
1972
Porous implant systems for prosthesis stabilization
Clinical Orthopaedics and Related Research 89: 220-229

Homsy CA
1973
Implant stabilization: chemical and biomechanical considerations
Orthopaedic Clinics of North America 4: 295-304

Huiskes R, Chao EYS
1983
A survey of FEA in orthopaedic biomechanics: the first decade
Journal of Biomechanics 16:385-409

Huiskes R, Strens PHGE, Van Heck J, Sloof TJJH
1985
Interface stresses in the resurfaced hip: FEA of load transmission in the femoral head
Acta Orthopaedica Scandinavica 56:474-478

Huiskes R
1987
Finite element analysis of acetabular reconstruction: noncemented threaded cups
Acta Orthopaedica Scandinavica 58:620-625

Huiskes R, Weinans H, Grootenboer HJ, Dalstra M, Fudala B, Slooff TJ
1987
Adaptive bone remodelling applied to prosthetic-design analysis
Journal of Biomechanics 20(11/12):1135-1150

Huiskes R, Weinans H, Van Rietbergen B
1992
The reationship between stress shielding and bone resorption around total hip stems and the effects of flexible materials
Clinical Orthopaedics and Related Research 274:124-134

Hungerford DS, Jones LC
1988
The rationale of cementless revision of cemented arthroplasty failures
Clinical Orthopaedics and Related Research 235:12-24

Hwang SK, Ahn JI, Kim HS
1991
Cementless total hip arthroplasty with PCA prostheses
Orthopaedics 14(10): 1135-1141

Inman J
1947
Functional aspects of the abductor muscles of the hip
Journal of Bone and Joint Surgery 29: 607-619

Jacob HAC, Huggler AH, Dietschi C, Schreiber A
1976
Mechanical function of subchondral bone as experimentally determined on the acetabulum of the human pelvis
Journal of Biomechanics 9: 625-627

Jacob HAC, Huggler AH, Schreiber A
1980
An investigation into biomechanical causes of prosthesis stem loosening within the proximal end of human femur
Journal of Biomechanics 13: 159-173

Jasty M, Harris WH
1988
Observations on factors controlling bony ingrowth into weight-bearing, porous canine total hip replacements
pp 175-189 Ed. RH Fitzgerald In: Non-cemented Total Hip Arthroplasty
Raven Press, New York

Johnston RC, Larson CB
1969
Biomechanics of cup arthroplasty
Clinical Orthopaedics and Related Research 66:56-69

Kapandji IA
1987
The Physiology of the Joints
Churchill Livingstone, Edinburgh London Melbourne & New York

Keating EM, Ritter MA, Faris PM
1990
Structures at risk from medially placed acetabular screws
Journal of Bone and Joint Surgery 72A:509-511

Kim WC, Grogan T, Amstutz HC, Dorey F
1987
Survivorship comparison of THARIES and conventional hip arthroplasty in patients younger than 40 years old
Clinical Orthopaedics and Related Research 214: 269-277

Kim YK, Kim VEM
1992
Results of the Harris-Galante cementless hip prosthesis
Journal of Bone and Joint Surgery 74B: 83-87

Kirkpatrick JS, Callaghan JJ, Vandemark RM, Goldner RD
1990
The relationship of the intrapelvic vasculature to the acetabulum: implications in screw-fixation acetabular components
Clinical Orthopaedics and Related Research 258:183-190

Knahr K, Böhler M, Frank P, Plenk H, Salzer M
1987
Survival analysis of an uncemented ceramic acetabular component in THA
Archives of Orthopaedic and Traumatic Surgery 106:297-300

Koch JC
1917
The laws of bone architecture
American Journal of Anatomy 21: 177-183

Kody MH, Kabo JM, Markolf KL, Dorey FJ, Amstutz HC
1990
Strength of initial mechanical fixation of screw ring acetabular components
Clinical Orthopaedics and Related Research 257:147-153

Ling RSM
1986
Observations on the fixation of implants to the bony skeleton
Clinical Orthopaedics and Related Research 210:80

Lionberger D, Walker PS, Granholm J
1985
Effects of prosthetic acetabular replacement on strains in the pelvis
Journal of Orthopaedic Research 3:372-379

Mallory TH, Vaughn BK, Lombardi AV, Reynolds HM, Koenig JA
1988
Threaded acetabular components: design rationale and preliminary clinical experience
Orthopaedic Review 17:305-314

Maistrelli G, Gerundini M, Bombelli R
1986
The inclination of the weight bearing surface in the hip joint
Orthopaedic Review 15:271-279

Maric Z, Karpman RR
1992
Early failure of noncemented porous coated anatomic total hip arthroplasty
Clinical Orthopaedics and Related Research 278: 116-120

McCoy TH, Salvati EA, Ranawat CS, Wilson PD
1988
A fifteen year follow-up study of one hundred Charnley low-friction arthroplasties
Orthopaedic Clinics of North America 19:467-476

McGann WA, Welch RB, Picetti GD
1988
Acetabular preparation in cementless revision total hip arthroplasty
Clinical Orthopaedics and Related Research 235:35-46

McKee GK
1970
Development of total prosthetic replacement of the hip
Clinical Orthopaedics and Related Research 72:85

McMinn, Hutchings
1977
A colour atlas of human anatomy
Wolfe Medical Publications Ltd, London

McLeish RD, Charnley J
1970
Abduction forces in the one-legged stance
Journal of Biomechanics 3: 191-209

Mehlhoff MA, Sledge CB
1990
Comparison of cemented and cementless hip and knee replacements
Arthritis and Rheumatism 33:293-297

Miyanaga Y, Tagawa H, Ninomiya S, Katoh F, Tateishi T, Shirasaki Y
1980
A new socket design for the dysplastic acetabulum in total hip replacement
Clinical Orthopaedics and Related Research 149:194-200

Mjöberg B
1986
Loosening of the cemented hip prosthesis: the importance of heat injury
Acta Orthopaedica Scandinavica 57:Suppl. 221, pp 14-18

Moreland JR, Gruen TA, Mai L, Amstutz HC
1980
Aseptic loosening of total hip replacement: incidence and significance
pp 281-291, Ed. LH Riley In: The Hip Society: Proceedings of the Eighth Open Scientific Meeting Of the Hip Society.
St Louis, CV Mosby

Morscher EW, Bereiter H, Lampert C
1989
Cementless press-fit cup
Clinical Orthopaedics and Related Research 249:12-20

Morscher EW, Dick W, Kernen V
1982
Cementless fixation of polyethylene acetabular component in total hip arthroplasty
Archives of Orthopaedic and Traumatic Surgery 99:223-230

Morscher E, Schmassmann
1983
Failures of total hip arthroplasty and probable incidence of revision surgery in the future
Archives of Orthopaedic and Traumatic Surgery 101:137-143

Morscher EW, Masar Z
1988
Development and first experience with an uncemented press-fit cup
Clinical Orthopaedics and Related Research 232:96-103

Morscher EW, Dick W
1983
Cementless fixation of "isoelastic" hip endoprostheses manufactured from plastic materials
Clinical Orthopaedics and Related Research 176:77-87

Morscher EW
1983
Cementless total hip arthroplasty
Clinical Orthopaedics and Related Research 181:76-91

Morscher E
1989
Endoprosthetic surgery in 1988
Annales Chirurgiae et Gynaecologiae 78:242-253

Noble PC, Scheller AD, Tullos HS, Levy RN, Turner RH
1987
Applied design criteria for total hip prostheses
pp 51-68 Ed. WT Stillwell In: The art of total hip arthroplasty.
Grune and Stratton, Inc

Oonishi H, Hasegawa T
1981
3D-finite element analysis of the pelvis and ceramic acetabulum
Proceedings: Orthopaedic Research Society, Nevada, Feb 24-26

Oonishi H, Isha H, Hasegawa T
1983
Mechanical analysis of the human pelvis and its application to the artificial hip joint - by means of the three dimensional finite element method
Journal of Biomechanics 16 (6): 427-444

PDA Engineering
1992
PATRAN User Manuals, Release 3.2
Costa Mesa, California, USA

Pedersen DR, Crowninshield RD, Brand RA, Johnston RC
1982
An axisymmetric model of acetabular components in total hip arthroplasty
Journal of Biomechanics 15:305-315

Pellicci PM, Wilson PD, Sledge CB, Salvati EA, Ranawat CS, Poss R, Callaghan JJ
1985
Long term results of revision total hip replacement
Journal of Bone and Joint Surgery 67A: 513-523

Petty W, Miller GJ, Piotrowski G
1980
In vitro evaluation of the effect of acetabular prosthesis implantation on human cadaver pelves
Bulletin of Prosthesis Research 17:80-89

Pilliar RM, Bratina WJ
1980
Micromechanical bonding at a porous surface structured implant interface: the effect on implant stressing.
Journal of Biomedical Engineering 2:49

Pilliar RM, Lee JM, Maniatopoulos C
1986
Observations on the effect of movement on bone ingrowth into porous-surfaced implants
Clinical Orthopaedics and Related Research 208: 108-115

Post D
1979
Photoelasticity
Experimental Mechanics 19: 176-192

Pupparo F, Engh C
1991
Comparison of porous-threaded and smooth-threaded acetabular components of identical design: 2- to 4-year results
Clinical Orthopaedics and Related Research 271:201-206

Rao SS
1989
pp 43-94 In: The Finite Element Method in Engineering
Pergamon, Oxford

Rapperport DJ, Carter DR, Schurman DJ
1987
Contact finite element stress analysis of porous ingrowth acetabular cup implantation, ingrowth, and loosening
Orthopaedic Research Society 5:548-561

Rohlmann A, Mössner U, Bergmann G, Kölbel R
1983
FEA and experimental investigation in a femur with hip endoprosthesis
Journal of Biomechanics 16:727-742

Rothman RH, Cohn JC
1990
Cemented versus cementless total hip arthroplasty
Clinical Orthopaedics and Related Research 254:153-169

Russotti GM, Coventry MB, Stauffer RN
1988
Cemented total hip arthroplasty with contemporary techniques: a five year minimum follow-up study
Clinical Orthopaedics and Related Research 235: 141-148

Salvati EA, Im VC, Aglietti P, Wilson D
1976
Radiology of total hip replacements
Clinical Orthopaedics and Related Research 121:74-82

Sarmiento A, Ebramzadeh E, Gogan WJ, McKellop HA
1990
Cup containment and orientation in cemented total hip arthroplasties
Journal of Bone and Joint Surgery 72B: 996-1002

Shaw JA, Bailey JH, Bruno A, Greer RB
1990
Threaded acetabular components for primary and revision total hip arthroplasty
Journal of Arthroplasty 5:201-215

Silber DA, Engh CA
1990
Cementless THA with femoral head bone grafting with hip dysplasia
Journal of Arthroplasty 5:231-240

Schmalzried TP, Harris WH
1992
The Harris-Galante porous-coated acetabular component with screw fixation
Journal of Bone and Joint Surgery 74A: 1130-1139

Schreiber A, Huggler AH, Dietschi C, Jacob H
1976
Complication after joint replacement - longterm follow-up, clinical findings and biomechanical research
pp 187-202 Eds. M Schaldach & D. Hohmann In: Advances in Artificial Hip and Knee Joint Technology
Springer-Verlag, Berlin Heidelberg New York

Schüller HM, Dalstra M, Huiskes R, Marti RK
1993
Total hip reconstructionin acetabular dysplasia. A finite element study.
The Journal of Bone and Joint Surgery 75B: 468-474

Snorrason F, Kärrholm J
1990
Primary migration of fully-threaded acetabular prostheses
Journal of Bone and Joint Surgery 72B:647-652

Spector M
1988
Current concepts of bone ingrowth and remodelling
pp 69-85 Ed. Fitzgerald RH In: Non-cemented Total Hip Arthroplasty
Raven Press, New York

Spirakis AA
1988
A qualitative holographic study of hemipelvic and acetabular deformation caused by different hip prostheses
Masters Thesis University of Cape Town, South Africa

Spirakis A, Learmonth ID, Gryzagoridis J, Davis BL
1992a
Pelvic and acetabular stresses and strains accompanying total hip arthroplasty: a review of experimental and mathematical studies
South African Journal of Science 88: 211-216

Spirakis A, Learmonth ID, Gryzagoridis J, Davis BL
1992b
Qualitative holographic study of hemipelvic deformation caused by loading different hip prostheses
Journal of Biomedical Engineering 14: 126-132

Starke GR, Spirakis A, Martin JB, Learmonth ID
1993
A numerical approach to simulating the strain related adaptive bone remodelling process
CERECAM Report No 197 (in preparation) FRD/UCT Centre for Research in Computational and Applied Mechanics, University of Cape Town, RSA

Stauffer RN
1982
Ten-year follow-up study of total hip replacement
Journal of Bone and Joint Surgery 64A:983-990

Stiehl JB, Hill D, Pavelic V
1990
Experimental finite element and invitro analysis of radial expansion press fit acetabular component
Annual International Conference of the IEEE Engineering in Medicine and Biology Society 12:2136-2137

Summagraphics SummaSketch II
1989
Summagraphics digitiser, software and manuals
Summagraphics Corporation
Connecticut, USA

Sutherland CJ, Wilde AH, Borden LS, Marks KE
1982
A ten-year follow-up of one hundred consecutive Müller curved-stem total hip replacement arthroplasties
Journal of Bone and Joint Surgery 64A: 970-980

Svensson NL, Valliapan S, Woods RD
1977
Stress analysis of human femur with with implanted Charnley prosthesis
Journal of Biomechanics 10: 581-588

Tanzer M, Drucker D, Jasty M, McDonald M, Harris WH
1992
Revision of the acetabular component with an uncemented Harris-Galante Porous-Coated prosthesis
Journal of Bone and Joint Surgery 74A: 987-994

Vasu R, Carter DR, Harris WH
1982
Stress distributions in the acetabular region - I. Before and after total hip replacement
Journal of Biomechanics 15:155-164

Vukicevic D, Vukicevic S, Vinter J, Sankovic K
1982
Holographic investigations of the human pelvis
pp 138-142 Eds. G. von Bally & P. Greguss In: Optics in Biomedical Sciences
Springer-Verlag, Berlin

Wasielewski RC, Cooperstein LA, Kruger MP, Rubash HE
1990
Acetabular anatomy and the transacetabular fixation of screws in THA
Journal of Bone and Joint Surgery 72A:501-508

Weisl H
1954a
The ligaments of the sacroiliac joint examined with particular reference to their function
Acta Anatomica 20: 201-213

Weisl H
1954b
The articular surfaces of the sacroiliac joints and their relation to the movements of the sacrum
Acta Anatomica 22: 1-14

Weisl H
1955
The movements of the sacroiliac joint
Acta Anatomica 23: 80-91

Williams JF, Svensson NL
1968
A force analysis of the hip joint
Biomedical Engineering 3: 366-370

Wilson-MacDonald J, Morscher E, Masar Z
1990
Cementless uncoated polyethylene acetabular components in total hip replacement
Journal of Bone and Joint Surgery 72B:423-430

Woo SL, Kvei SC, Amiel D
1981
The effect of prolonged physical training on the properties of long bone: A study of Wolff's Law
Journal of Bone and Joint Surgery 63A:780-786

Wykman A, Olsson E, Axdorph G, Goldie I
1991
Total hip arthroplasty: a comparison between cemented and press-fit noncemented fixation
Journal of Arthroplasty 6:19-29

Zienkiewicz OC
1977
The finite element method
McGraw-Hill, London.